PROCEEDINGS

of the

Thirteenth
International Tissue Elasticity Conference™

Snowbird, Utah, USA
September 7 – 10, 2014

PROCEEDINGS

of the
Thirteenth International Tissue Elasticity Conference™

Snowbird, Utah, USA
September 7-10, 2014

Table of Contents

Foreword

Dear Conference Delegate:

On behalf of the general organizing team, welcome to the 13th annual International Tissue Elasticity Conference™ (ITEC™), and to the scenic mountains of Salt Lake County, Utah. We are returning to the Snowbird Resort, voted by you as a very popular venue on two previous occasions. The venue provides a comfortable retreat, with excellent conference facilities and a relaxing atmosphere within which we can present and discuss our science, as well as renew and create friendships. You may wish to take the time to indulge in a walk. The air is fresh and the views are worth the effort; here is a picture taken during ITEC 2006, looking west (towards Salt Lake City) from near where the aerial tram stops at the top of its run.

For our free evening, on the Tuesday this year, we are providing a bus to Park City, in Summit County, Utah, just over the mountains in the opposite direction to Salt Lake City. An old mining town, Park City is named by Forbes Traveler Magazine as among the 20 prettiest towns in the USA. It also has the largest collection of factory outlet stores in northern Utah. To help you enjoy your free evening in Park City our Local Events Organizer, Helen Feltovich, has kindly obtained discount coupons for great deals in various restaurants. Helen, thank you so much for all your help with numerous local details. Your assistance has been so important for the success of ITEC 2014.

I am greatly looking forward to the performance by vocalist and composer, Emily Merrell (http://www.emilymerrell.com/), shown in the picture on the right. Emily is a recent graduate in Jazz Performance of the University of North Texas, and will provide our musical entertainment to follow the Conference Dinner on the Monday evening.

I am very sad to report that Jonathan and Karen Ophir will not be able to join us this year. Jonathan and Karen are two of the Founding Organizers of ITEC, and they were the principle driving force behind the ITEC series of conferences from 2002-2012. They had hoped to attend ITEC 2014 but it was not to be, as explained in their letter below. Jonathan, we all send you our good wishes for a continued and speedy recovery from your surgery, and Karen we hope that your treatment goes well. We hope to involve you both in the conference at various points, via Skype.

This year we will kick-off two of the days, Monday and Wednesday, with tutorial speakers. I am delighted that David Cosgrove has agreed, on Monday, to open ITEC 2014 with a lecture that discusses the medical applications where elastography is able to make a genuine clinical difference right now, and explores possible applications where it can be expected to make a difference in the future. David is a world-renowned ultrasound educator and I am delighted that he will be leading this discussion to open the conference. Our tutorial on Wednesday will be in the important and rapidly developing technological area of ultrasonic beam forming, a hot topic in ultrasound in general for the last few

years, and one which is now having a substantial impact on performance and capability of elastography. This is a topical theme that runs through some of the abstracts submitted this year for proffered papers. I am therefore very pleased indeed that Marvin Doyley, whose research team has been specialising in this area, has agreed to provide a tutorial on the various beam and image formation methods available and how they can be employed to the benefit of elasticity imaging. It is a substantial task to prepare an ITEC tutorial, and I am grateful to both David and Marvin for agreeing to pass on their knowledge and experience in this way.

Many volunteers and colleagues have helped to bring about this conference, especially our conference secretary, Cheryl Taylor. Please join me in thanking Cheryl for, once again, working tirelessly to make the conference a timely success. It is a pleasure also to acknowledge contributions from the administration of the Institute of Cancer Research, especially Liam Blake and Alan Hill for assistance in financial and legal matters, and Elise Glenn and Neil Walford for assistance with audio-visual equipment. Finally, we are extremely grateful to all those who have participated as helpers, sponsors, reviewers, session chairs, award judges and contributors, without whom the conference could not happen.

When Jonathan Ophir and Kevin Parker first conceived this conference series they expressed the purpose as "to advance the field of measurement and imaging of the elastic attributes of soft tissues through tutorials and scientific presentations of the state of the art in the field, within a unique and unified forum that would bring together researchers from several countries and ultimately contribute to the rapid development and clinical introduction of this new medical imaging technology". Our presence here suggests that we all strongly agree that we continue to value such a conference. However, ITEC must evolve if it is to continue to serve the needs of researchers and practitioners in the field of tissue elasticity measurement and imaging. Please complete the feedback forms in this Proceedings Book and join us for the discussion session just prior to the Group Photo on Tuesday. They will be of immense value to us as we plan future ITECs.

May your research be inspired by the presentations and discussions during the 13th ITEC, and may you make new friends, establish productive collaborations and renew old acquaintances.

Jeffrey Bamber
General Conference Organizer
Snowbird, USA, September 7-10, 2014

Message from the Founding Organizers

Dear friends and colleagues:

We are writing you this note in lieu of greeting you in person at ITEC '14 in Utah. As some of you may know, Karen has been having serious health issues for over a decade. All the while, she volunteered to organize the Conference and contribute to its success. In the last years this task has become more burdensome and time consuming for her and this was the reason that we decided that in 2013 it was a good time to transfer the organization of the Conference to Jeff Bamber's team in the UK. The transfer was successful and the Conference continues to thrive under the capable new leadership.

The transfer did not occur a moment too soon; in the past months I (Jonathan) was diagnosed with a serious health issue. I recently underwent major surgery and continue to recuperate at home.

These issues all together made it impossible for us to attend this year's Conference, but we will do whatever we can to attend next year.

We will miss seeing our friends and colleagues as well as meeting the new delegates. We hope that you will have a stimulating academic experience and much wonderful camaraderie.

All the best,

Jonathan and Karen Ophir
Founding Organizers

Welcome

Dear Conference Delegate:

I am delighted to welcome you to the mountains of Utah, Snowbird, for the 13th annual International Tissue Elasticity Conference™, 7-10th September, and to Park City, for the evening on Tuesday 8th September.

Helen Feltovich
Local Events Organizer
Snowbird, USA, September 7-10, 2014

CONFERENCE–AT–A–GLANCE
Thirteenth International Tissue Elasticity Conference™
Snowbird Ski and Summer Resort – Salt Lake County, Utah, USA   September 7–10, 2014

Sunday, September 7

11:00A – 4:00P	**Set Up:**	Oral Presenters load presentations (CD or USB Stick)	Ballroom III
11:00A – 6:00P		Registration Desk Open	Ballroom Foyer
11:00A – 2:00P		Exhibitors set up	Ballroom II
2.00P – 4.00P		*Coffee Available*	Ballroom II
2:00P- 6.00P	**Session EEX:**	Equipment Exhibit	Ballroom II
6:30P – 8:30P		*Opening Dinner Reception*	Ballroom II

Monday, September 8   9:00A – 10:00P

9:00A – 5:00P		Registration Desk Open	Ballroom Foyer
9:00A – 5:00P	**Session EEX:**	Equipment Exhibit	Ballroom II
8:45A – 9:00A		Opening Remarks	Ballroom III
9:00A – 10:00A	**Session TUT-1:**	**Tutorial A**	Ballroom III
10:00A – 10:30A		*Coffee Break*	Ballroom II
10:30A – 12:30P	**Session SAS:**	**Student Awards Finalists Session**	Ballroom III
12:30P – 2:00P		*Group Lunch*	Golden Cliff/Eagles Nest
2:00P – 3:15P	**Session MIP–1:**	**Methods for Imaging Elastic Tissue Properties – I**	Ballroom III
3:15P – 3:45P		*Coffee Break*	Ballroom II
3:45P – 4:15P	**Session CAA -1:**	**Clinical and Animal Applications**	Ballroom III
7:00P – 10:00P		*Conference Dinner*	Ballroom I

Tuesday, September 9   9:00A – 5:00P

8:30A – 5:00P		Registration Desk Open	Ballroom Foyer
8:30A – 5:00P	**Session EEX:**	Equipment Exhibit	Ballroom II
9:00A – 10:15A	**Session MIP–2:**	**Methods for Imaging Elastic Tissue Properties – II**	Ballroom III
10:15A – 10:45A		*Coffee Break*	Ballroom II
10:45A – 11:30A	**Session MPT:**	**Mechanical Properties of Tissues**	Ballroom III
11:30P – 12:15P	**Session SIP–1:**	**Signal and Image Processing – I**	Ballroom III
12:15P – 1:45P		*Group Lunch*	Golden Cliff/Eagles Nest
1.45P – 4:00P	**Session CVE:**	**Cardiovascular Elasticity**	Ballroom III
4:00P – 4:30P		*Coffee Break*	Ballroom II
4.30P – 5:00P		**Discussion**	Ballroom III
5.00P – 5:15P		**Group Photo**	Ballroom III
5:50P – 10:00P		Boarding Coach to Parkside (departs at 6:00P)	TBA

Wednesday, September 10   9:00A – 9:00P

8:30A – 5:00P		Registration Desk Open	Ballroom Foyer
8:30A – 5:00P	**Session EEX:**	Equipment Exhibit	Ballroom II
9:00A – 10:00A	**Session TUT-2:**	**Tutorial B**	Ballroom III
10:00A – 10:30A		*Coffee Break*	Ballroom II
10:30A – 11:45P	**Session CAA -2:**	**Clinical and Animal Applications**	Ballroom III
11:45P – 1:30P		*Group Lunch*	Golden Cliff/Eagles Nest
1:30P – 2:15P	**Session MIP–3:**	**Methods for Imaging Elastic Tissue Properties – III**	Ballroom III
2:15P – 2:58P	**Session SIP–2:**	**Signal and Image Processing – II**	Ballroom III
3:00P – 3:30P		*Coffee Break*	Ballroom II
3:30P – 4:15P	**Session BTM:**	**Biomechanical Tissue Modeling**	Ballroom III
4:15P – 5:15P	**Session FIP:**	**Forward and Inverse Problems**	Ballroom III
6:15P – 9:00P		*Closing Pizza Party (Proceedings Book Signing)*	Atrium Lounge

PROGRAM
Thirteenth International Tissue Elasticity Conference™
Snowbird, Utah, USA
September 7-10, 2014

Sunday, September 7	**11:00A – 8:30P**

11:00A – 4:00P   Presentation Set Up
All Oral Presenters load presentations onto Conference computers   Ballroom III

11:00A – 2:00P Exhibitors set up exhibits   Ballroom II

11:00A – 6:00P Registration Desk Open   Ballroom Foyer

2:00P – 6:00P   Session EEX: Equipment Exhibit   Ballroom II

2:00P – 4:00P COFFEE AVAILABLE   Ballroom II

Sunday   6:30P – 8:30P
Opening Dinner Reception   Ballroom II

Monday, September 8	**9:00A – 10:00P**

9:00A – 5:00P Registration Desk Open   Ballroom Foyer

9:00A – 5:00p   Session EEX: Equipment Exhibit   Ballroom II

Monday   8:45A – 9:00A
OPENING REMARKS
JC Bamber   Ballroom III

Monday   9:00A – 10:00A
Session TUT-1:   Tutorial A
Chair: JC Bamber, UK   *Co–Chair: C Sumi, Japan*   Ballroom III

Page No.

9:00A – 9:45A
058   CLINICAL USEFULNESS OF ULTRASOUND ELASTOGRAPHY: IMPACT ON MANAGEMENT.   20
   D Cosgrove[1]*
   [1]Imperial and King's Colleges, London, England, UK.

9:45A – 10:00A   Discussion

10:00A – 10:30A
          COFFEE BREAK   Ballroom II

Session SAS: **Oral Presentations of Finalists for Student Awards Session**

Chair: TJ Hall, USA   *Co–Chair: HHG Hansen, The Netherlands*   Ballroom III

Page No.

10:30A – 10:45A

015   MULTI-ELEMENT SYNTHETIC APERTURE VASCULAR ELASTOGRAPHY FOR CAROTID   21
IMAGING.
R Nayak*, P Verma, MM Doyley.
University of Rochester, Rochester, New York, United States.

10:45A – 11:00A

016   QUANTIFYING DISPERSION OF SHEAR WAVES PRE AND POST-INDUCTION OF LABOR.   22
L Carlson[1]*, H Feltovich[1,2], ML Palmeri[3], S Romero[2], TJ Hall.[1]
[1]University of Wisconsin, Madison, WI, USA; [2]Intermountain Healthcare, Intermountain
Medical Center, Murray, UT, USA; [3]Duke University, Durham, NC, USA.

11:00A – 11:15A

019   MULTI SLICE RADIAL STRAIN IMAGING OF AN ATHEROSCLEROTIC CAROTID ARTERY BY   23
CROSS-SECTIONAL STRAIN ESTIMATIONS USING MULTI ANGLE SIMULATED PLANE WAVE
ULTRASOUND TRANSMISSIONS.
S Fekkes[1]*, AES Swillens[2], HHG Hansen[1], AECM Saris[1], MM Nillesen[1], F Iannacone[2],
P Segers[2], CL de Korte[1].,
[1]Radboud University Medical Center, Nijmegen, THE NETHERLANDS; [2] Ghent University,
Ghent, BELGIUM.

11:15A – 11:30A

020   PLANE WAVE DISPLACEMENT COMPOUNDING FOR ESTIMATION OF LARGE   24
DISPLACEMENTS.
AECM Saris[1]*, HHG Hansen[1], S Fekkes[1], MM Nillesen[1], MCM Rutten[2], CL de Korte[1]
[1]Radboud University Medical Center, Nijmegen, THE NETHERLANDS; [2]Eindhoven
University of Technology, Eindhoven, THE NETHERLANDS.

11:30A – 11:45A

023   QUANTITATIVE SONOELASTOGRAPHY OF THE UTERINE CERVIX BY INTERPOSITION OF A   25
SYNTHETIC REFERENCE MATERIAL AND INTRA-INTEROBSERVER EVALUATION.
A K Leonhard[1]*, L Hee[1], P Sandager[12], O Petersen[2], C K Rasmussen[1], J M Schlütter[1], N Ulbjerg[12],
[1]Institute of Clinical Medicine, Aarhus University, Aarhus, DENMARK; [2]Aarhus University
Hospital, Skejby Aarhus, DENMARK.

11:45A – 12:00P

029   A NEW APPROACH TO MEASURE THE MECHANICAL HETEROGENEITY OF BREAST   26
MASSES.
T. Liu[1]*, O.A. Babaniyi[2], T.J. Hall[3], P.E. Barbone[2], A.A. Oberai[1],
[1]Rensselaer Polytechnic Institute, Troy, NY, USA; [2]Boston University, Boston, MA, USA;
[3]University of Wisconsin, WI, USA.

12:00P – 12:15P

037   *IN VIVO* CHARACTERIZATION OF ATHEROSCLEROTIC PLAQUE IN HUMAN CAROTID   27
ARTERIES WITH HISTOPATHOLOGICAL CORRELATION USING ACOUSTIC RADIATION
FORCE IMPULSE (ARFI) ULTRASOUND.
TJ Czernuszewicz[1⃝], JW Homeister[1], MC Caughey[1], MA Farber[1], JJ Fulton[1], PF Ford[1],
WA Marston[1], R Vallabhaneni[1], TC Nichols[1], CM Gallippi[1].
[1]University of North Carolina, Chapel Hill, NC, USA.

Monday   2:00P – 3:15P
Session MIP–1:   Methods for Imaging Elastic Tissue Properties – I
Chair: RGP Lopata, The Netherlands   Co–Chair: PE Barbone, USA   Ballroom III
Page No.

Monday   **3:45P – 4:15P**
Session CAA–1:   Clinical and Animal Applications – I
Chair: HW Chan, UK   *Co–Chair: D Cosgrove, UK*   Ballroom III

Monday   **7:00P – 10:00P**
Conference Dinner   Ballroom I
Proceedings Book Signing

          Music by Emily Merrell

Tuesday, September 9   9:00A – 5:00P

8:30A – 5:00P
          Registration Desk Open   Ballroom Foyer
8:30A – 5:00p   Session EEX: Equipment Exhibit   Ballroom II

Tuesday   **9:00A – 10:15A**
Session MIP–2:   Methods for Imaging Elastic Tissue Properties – II
Chair: R Souchon, France   *Co–Chair: EE Konofagou, USA*   Ballroom III

* indicates Presenter   10

9:30P – 9:45P

008   ACCURATE MEASUREMENTS OF TISSUE DISPLACEMENT IN TWO DIMENSIONS USING   38
HIGH FRAME RATE ULTRASOUND IMAGING.
P Kruizinga[1]*, F Mastik[1], N de Jong[1,2,3,], JG Bosch[1], G van Soest[1,] AFW van der Steen[1,2,3,4]
[1]Thorax Center, Erasmus Medical Center, Rotterdam, THE NETHERLANDS. [2]Delft University
of Technology, Delft, THE NETHERLANDS. [3]Interuniversity Cardiology Institute of The
Netherlands, Utrecht, THE NETHERLANDS. [4]Shenzhen Institutes of Advanced Technology,
Shenzhen, CHINA.

9:45A – 10:00A

051   THE APPLICABILITY OF PLANE WAVE IMAGING TO POROELASTOGRAPHY.   39
M Theodorou[1]*, J Fromageau[1], N de Souza[1], JC Bamber[1].
[1]Institute of Cancer Research and Royal Marsden NHS Foundation Trust, London, UK.

10:00A – 10:15A

038   ESTIMATION OF TISSUE VISCOELASTICITY USING INVERSE FILTER AND MULTIPLE-   40
POINT SHEAR WAVE GENERATION.
T Kitazaki[1]*, K Kondo[1,] M Yamakawa[1,] T Shiina[1].
[1]Kyoto University, Kyoto, JAPAN.

10:15A – 10:45A

        COFFEE BREAK   Ballroom II

Tuesday   **10:45A – 11:30A**
Session MPT: **Mechanical Properties of Tissues**
Chair: R Lopata, The Netherlands   *Co–Chair: HHG Hansen, The Netherlands*   Ballroom III
                                                        Page No.

10:45A – 11:00A

047   *IN VIVO* 3D SKELETAL MUSCLE DEFORMATION: METHODS AND INITIAL RESULTS.   41
K Gijsbertse[1]*, AMJ Sprengers[1], NJJ Verdonschot[1,2], CL de Korte[1].
[1] Radboud University Medical Center, Nijmegen, THE NETHERLANDS. [2]University of
Twente, Enschede, THE NETHERLANDS.

11:00A – 11:15A

028   *IN VIVO* SHEAR WAVE DISPERSION MEASUREMENT USING MULTIFREQUENCY   42
VIBRATION-CONTROLLED TRANSIENT ELASTOGRAPHY: FIRST RESULTS TO LIVER
STEATOSIS QUANTIFICATION.
JP Remenieras[1]*, M Dejobert[2], C Bastard[3], V Miette[2], JM Perarnau[2], F Patat[1,2].
[1]INSERM, Tours, France, [2]Echosens, Paris, FRANCE.

11:15A – 11:30A

027   MEASUREMENT OF SHEAR WAVE SPEED DISPERSION IN PLACENTA USING TRANSIENT   43
ELASTOGRAPHY: A PRELIMINARY *EX VIVO* STUDY.
S Calle[1]*, E Simon[1,2], E Nicolas[1], R Ternifi[1], F Perrotin[1,2], JP Remenieras[1.]
[1] INSERM, Tours, FRANCE, [2]University Hospital Center of Tours, Tours, FRANCE.

Tuesday   11:30A – 12:15P
Session SIP-1:   Signal and Image Processing
Chair: EE Konofagou, USA   *Co–Chair: J Jiang, USA*   Ballroom III

Tuesday   1:45P – 4:00P
Session CVE: Cardiovascular Elasticity
Chair: CL de Korte, The Netherlands   *Co–Chair: R Daigle, USA*   Ballroom III

2:45P – 3:00P

005   3-D SPECKLE TRACKING WITH TWO-PASS PROCESSING AND PHASE-ROTATED   51
      CORRELATION COEFFICIENT FILTERING FOR 4-D ECHOCARDIOGRAPHIC STRAIN
      ESTIMATION.
      EY Wong[1]*, CB Compas[2], BA Lin[2], AJ Sinusas[2], JS Duncan[2], M O'Donnell[1].
      [1]University of Washington, Seattle, Washington, USA; [2]Yale University, Connecticut, USA.

3:00P – 3:15P

056   IN VITRO VALIDATION OF VASCULAR ELASTOGRAPHY: FROM INFLATION TEST TOWARDS   52
      IN VIVO MEASUREMENTS.
      Edgar J. S. Mascarenhas, Mathijs F.J. Peters, Marcel C.M. Rutten,
      Frans N. van de Vosse, R G.P. Lopata.*
      Eindhoven University of Technology, Eindhoven, THE NETHERLANDS.

3:15P – 3:30P

002   FATTY PLAQUE PHANTOM FOR ULTRASOUND IMAGING.   53
      RW Boekhoven[1]*, MC Rutten[1], F van de Vosse[1], RG Lopata[1].
      [1]Eindhoven University of Technology, Eindhoven, THE NETHERLANDS.

3:30P – 3:45P

007   INTRAVASCULAR ARFI TRANSDUCER FOR ELASTICITY IMAGING OF   54
      CORONARY ARTERIES.
      CD Herickhoff[1]*, JJ Dahl[1].
      [1]Duke University, Durham, NC, USA.

3:45P – 4:00P

032   MECHANICAL CHARACTERIZATION OF ASCENDING THORACIC AORTIC ANEURYSMS   55
      USING 4-D ULTRASOUND.
      EM van Disseldorp[1]*, J Nijs[2], M Erwin SH Tan[3], MR. van Sambeek[3], F van de Vosse[1], RG Lopata[1.]
      [1]Eindhoven University of Technology, Eindhoven, THE NETHERLANDS; [2]University Hospital
      Brussels, Brussels, BELGIUM; [3]Catharina Hospital Eindhoven, Eindhoven, THE NETHERLANDS.

4:00P – 4:30P

                    COFFEE BREAK   Ballroom II

Tuesday   4:30P – 5:00P
Session: General Discussion
Chair: JC Bamber, UK   Ballroom III

5:00P – 5:15P

                    GROUP PHOTO   Ballroom III

After 5:15P   No conference Activities

5:50P – 10:00P   Boarding Coach to Park City (departs at 6:00P)   TBA

8:30A – 5:00P

    Registration Desk Open   Ballroom Foyer

8:30A – 5:00p   **Session EEX: Equipment Exhibit**   Ballroom II

Wednesday   9:00A — 10:00A
Session TUT-2:   Tutorial B

Chair: C Sumi, Japan   *Co–Chair: JC Bamber, UK*   Ballroom III

                                                             Page No.

9:00A – 9:45A

057 BEAM-FORMING CHOICES: WHAT ARE THEY, HOW DO THEY WORK, AND WHAT IS   56
THEIR IMPACT FOR ELASTOGRAPHY.
MM Doyley[1]*.
[1]University of Rochester, Rochester, NY, USA.

9:45A – 10:00A   Discussion

10:00A – 10:30A

        COFFEE BREAK   Ballroom II

Wednesday   10:30A — 11:45A
Session CAA–2:   Clinical and Animal Applications – II

Chair: D Cosgrove, UK   *Co–Chair: HW Chan, UK*   Ballroom III

                                                             Page No.

10:30A – 10:45A

036 *IN VIVO* ARFI SURVEILLANCE OF SUBCUTANEOUS HEMORRHAGE (ASSH) FOR   57
MONITORING RCFVIII DOSE RESPONSE IN HEMOPHILIA A DOGS Response in Hemophilia
A DOGS.
RE Geist[1]*, TC Nichols[2,3], EP Merricks[3], MC Caughey[2], and CM Gallippi[1,4,5].
[1]University of North Carolina at Chapel Hill, Chapel Hill, North Carolina, USA.

10:45A – 11:00A

021 AGE-DEPENDENT EVOLUTION OF NATURAL BRAIN TISSUE PULSATILITY: A CLINICAL   58
UNLTRASOUND STUDY.
R Ternifi[1]*, G Chassagnon [2,3], C Destrieux [1,2], F Patat [1,2,3], JP Remenieras [1].
[1]University of North Carolina, Chapel Hill, NC, USA.

11:00A – 11:15A

053 VISCOELASTICITY AS A BIOMARKER OF CELL DEATH: A COMPARISON WITH ADC IN AN   59
ORTHOTOPIC BREAST CANCER XENOGRAFT MODEL.
J Li[1], Y Jamin[1], JKR Boult[1], JC Waterton[2], R Sinkus[3], MD Garrett[1], JC Bamber[1]*, SP Robinson[1].
[1] Institute of Cancer Research and Royal Marsden NHS Foundation Trust, London, UK;
[2]AstraZeneca, Macclesfield, UK; [3]King's College London, King's Health Partners,
St Thomas' Hospital, London, UK.

---

* indicates Presenter   14

11:15A – 11:30A

049 INVESTIGATING THE EFFECT OF PIA ON THE YOUNG'S MODULUS MEASUREMENTS OF GREY AND WHITE MATTER IN *EX VIVO* PORCINE BRAINS USING SHEAR WAVE ELASTOGRAPHY.   60

HW Chan[1,2]*, C Uff[2], A Chakraborty[3], N Dorward[2], JC Bamber[1].
[1]Institute of Cancer Research and Royal Marsden NHS Foundation Trust, London, UK;
[2]The National Hospital for Neurology and Neurosurgery, London, UK.
[3]Southampton General Hospital, Southampton, England, UK.

11:30A – 11:45A

050 DETECTING MRI-NEGATIVE EPILEPTOGENIC LESIONS WITH INTRAOPERATIVE SHEAR WAVE ELASTOGRAPHY.   61

HW Chan[1,2]*, C Uff[2], A Chakraborty[3], N Dorward[2], JC Bamber[1].
[1]Institute of Cancer Research and Royal Marsden NHS Foundation Trust, London, UK;
[2]The National Hospital for Neurology and Neurosurgery, London, UK.
[3]Southampton General Hospital, Southampton, England, UK.

11:45A – 1:30P

GROUP LUNCH   Golden Cliff/Eagles Nest

Wednesday   1:30P – 2:15P

Session MIP–3:   Methods for Imaging Elastic Tissue Properties – III

Chair: PE Barbone, USA   Co–Chair: MM Doyle, USA   Ballroom III

Page No.

1:30P – 1:45P

003 PHASE-SENSITIVE OPTICAL COHERENCE TOMOGRAPHY AND CODED ACOUSTIC RADIATION FORCE FOR SHEAR WAVE ELASTOGRAPHY.   62

TM Nguyen[1]*, S Song[1,2], B Arnal[1], EY Wong[1], RK Wang[1,3], M O'Donnell[1].
[1]University of Washington, WA, USA; [2]University of Dundee, Dundee, Scotland, UK;
[3]University of Washington, Seattle, WA, USA.

1:45P – 2:00P

055 SHEAR-WAVE ELASTOGRAPHY USING MULTI-CHANNEL OPTICAL COHERENCE TOMOGRAPHY: A COMPARISON OF RELATIVE AND ABSOLUTE SHEAR-WAVE TIME OF FLIGHT METHODS.   63

E Elyas[1], A Grimwood[2], J Erler[3], SP Robinson[1], T Cox[3], D Woods[4], P Clowes[1], JC Bamber[1]*
[1]Institute of Cancer Research and Royal Marsden NHS Foundation Trust, London, UK;
[2]Royal Surrey County Hospital, Guildford, Surrey, UK; [3]University of Copenhagen,
Copenhagen, Denmark; [4]Michelson Diagnostics, Orpington, Kent, UK.

2:00P – 2:15P

052 UNWRAPPING PHASE IN SWEPT-SOURCE OPTICAL COHERENCE ELASTOGRAPHY USING THE COMBINED AUTOCORRELATION METHOD.   64

A Grimwood[1], JC Bamber[2]*.
[1]Royal Surrey County Hospital, Guildford, Surrey, UK; [2]Institute of Cancer Research,
London, England, UK.

Wednesday   2:15P – 2:58P

Session SIP-2:   Signal and Image Processing – II

Chair: P Kruizinga, The Netherlands   Co–Chair: JC Bamber, UK   Ballroom III
Page No.

2:15P – 2:22P

012   ANALYTICAL PHASE TRACKING BASED STRAIN ESTIMATOR FOR QUASI-STATIC   65
ELASTOGRAPHY.
L Yuan[1], PC Pedersen[1].*
[1]Worcester Polytechnic Institute, Worcester, MA, USA.

2:22P – 2:29P

011   A FAST HYBRID MOTION TRACKING ALGORITHM FOR 3D ULTRASONIC ELASTICITY   66
IMAGING.
Y Wang[1], TJ Hall[1].*
[1]University of Wisconsin, Madison, WI, USA.

2:29P – 2:36P

006   ASSESSMENT OF MYOCARDIAL STRAIN USING ADAPTIVE SIGNAL PROCESSING FOR   67
THE SUPPRESSION OF HIGH-INTENSITY INTERFERENCES: A SIMULATION STUDY.
S Okumura[1], A Kita[2], H Taki[1], T Sato[1].*
[1]Kyoto University, Kyoto, Japan; [2]Sakai Rumi, Hyogo, Japan.

2:36P – 2:43P

014   TWO-DIMENSIONAL ULTRASOUND STRAIN IMAGING IN A TRANSVERSELY ISOTROPIC   68
MEDIUM.
H Li[1]; W-N Lee[1].*
[1]The University of Hong Kong, Hong Kong, CHINA.

2:43P – 2:58P

030   OVER-DETERMINED SYSTEMS USING PLURAL STEERED BEAMS OR PLANE WAVES FOR   69
DISPLACEMENT VECTOR MEASUREMENT AND SUPER-RESOLUTION IMAGING.
C. Sumi[1].*
[1]Sophia University, Tokyo JAPAN.

3:00P – 3:30P

COFFEE BREAK   Ballroom II

Wednesday   3:30P – 4:15P

Session BTM: Biomechanical Tissue Modeling

Chair: MM Doyle, USA   Co–Chair: TJ Hall, USA   Ballroom III
Page No.

3:30P – 3:45P

045   LONGITUDINAL SHEAR WAVE AND TRANSVERSE COMPRESSIONAL WAVE IN ELASTIC   70
SOLIDS.
R.Souchon[1], S. Catheline[1], N. Benech[2].*
[1]University of Lyon, Lyon, FRANCE; [2]Instituto de Física, Montevideo, URUGUAY.

3:45P – 4:00P

009   DEVELOPMENT OF AN EXPERIMENTALLY VALIDATED NUMERICAL TOOL TO ASSESS   71
THE ACCURACY OF SHEAR WAVE ELASTOGRAPHY.
A Caenen[1], D Shcherbakova[1], B Verhegghe[1], C Papadacci[2], M Pernot[2], P Segers[1], A Swillens[1].*
[1]Ghent University, Ghent, BELGIUM; [2]Institut Langevin, Paris, FRANCE.

* indicates Presenter   16

4:00P – 4:15P

031 DEVELOPMENT OF OPEN-SOURCE TOOLS TO VALIDATE SHEAR WAVE IMAGING: AN   72
        INTEGRATED QIBA EFFORT.

J Jiang[1]*, S McAleavey[2], J Langdon[2], ML Palmeri[3].
[1]Michigan Technological University, Houghton, Michigan, USA; [2]Universtiy of Rochester, Rochester, New York, USA; [3]Duke University, Durham, North Carolina, USA.

Wednesday   4:15P – 5:15P
Session FIP: Forward and Inverse Problems

Chair: J Jiang, USA   *Co–Chair: R Souchon, France*   Ballroom III
                                                                                                    Page No

4:15P – 4:30P

017 STRAIN-BASED SPARSITY REGULARIZATION FOR DIRECT FEM INVERSION OF TISSUE   73
        ELASTOGRAPHY.

M Honarvar[1], R Rohling[1]*, S E Salcudean[1].
[1] The University of British Columbia, Vancouver, CANADA.

4:30P – 4:45P

048 EFFECT OF ISOTROPIC ASSUMPTION ON MATERIAL PROPERTY MAPS OF THE HUMAN   74
        BRAIN USING NON-LINEAR INVERSION FOR MR ELASTOGRAPHY.

A Anderson[1], C Johnson[1], J Holtrop[1], E Van Houten[2], M McGarry[3], K Paulsen[3],
B Sutton[1], J Georgiadis[1].*
[1]University of Illinois at Urbana-Champaign, Urbana, IL, USA; [2]Universite of Sherbrooke, Quebec, CANADA; [3]Dartmouth College, Hanover, NH, USA.

4:45P – 5:00P

034 ALGORITHMS FOR QUANTITATIVE QUASI-STATIC ELASTITY IMAGING USING FORCE   75
        DATA.

M Tyagi[1]*, S Goenezen[2], PE Barbone[3], AA Oberai[1].
[1]Rensselaer Polytechnic Institute, Troy, NY, USA; [2]Texas A&M University, TX, USA;
[3]Boston University, Boston, MA, USA.

5:00P – 5:15P

024 CALIBRATION-FREE BLOOD PRESSURE ESTIMATION USING A MODIFIED   76
        ELASTOGRAPHY APPROACH: SIMULATION RESULTS.

A.M. Zakrzewski[1]*, B.W. Anthony[1].
[1]Massachusetts Institute of Technology, Cambridge, MA, USA.

Wednesday   6:15P – 9:00P
Closing Reception   *Proceedings Book Signing*   Atrium Restaurant

Session EEX: Equipment Exhibit   Ballroom II

AUTHOR INDEX

**Session TUT-1:   Tutorial: Clinical Usefulness of Ultrasound Elastography:
Impact on Management**
Monday, September 8   9:00A – 10:00A

058   **CLINICAL USEFULNESS OF ULTRASOUND ELASTOGRAPHY: IMPACT ON MANAGEMENT.**
David Cosgrove[1]*
[1]Imperial and King's Colleges, London, England, UK.

Elastography using ultrasound has attracted much attention since its introduction in the 90s [1], and systems are now offered by all major system manufacturers. One, the Fibroscan, is dedicated just to elastography. The evidence of the clinical value of elastography as an addition to conventional ultrasound imaging has been summarised in recently published guidelines [2], but there remains controversy over the extent of its value and over which technique to apply.

Two main methods are clinically available, strain and shear wave [3], and two main clinical applications have emerged, the breast for classifying masses, and the liver for assessing fibrosis.

Strain elastography for the breast was an early commercial implementation. With its use pioneered by Japanese workers [4], a subjective score supplemented by a semiquantitative index of the stiffness relative to the surrounding tissue (ideally, fatty tissue) picked out cancers, especially invasive cancers, as being stiffer than benign masses and improved on the BI-RADS score, especially in reclassifying BI-RADS 3 and 4a lesions so that biopsy would be prompted for the former and 6-month review for the latter. A useful additional way to classify breast masses hinges on the observation that cancers appear larger on strain elastograms than on B-mode, while benign masses are smaller or equal in size [5]. There remain misclassifications, the most worrying of which concern intrinsically soft malignancies (colloid and mucinous cancers) for which elastography is falsely reassuring. This method has more recently been supplemented by shear wave elastography which has the advantages of being quantitative (results in m/s convertible to kPa) and of being less operator-dependent (because the system's push pulses generate the tissue distortion) [6]. However, it has a problem with very stiff cancers which sometimes show no stiff region at all, although in most at least a peripheral rim of stiff tissue is found.

The liver is the other well-evidenced clinical application, where elastography is mainly used for diffuse diseases and especially for fibrosis. Strain elastography is difficult to apply to this well-shielded organ but shear wave methods work well. The oldest is the Fibroscan [7], a dedicated non-imaging method that requires experience but has been widely accepted amongst hepatologists and is routinely used to track changes in liver stiffness. Typically measurements are made before the patient sees the clinician and its use has resulted in a reduction in biopsies [8]. The lack of imaging can pose problems because parts of the liver are innately stiffer (the sub capsular region and major blood vessels), so imaging versions have gained some advantage here, despite the somewhat higher cost [9]. The advantages over biopsies are obvious (risk, discomfort, undersampling), though these non-invasive methods do not inform about inflammation or steatosis and they are more reliable for more severe degrees of fibrosis.

Of the numerous other potential clinical applications, perhaps the thyroid is amongst the most pressing because of the large number of negative FNAs that are performed for found nodules; the evidence here is mixed and conclusions are hard to draw despite extensive studies [10]. Many other applications are intriguing (cervical stiffness for assessing the risk of premature birth, intra-operative applications to guide surgery, musculo-skeletal disorders, prostate, renal transplants) but they have not yet been sufficiently evaluated to warrant recommendation as routinely useful tools.

References: [1] Ophir, J, et al., Proc Inst Mech Eng. Part H, J Eng Med, 213:203-33, 1999. [2] Cosgrove D, et al., Ultraschall in Med, 34:238-253, 2013. [3] Bamber, J, et al., Ultraschall Med, 34:169-84, 2013. [4] Itoh, A, et al., Radiology, 239: 341-50, 2006. [5] Barr, RG, J Ultrasound Med, 31: 773-83, 2012. [6] Berg WA, et al., Radiology, 262:435-49, 2012. [7] Sandrin L, et al., Ultrasound Med Biol, 29:1705-13, 2003. [8] Wong GL, Gastroent Rep (Oxf), 1:9-26, 2013. [9] Ferraioli G, et al., Eur Radiol, 2014. [10] Sebag F, et al., J Clin Endocrin & Metab, 95: 5281-8, 2010.

015   **MULTI-ELEMENT SYNTHETIC APERTURE VASCULAR ELASTOGRAPHY FOR CAROTID IMAGING.**

Rohit Nayak*, Prashant Verma and Marvin M. Doyley.
University of Rochester, Department of Electrical and Computer Engineering, Rochester, NY, USA.

Background: Plaque rupture may trigger myocardial and cerebral infarctions. Clinicians could use mechanical property images to detect rupture-prone plaques. Synthetic aperture vascular elastography (SAVE) visualizes the strain distribution within vascular tissues with high precision [1]. However, there are concerns that the low transmit power of SAVE will degrade clinical utility. In this study, we hypothesize that increasing the number of transmission elements will overcome this limitation. More specifically, we propose to use parabolic defocussing delays to produce a virtual source with a spherical beam pattern [2].

Methods: To corroborate this hypothesis, we performed simulation studies on two groups of vessels with attenuation coefficients of: (a) 0 dB/cm/MHz (to represent the ideal case, where power is not a limiting factor) and (b) 1.5 dB/cm/MHz (at diagnostic level of attenuation [3]). The simulated vessels had inner radius of 1.5 mm, outer radius of 6 mm, elastic modulus of 45 kPa, and a Poisson's ratio of 0.495. The inner vessel wall was subjected to an intra-luminal pressure of 5 mm of Hg. We simulated a linear array that had 128 elements, each of size 0.2 mm (width) x 4 mm (height); pitch of 0.03 mm, and center frequency of 5 MHz. We performed sparse array imaging by transmitting an acoustic signal from 16 groups of elements (subaperture), sequentially [1,2]. The transmit subapertures were uniformly distributed over the entire aperture of the transducer. We varied the size of the subaperture from 1 to 21 elements. For all cases, we placed the virtual source 1 mm behind the transducer. We used the delay-and-sum technique to beamform the RF echo frames. Displacement elastograms were computed by applying a 2D cross-correlation-based echo-tracking technique to the pre- and post-dilated RF echo frames [1]. The elastographic signal to noise ratio (SNRe) and the root mean square error (RMSE) were used to evaluate the quality of the strain elastograms. The RMSE metric was normalized over the full range of applied strain, as described in [1].

Results: Figure 1 shows SNRe and RMSE, plotted as a function of subaperture size. For both radial and circumferential strain elastograms, SNRe improved with increased subaperture size, up to 7 elements, and then degraded with further increase (see Fig. 1 a & b). In the RMSE plots, the smallest error occurred when we transmitted with 7 elements (see Fig. 1 c & d). For the non-attenuating vessel, the peak SNRe (radial strain) of SAVE (1 element) and multi-element SAVE (7 elements) were comparable. For 1.5 dB/cm/MHz attenuation, the peak SNRe (radial strain) of SAVE and multi-element SAVE (mSAVE) reduced to 7.33 dB and 11.41 dB, respectively. Similarly, for the non-attenuating vessels, the peak RMSE (radial strain) of SAVE and mSAVE were 13.40% and 13%, respectively. On increasing attenuation to 1.5 dB/cm/MHz, the peak RMSE (radial strain) for SAVE and mSAVE increased to 32.58% and 17.70%, respectively.
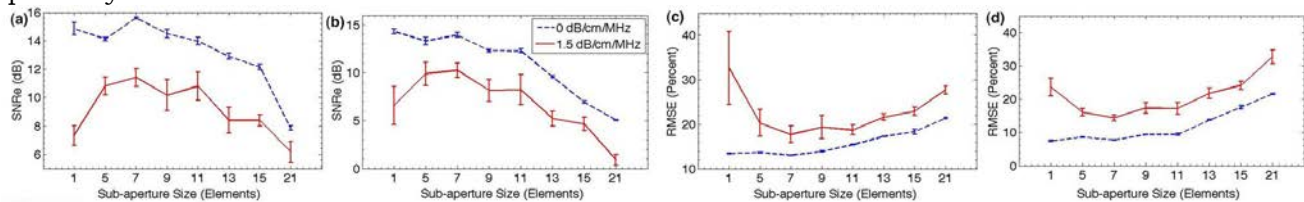
Figure 1: SNRe (a & b) and RMSE (c & d) plots obtained from radial (a & c) and circumferential strain (b & d) elastograms, as a function of aperture size. The error bars represent the standard deviation obtained from 5 independent simulations.

Conclusions: These results suggest that mSAVE can produce useful strain elastograms, at the diagnostic level of attenuation. These simulation results encourage further development of the proposed technique. Our future work will involve ex vivo study using excised carotid artery, and subsequent in vivo validation on human subjects.

References: [1] S. Korukonda, R. Nayak, N. Carson, G. Schifitto, V. Dogra and M.M. Doyley: IEEE UFFC, 60(2), pp. 332-342, 2013. [2] R. Nayak, S. Korukonda and M.M. Doyley: Proc. of SPIE Medical Imaging, Florida, 2013. [3] H. Shi, T. Varghese, R.J. Dempsey, M.S. Salamat, J.A. Zagzebski: UMB, 34(10), pp.1666-1677, 2008.

016 **QUANTIFYING DISPERSION OF SHEAR WAVES PRE AND POST-INDUCTION OF LABOR.**

Lindsey C. Carlson[1]*, Helen Feltovich[1,2], Mark L. Palmeri[3], Stephanie Romero[2], Timothy J. Hall[1]
[1]University of Wisconsin, 1005, Madison, WI, USA; [2]Intermountain Healthcare, Intermountain Medical Center, Murray, UT, USA. [3]Duke University, Pratt School of Engineering, Durham, NC, USA.

Background: During pregnancy, the cervix undergoes significant remodeling and softening [1]. Premature changes that may occur during this process could lead to preterm birth. Currently, there is no objective method to assess the softness of the cervix. Shear wave speed (SWS) estimation is a non-invasive quantitative method to quantify the mechanical properties of tissue [2]. Most soft tissues are considered viscoelastic and therefore at least somewhat dispersive. Using shear wave data, dispersion can be quantified based on phase velocities. Changes in the tissue microstructure likely result in changes in shear wave dispersion.

Aims: The aim of this study is to quantify dispersion in propagating shear waves in the pregnant cervix during induction of labor to determine if there is a significant difference in the slope of phase velocity vs. frequency pre- vs. post-softening.

Methods: Female patients (n = 20) scheduled for induction of labor at term with cervical ripening were recruited, and a subset (m = 10) of these did not have an onset of labor. Scanning was performed using a Siemens Acuson S2000 Ultrasound system. A prototype catheter transducer (128 elements, 14mm aperture, 3mm diameter) operated in linear array mode was used to scan the outside of the cervix. The probe was secured to clinician's hand, with the active aperture on her fingertip, and then placed into a sterile glove filled with gel for acoustic coupling. The clinician's finger was placed on top of the anterior cervix and aligned parallel to endocervical canal in the mid-position along the length of the canal. 10 replicate SWS measurements were made at this location before and four hours after a cervical ripening agent was administered to the patient. Displacements were estimated using the Loupas' algorithm [3] and phase velocities were calculated using the displacements near the focal plane.

Results: Patients that did not exhibit onset of labor (m = 10) were chosen for initial analysis. Those patients exhibiting the onset of labor demonstrated increased shear wave speeds due to uterine contractions and/or fetal movement toward the lower uterine segment, as previously reported [4]. The mean not-in-labor pre-ripening slope in phase velocities was 5.03 ± 3.15 $m \cdot s^{-1} \cdot kHz^{-1}$ versus 3.21 ± 0.78 $m \cdot s^{-1} \cdot kHz^{-1}$ for post-ripening. Using a paired Wilcoxon signed rank test a p-value of 0.10 was obtained indicating a marginal significance in pre vs. post-ripening dispersion (marginal significance defined as $0.05 < p < 0.15$).

Conclusions: Although pre- and post-ripening changes were not statistically significant, a trend toward decreased slope in phase velocities was shown in the post-ripened cervix. It is not unexpected that statistical significance was not reached because all patients were in the final stages of pregnancy in which the cervix has already undergone significant remodeling. Larger changes in dispersion will likely be seen in early vs. late stage pregnancy, and could prove a useful tool for monitoring cervical changes during pregnancy.

References:
[1] Word RA, Li XH, Hnat M, Carrick K. Dynamics of Cervical Remodeling during Pregnancy and Parturition: Mechanisms and Current Concepts. Semin Reprod Med; 25: pp. 69-79. [PMID: 17205425] 2007.
[2] Loupas T, Powers JT, Gill RW. An Axial Velocity Estimator for Ultrasound Blood Flow Imaging, Based on a Full Evaluation of the Doppler Equation by Means of a Two-Dimensional Autocorrelation Approach. IEEE Trans Ultrason Ferrorelectr Freq Control; 42**,** pp. 672-688, 1995.
[3] Pinton, GF, Dahl, JJ, Trahey, GE. Rapid Tracking of Small Displacements with Ultrasound. IEEE Trans Ultrason Ferrorelectr Freq Control; 53, pp. 1103-1117. [PMID: 16846143] 2006.
[4] Carlson LC, Romero ST, Palmeri ML, Munoz del Rio A, Esplin SM, Rotemberg VM, Hall TJ, Feltovich H. Changes in Shear Wave Speed Pre and Post Induction of Labor: A Feasibility Study. Ultrasound Obstet Gynecol 2014.

019 MULTI SLICE RADIAL STRAIN IMAGING OF AN ATHEROSCLEROTIC CAROTID ARTERY BY CROSS-SECTIONAL STRAIN ESTIMATIONS USING MULTI ANGLE SIMULATED PLANE WAVE ULTRASOUND TRANSMISSIONS.

Stein Fekkes[1]*, Abigail E.S. Swillens[2], Hendrik H.G. Hansen[1], Anne E.C.M. Saris[1], Maartje M. Nillesen[1], Francesco Iannacone[2], Patrick Segers[2], Chris L. de Korte[1].
[1]Department of Radiology and Nuclear Medicine, Radboud University Medical Center, Nijmegen, THE NETHERLANDS; [2]Department of Electronics and Information Systems, Ghent University, BELGIUM.

Background/Aim: Three-dimensional vascular strain estimation is crucial for assessment of the distribution of high strain regions in the carotid artery. This study introduces a semi-3D radial strain imaging method which is tested in a 3D model of an atherosclerotic carotid artery.

Methods: A 3D finite element model of a patient-specific, pulsating atherosclerotic carotid artery (pulse pressure 60 mmHg) was generated with Abaqus. Radiofrequency (RF) data were simulated in Field II by moving point scatterers (~vessel wall) according to the calculated deformation patterns (*ground truth*). RF element data were simulated for a linear array transducer (f_c = 9 MHz, pitch = 198 μm, 192 elements) that transmitted plane waves at 3 sequentially alternating angles (+20°, 0°, -20°) at a pulse repetition frequency of 12 kHz. Simulations with 25 ms inter-frame time were performed for 25 equally spaced (0.5 mm) transversal positions of the internal carotid artery containing fatty and calcified areas. After delay-and-sum beamforming, inter-frame axial displacements were estimated using a coarse-to-fine normalized cross-correlation method. The 0° axial displacement was used as vertical displacement component. Projection of the +20° and -20° axial displacements yielded the horizontal displacement component [1]. Tracking was performed to accumulate displacements for each transversal position. A polar grid and the lumen center were defined in the end-diastolic frame of each transversal position and used to convert the tracked axial and lateral displacements to radial displacements. Least squares strain estimation was performed to acquire accumulated radial strain. Strains derived from the model dynamics and estimated strains were compared by the Root Mean Squared Error (RMSE).

Results: Good agreement between the ground truth and the estimated radial strain was observed for all volumes over the entire pressure cycle. Figure 1 shows the cumulative strains at maximum pressure difference revealing a ~-7% strain region corresponding to a fatty region and a ~-2% strain region corresponding to a calcified region.
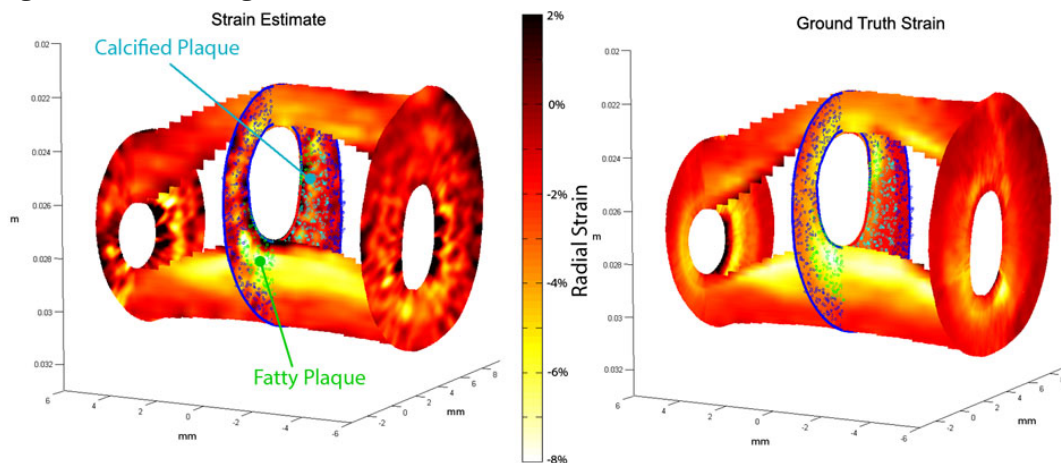
Figure 1: semi-3D strain imaging of a atherosclerotic carotid artery at the maximum systolic pressure indicating correspondence between high strain regions and fatty plaque location (green scatterers = fatty, cyan scatterers = calcified, blue scatterers = healthy tissue). For clarification only 3 of 25 transversal slices are shown.

Conclusions: The RMSE between the ground truth and estimated strain was 1.9% at the maximum systolic pressure. These results show the feasibility of 3D carotid strain imaging although this is only the first step towards full 3D strain estimation.

References:
[1] Hansen et al.: Journal of Biomechanics, 47(4), pp. 815-23, 2014

020 **PLANE WAVE DISPLACEMENT COMPOUNDING FOR ESTIMATION OF LARGE DISPLACEMENTS.**

Anne E.C.M. Saris[1]*, Hendrik H.G. Hansen[1], Stein Fekkes[1], Maartje M. Nillesen[1], Marcel C.M. Rutten[2], Chris L. de Korte[1].
Radboud University Medical Center, Nijmegen, THE NETHERLANDS; Eindhoven University of Technology, Eindhoven, THE NETHERLANDS.

Background: RF based quantification of large displacements and high strain values in tissue requires fast and dedicated transmission schemes. Plane wave imaging enables the assessment of the entire displacement field for a full field of view at kHz frame rates. However, performing 2D displacement estimation can be difficult, due to the low contrast and off-axis spatial resolution in plane wave images. 2D displacement compounding, a technique originally developed for vascular strain imaging [1], uses only axial displacement estimates at two angled plane waves to derive the entire 2D displacement vector.

Aim: This study compares the performance of 0° and compound 2D vector velocity estimation, using plane wave transmissions at two different frame rates.

Methods: To obtain high displacements and large displacement gradients, fluid-structure interaction modeling was used to generate realistic 3D flow velocity fields inside a curved carotid artery [2]. This 3D velocity field was used as input to Field II, to simulate ultrasound radiofrequency element data for a linear array transducer (f_c = 9 MHz, pitch = 198 µm, 192 elements). Plane waves were emitted at pulse repetition frequencies (PRF) of 2 and 12 kHz, at sequentially changing angles of 0°, -20° and 20°, resulting in effective frame rates (FR) of about 666 Hz and 4 kHz. Delay-and-sum beamforming was performed to generate RF data in the direction of the steered plane waves. A 2D normalized cross-correlation-based method was used to estimate the displacements at a diastolic (low velocity) and systolic (high velocity) phase of the cardiac cycle, rendering the velocity by multiplication with the FR. The velocity components were determined in 2 ways: 1) directly fromthe0° acquisitions (PW0), or 2) by compounding the axial velocity components obtained from the -20° and +20° acquisitions (PW$_C$). The performance of the methods at both frame rates was compared by calculating the root mean squared error (RMSE) between estimated and true horizontal (v_x) and vertical (v_y) velocity components.

Results: Figure 1 shows the velocity estimates and ground truth. The compounding technique only outperforms the PW0 method in estimating the horizontal velocity (v_x) component at diastole, using a PRF of 12 kHz (RMSE PW0: 52.6 mm/s versus RMSE PW$_C$: 25.8 mm/s). In all other cases the PW0 method provides more accurate velocity estimates, i.e., lower RMSEs as compared to PW$_C$.
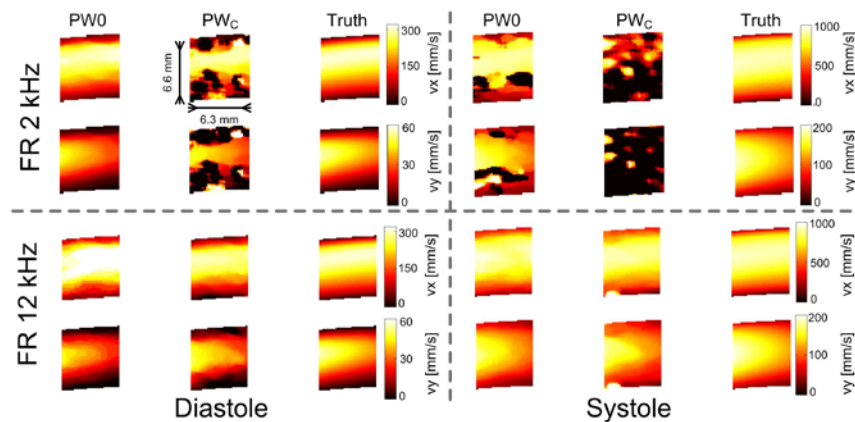
Conclusions: 2D displacement compounding for displacement estimation is only beneficial if sub-line inter-frame displacements occur. This is in accordance with vascular strain imaging applications, where horizontal displacements are mainly within the sub-line range. When larger inter-frame displacements need to be captured, the PW0 method seems to provide more robust velocity estimates.

References:
[1] Hansen et al.: Journal of Biomechanics, 47(4), pp. 815-23, 2014
[2] Beulen et al.: Journal of Fluids and Structures, 25, pp. 954-966, 2009

023 **QUANTITATIVE SONOELASTOGRAPHY OF THE UTERINE CERVIX BY INTERPOSITION OF A SYNTHETIC REFERENCE MATERIAL AND INTRA-INTEROBSERVER EVALUATION.**

Anne Katrine Leonhard[1,2]*, Lene Hee[1], Puk Sandager[1,2], Olav Petersen[1], Christina Kjærgaard Rasmussen[1], Jacob Mørup Schlütter[1], Niels Ulbjerg[1,2]
[1]Institute of Clinical Medicine, Aarhus University, Aarhus, DENMARK; [2]Aarhus University Hospital, Aarhus, DENMARK.

Background: Elastography has been introduced to evaluate the stiffness (compressibility) of the uterine cervix ([1]). However, elastography of the cervical tissue is restricted by the absence of natural reference material in that anatomical area. Thus, it has until now not been possible to make an inter-individual comparison of the uterine cervix.

Aims: To test elastography on phantoms regarding distance dependence and the influence of a heterogeneous material. To develop a reference material that allows for quantitative elastography of the cervix by calculating tissue stiffness expressed as the approximate Young's modulus in N/mm^2 (E). To make inter-intra observer evaluations.

Methods: The scanning was conducted using a 2D transvaginal ultrasound transducer (IC5-9-D) connected to a Voluson E8 Expert scanner with the BT13 software. The strain ratio between the selected ROIs (Region of Interest) was calculated by the H48681GB software (all GE, Healthcare Austria, Zipf, Austria). Three cylinder-shaped phantoms were used (produced by Danish Phantom Design, DPD). Two were made of homogeneous material but with different E (0.22 N/mm^2 and 0,07 N/mm^2), and the third (E 0.22 N/mm^2) had a 5-mm soft layer (E 0.07 N/mm^2) introduced 5 mm below the surface, to imitate the uterine cervix with its less stiff cervical canal. Four ROIs were placed 0–5 mm (reference ROI), 5–10, 10–15 and 15–20 mm from the transducer, respectively. The reference ROI was given the E of the phantom, whereas the approximated E of the other ROIs was calculated by multiplying the strain ratio by the E of the phantom. We developed three 5-mm-thick reference caps made of silicone and oil. The caps had an E of 0.40 N/mm^2, 0.32 N/mm^2 and 0.22 N/mm^2. To evaluate the reference caps, we performed elastography on 6 mid- and 5 full-term pregnant women. In the elastography analysis, the ROI's were placed corresponding to the reference cap and the anterior cervical lip. To assess the intra- and inter-observer reliability two observers scanned 29 women, all undergoing induction of labor ([2]). Each observer performed three scans, and the transducer was pulled back between each scan, so the cervix had to be relocated before the next scan.

Results: The recordings of the phantoms revealed that the calculation of the approximate E became unreliable at distances above 10–15 mm from the transducer. This was further increased for ROI on the other side of the soft layer in the third phantom; please see the table below. The approximate E obtained from the anterior cervical lip using the reference caps were 0.08 N/mm^2 in mid-term and 0.03 N/mm^2 in full-term pregnant women. The average approximate E measured with the soft reference cap was significantly different between the two groups; p=0,01. The results obtained with the medium hard and hard reference caps showed the same tendency. The intra-and inter-observer ICC was 88% and 58%, respectively.

Approximate Young's modulus, N/mm2						
	Phantom A (0,22 N/mm2)		Phantom B (0,07 N/mm2)		Phantom C (0,22 and 0,07 N/mm2)	
Distance from the probe	Mean	Range	Mean	Range	Mean	Range
0,5 mm	0,22		0,07		0,22	
5-10 mm	0,22	0,22-0,23	0,07	0,07-0,07	0,19	0.18-0,20
10-15 mm	0,27	0,26-0,29	0,07	0,07-0,10	0,29	0,28-0,31
15-20 mm	0,33	0,32-0,36	0,09	0,07-0,15	0,39	0,37-0,40
p-value, Friedman test	0,03		0,01		0,01	

Conclusions: The reference cap constitutes a promising tool for quantitative elastography of the anterior cervical lip. Figures obtained from the posterior cervical lip are less plausible due to the distance from the transducer and the heterogeneity introduced by the cervical canal. Since these studies ended, a new cap material has been found, which has properties superior to the old material. This will be presented at the conference. The method has the potential to be used to supplement cervical length assessment when evaluating women at risk of preterm delivery and when planning induction of labor.

References: [1] Fruscalzo A, Schmitz R, Klockenbusch W, Steinhard J. Reliability of Cervix Elastography in the Late First and Second Trimester of Pregnancy. Ultraschall Med; 33(7), E101-E107, 2012. [2] Hee L, Kjærgaard CK, Schlütter JM, Sandager P, Uldbjerg N. Quantitative Sonoelastography of the Uterine Cervix Prior to Induction of Labor as a Predictor of Cervical Dilation Time, 2014.

029 **A NEW APPROACH TO MEASURE THE MECHANICAL HETEROGENEITY OF BREAST MASSES.**

T. Liu[1]*, O.A. Babaniyi[2], T.J. Hall[3], P.E. Barbone[2], A.A. Oberai[1],
[1]Rensselaer Polytechnic Institute, Troy, NY, USA; [2]Boston University, Boston, MA, USA; [3]University of Wisconsin, WI, USA.

Background: In gross pathology, cancerous tumors appear to be heterogeneous and have rough margins. This is because of the desmoplastic reaction which is usually only associated with malignant tumors. Desmoplasia is characterized by the pervasive growth of dense collagen fibers. More collagen fibers imply higher elastic modulus. Therefore it is reasonable to expect that malignant tumors would appear as heterogeneous masses in elastic modulus images. We verify this hypothesis in this study and determine whether it can be used to diagnose cancerous lesions.

Aims: The aim of this work is to (a) develop and implement methods for creating high-resolution images of Young's modulus of breast tissue. (b) Develop a new measure that quantifies the spatial mechanical heterogeneity within a tumor. (c) To quantify the accuracy of this measure in diagnosing malignant lesions.

Methods: Using free-hand ultrasound elastography ultrasound data was acquired on a set of ten patients with five fibroadenomas (FA) and five invasive ductal carcinomas (IDC). During this process the breast was compressed to about 12% strain. The ultrasound rf. data was used to determine displacement field within the breast at a resolution of about 150 microns. This displacement data was used in an inverse algorithm to determine the spatial distribution of the shear modulus at the same resolution. Using 50% of the peak modulus value within the tumor as a guideline, the margins of the tumor were identified in the shear modulus images. Thereafter a heterogeneity parameter (denoted by H) which is roughly equal to the ratio of the tumor size to the correlation length of the modulus distribution within the tumor, was evaluated for each tumor.

Results: Visual inspection of the modulus images indicated that the malignant tumors were mechanically more heterogeneous when compared with benign tumors (see Figures 1 and 2). This was quantitatively verified by evaluating the heterogeneity parameter, H. It was found that the value of this parameter was higher for cancerous tumors. By using $H > 0.6$ as a criterion for malignancy we achieved an accuracy of 90%(100% sensitivity and 80% specificity).

Conclusions: Through high-resolution quasi-static elasticity imaging it was verified the malignant lesions are mechanically more heterogeneous than benign lesions, and that a quantitative measure of heterogeneity has the potential to accurately diagnose these lesions.
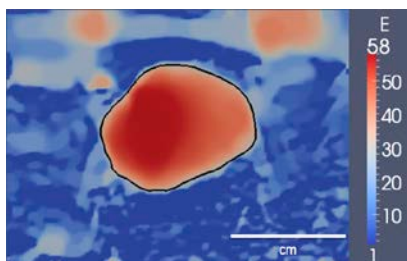
Figure 1 Distribution of Young's modulus for a typical fibroadenoma(FA)
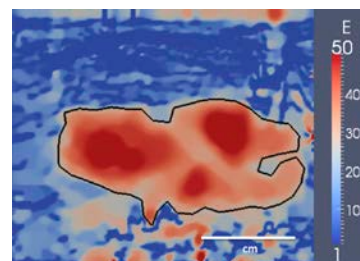
Figure 2 Distribution of Young's modulus for a typical invasive ductal carcinoma(IDC)

037 ***IN VIVO* CHARACTERIZATION OF ATHEROSCLEROTIC PLAQUE IN HUMAN CAROTID ARTERIES WITH HISTOPATHOLOGICAL CORRELATION USING ACOUSTIC RADIATION FORCE IMPULSE (ARFI) ULTRASOUND.**

Tomasz J. Czernuszewicz[1]*, Jonathon W. Homeister[1], Melissa C. Caughey[1], Mark A. Farber[1], Joseph J. Fulton[1], Peter F. Ford[1], William A. Marston[1], Raghuveer Vallabhaneni[1], Timothy C. Nichols[1], Caterina M. Gallippi[1].
[1]The University of North Carolina at Chapel Hill, Chapel Hill, NC, USA.

Background: Stroke is one of the leading causes of death and long-term disability in the US. The vast majority of strokes are related to ischemia secondary to atheroembolism originating from unstable plaques located in neck vasculature. Specifically, plaques that are composed of mechanically-soft lipid/necrotic regions covered by thin fibrous caps are the most vulnerable to rupture. Atherosclerotic plaque characterization with ARFI [1] has recently been developed using phantoms and atherosclerotic pigs [2]–[4], but has yet to be validated in vivo in humans. We present initial results from an ongoing clinical trial investigating in vivo ARFI imaging of human carotid plaque with spatially-matched histopathology.

Aims: Our goal was to characterize human carotid plaque in vivo with transcutaneous ARFI imaging and correlate results with pathologic findings.

Methods: Patients undergoing clinically-indicated carotid endarterectomy (CEA) were recruited from UNC Hospitals and imaged with ARFI implemented on a Siemens Acuson Antares with modifiable beam sequencing and a VF7-3 linear array. ARFI excitation pulses were 300 cycles at 4.21 MHz (F/1.5), while tracking pulses were 2 cycles at 6.15 MHz. Imaging was performed pre-operatively by focusing on the carotid bifurcation. After surgery, the extracted specimen was sectioned according to noted arterial geometry for spatial registration to the ultrasound imaging plane. The sections were stained with H&E, combined Masson's elastin, and Von Kossa for calcium, and compared to parametric 2D ARFI images of peak displacement (PD). Data is presented from five patients.

Results: In two asymptomatic patients with predominantly calcified plaques, ARFI PDs were small (2.1 ± 1.5 μm and 1.8 ± 0.8 μm respectively) suggesting large amounts of stiff tissue. In two symptomatic patients, plaques were composed of a mixture of necrotic core, mild intra-plaque hemorrhage, small focal calcifications, and fibrosis. ARFI PDs in regions corresponding to either necrotic core or intra-plaque hemorrhage were observed to be increased by 2 or 3-fold compared to surrounding fibrotic tissue. Fibrous cap thickness in these patients was estimated with <10% error in caps larger than 0.8 mm. In a fifth patient, also symptomatic, an ulcerated plaque with extensive organized thrombus was observed. ARFI displacements in regions corresponding to thrombus were small (~1-2 μm), similar to that in the fibrotic/calcified plaques.

Conclusions: The results of this study indicate that areas of relatively large displacement by ARFI imaging correlate with lipid/necrotic cores and/or inflammation, which may confer an increased chance of plaque rupture and future ischemic event. Interestingly, in the ulcerated plaque with organized thrombus, ARFI-induced displacements were relatively small, suggesting stiffer and more stable plaque. Discrimination of organized thrombus from other stiff atherosclerotic features may be improved by more advanced imaging techniques that evaluate both viscous and elastic properties of plaque.

References:
[1] K. Nightingale, M. S. Soo, R. Nightingale, and G. Trahey: Acoustic Radiation Force Impulse Imaging: *In Vivo* Demonstration of Clinical Feasibility, Ultrasound Med. Biol, vol. 28,(2), pp. 227–35, 2002.
[2] D. Dumont, R. H. Behler, T. C. Nichols, E. P. Merricks, and C. M. Gallippi: ARFI Imaging for Noninvasive Material Characterization of Atherosclerosis: Ultrasound Med. Biol, vol. 32, (11) pp. 1703–11, 2006.
[3] R. H. Behler, T. C. Nichols, H. Zhu, E. P. Merricks, and C. M. Gallippi: ARFI Imaging for Noninvasive Material Characterization of Atherosclerosis Part II: Toward *In Vivo* Characterization; Ultrasound Med. Biol., vol. 35,(2), pp. 278–295, 2009.
[4] R. Behler, T. Czernuszewicz, C. Wu, T. Nichols, H. Zhu, J. Homeister, E. Merricks, and C. Gallippi: Acoustic Radiation Force Beam Sequence Performance for Detection and Material Characterization of Atherosclerotic Plaques: Preclinical, *Ex Vivo* Results; IEEE Trans. Ultrason. Ferroelectr. Freq. Control, vol. 60, (12), pp. 2471–87, 2013.

043   *IN VIVO* ULTRASOUND ELASTICITY IMAGING OF THE HUMAN POSTERIOR TIBIAL TENDON.

Liang Gao[1]*, Justin S. Yuan[1], Samantha McGlone[1], L. Daniel Latt[1], Russell S. Witte[1].
[1]University of Arizona, Tucson, AZ, USA.

Background: Tendinopathies are common causes of pain and disability. Posterior tibial tendon dysfunction (PTTD), for example, is often related to degenerative disease from chronic overload of the muscle-tendon unit. Although severe cases often require surgery, many others resume normal gait following rest and rehabilitation. However, patient history and physical exam by themselves do not reliably predict the outcome of therapy. This leads to prolonged unsuccessful conservative treatment in some patients and premature surgical intervention in others. This study evaluates Ultrasound Elasticity Imaging (UEI) as a noninvasive tool for measuring the mechanical properties of the PTT to eventually help guide treatment decision-making.

Aims: 1) Develop noninvasive methods to evaluate the mechanical properties of the human PTT using UEI. 2) Obtain preliminary results using an in vivo UEI platform to determine whether there are detectable and quantifiable differences between healthy tendons and those with advanced-stage tendinopathies related to PTTD. A custom 2D phase-sensitive cross correlation speckle tracking [1] is performed with the ultrasound images to determine the mechanical properties of the human PTT under a custom designed ankle inversion task.

Methods: Five volunteers were recruited (Two healthy volunteers and three PTTD patients) to participate in an ankle inversion task during which a sequence of ultrasound images were acquired. Each volunteer was asked to place the ankle of one foot in maximal plantarflexion, and the side of the forefoot was placed against a dynamometer [Fig.1]. The volunteer was asked to exert a maximal ankle inversion force on the dynamometer and then relax during a six-second window. Ultrasound RF data (phase and amplitude) of the PTT in motion were collected at 50Hz using a clinical ultrasound scanner with a 14MHz probe (Zonare Medical System, L14-5). Frame-to-frame displacements were computed using a custom 2D phase-sensitive cross correlation algorithm. The strain of the PTT was calculated from the gradient of the displacement images. Transverse B mode images were also obtained to determine the average cross-sectional area of the PTT required for calculating the elastic modulus. The force on the PTT was estimated from the inversion force and a scaling factor (8.3) from previous human cadaver experiments [2]. Finally, the elastic modulus was calculated for each subject and each limb.

Results: The maximum strain of all PTTs ranges from 5% to 30%, due to the large range of the maximum inversion force applied by different subjects (from 30N to 195N). The elastic modulus shows a linear dependence on the inversion force. The slope of elastic modulus vs inversion force is 0.15±0.11MPa/N for healthy PTT, and 0.27±0.12 MPa/N for patients [Fig. 2].

Conclusions: The elastic modulus of diseased PTTs is more sensitive to the increase of inversion force than healthy PTTs. UEI has great potential as a portable real-time, noninvasive modality to gauge the severity of tendon degeneration and help guide treatment decision-making for tendinopathies like PTTD.

References:
[1] Lubinski MA, Emelianov SY, and O'Donnell M. Speckle Tracking Methods for Ultrasonic Elasticity Imaging using Short-Time Correlation; IEEE Trans. Ultrason., Ferroelect., Freq. Contr., vol. 46, no. 1, pp. 82–96, 1999.
[2]. Gao L, Yuan JS, Heden GJ, Szivek JA, Taljanovic MS, Latt LD, Witte RS. 2014. Ultrasound Elasticity Imaging for Determining the Mechanical Properties of the Human Posterior Tibial Tendon: A Cadaveric Study. Submitting to Journal of Orthopaedic Research.

Figure 1. *In vivo* UEI setup.
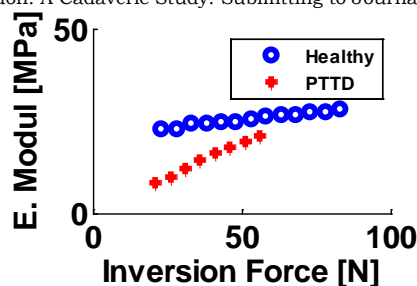
Figure 2. Elastic modulus vs inversion force of a healthy PTT and a diseased PTT.

022   **DISPLACEMENT   UNDERESTIMATION   CORRECTION   BY   SHEARWAVE-INDUCED DISPLACEMENT TRACKING IN VISCOELASTIC RESPONSE (VISR) ULTRASOUND.**

Mallory R. Selzo[1]*, Tomasz J. Czernuszewicz[1], Caterina M. Gallippi[1].
[1]The University of North Carolina at Chapel Hill, Chapel Hill, NC, USA.

Background: We have proposed an imaging technique called Viscoelastic Response (VisR) ultrasound that uses two acoustic radiation force (ARF) impulses for assessing the viscoelastic properties of tissue [1]. Using two successive ARF impulses and monitoring the induced displacements, VisR fits displacements to a mechanical model to measure the relaxation time constant, τ, given by the ratio of viscosity to elasticity. In this method, radiation force pulses are generated by the same transducer that is used to track motion. Thus, the displacements are susceptible to shearing decorrelation and underestimation, which will introduce error into our measurement of τ [2].

Aims: This study aims to test the hypothesize that by tracking displacements outside the region of excitation (ROE), where shearing decorrelation is minimized, we can better estimate displacements and generate τ measurements that more closely represent the material.

Methods: ViSR imaging was performed with a Siemens Antares scanner and VF7-3 linear array with excitation impulses centered at 4.21 MHz with an F/1.5 focal configuration. VisR was implemented using two 300-cycle ARF excitations, separated by 0.6 ms in time. Tracking pulses were centered at 6.15 MHz with an F/1.5 focal configuration. Acoustic displacement measurements were experimentally validated using optical tracking as described in [3]. Raw rf and optical data were acquired with three repeated measures on each bead. Motion tracking was performed using normalized cross-correlation for both acoustic and optical data sets. The experiment was repeated with the ARF excitations and tracking pulses focused in the same lateral position, and with tracking pulses focused 4.25 mm lateral to the ARF excitations.

Results: In the ROE, displacements measured acoustically were 83.9 ± 20.8% of the optical displacement on average, whereas, acoustic displacements measured 4.25 mm lateral to the ROE were measured to be 102.0 ± 24.3% of the optical displacement on average. In the ROE, τ was significantly larger when using acoustic displacement estimates (1.40 ± 0.03 ms) versus optical displacement estimates (0.75 ± 0.07 ms) (p<0.01). 4.25 mm outside the ROE, however, acoustically- and optically-derived values of τ (0.76 ± 0.05 ms and 0.75 ± 0.09 ms, respectively) were not significantly different (p=0.83) and were consistent with the optically-derived value of τ made in the ROE (p=0.94). Optical and acoustic displacements inside and outside the ROE and their associated VisR fits are shown in figure 1.
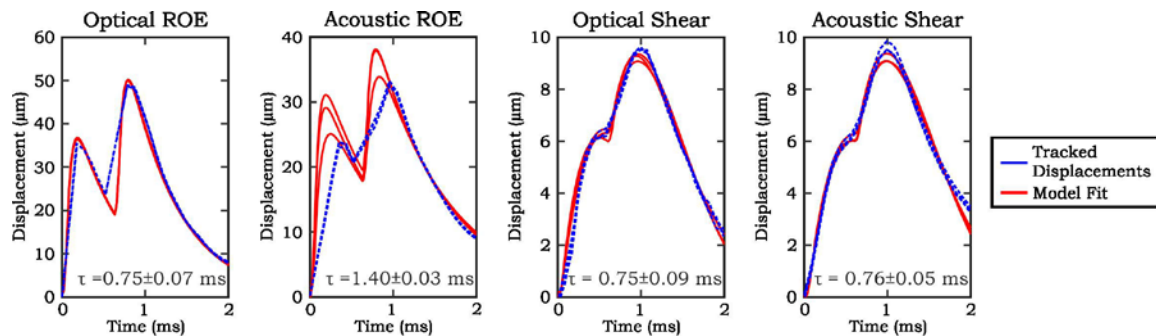
Figure 1. Displacement through time measured acoustically and optically in the ROE
and 4.25 mm outside of the ROE and their associated VisR fits.

Conclusions: These results show that acoustic displacement underestimation impacts VisR derived τ measurement, but that this error can be reduced by using shearwave-induced displacement tracked outside the ROE.

References:
[1] MR Selzo, CM Gallippi. IEEE Trans. Ultrason., Ferroelectr., Freq. Control, 60(12), pp. 2488–500, 2013.
[2] SA McAleavey, KR Nightingale, GE Trahey. IEEE Trans. Ultrason., Ferroelectr., Freq. Control, 50(6),pp. 631–41, 2013
[3] TJ Czernuszewicz, JE Streeter, PA Dayton, CM Gallippi. Ultrasonic Imaging, 35(3), pp. 196–213, 2013.

ENHANCEMENT OF ULTRASOUND RADIATION FORCE EFFICIENCY WITH OPTIMIZATION OF THE ELEVATIONAL FOCUS.

Bastien Arnal[1], Thu-Mai Nguyen*[1], Matthew O'Donnell[1].
[1]University of Washington, Department of Bioengineering, Seattle, WA 98105, USA.

Background: Ultrasound radiation force is commonly used in elastography to remotely displace tissues. Most techniques employ focused single-element transducers or linear arrays, which have primarily been designed for therapy or imaging purposes respectively and are not optimal for radiation force.

Aims: Here, we propose to investigate the role of the elevational focus in radiation force efficiency. We designed toric lenses to extend the focus of a spherically-focused single-element along the elevation direction.

Methods: For this study, a 7.5-MHz, spherically-focused transducer (Sonic Concept, Bothell, WA, USA) was used. The toric lens was fabricated in PDMS to obtain variable sizes of the focal spot in the elevation direction (see Fig. 1a). The corresponding pressure field was first simulated using Field II software. The expected displacements were modeled using an elastic Green's function approach. Then, several lenses were manufactured, mounted on the transducer and the experimental pressure fields were measured with a hydrophone (ONDA HNC 1000, Sunnyvale, CA, USA). 200-μs pulses were focused in tissue-mimicking phantoms. The resulting displacements were tracked at 10 kHz frame rate with a linear array (AT8L12-5 50 mm, 9 MHz, Broadsound, Taiwan) driven by a Verasonics system (Redmonds, WA, USA). We compared the displacement magnitude close to the source with and without lens.

Results: We tested lenses corresponding to focus aspect ratios from 2.8 to 7.7 (elevation width/lateral width). The loss of pressure at the focus was < 9 dB for all lenses and is mainly due to diffraction. At a pressure of 2 MPa, the maximum displacements magnitude observed in a 5%-gelatin phantom were 1.7 to 8.7 times higher with the different lenses than without lens (see Fig. 1b and c). We obtained comparable values from the Green's function simulations.

Conclusions: We underlined the importance of the elevation focus and demonstrated a tunable approach to optimize transducers for radiation force generation. We envision that such an approach will be ideally implemented on 2D-arrays, in which the focal aspect ratio can be instantaneously tuned with electronic delays. More detailed studies will be conducted to determine the optimal focus aspect ratio depending on the target application.
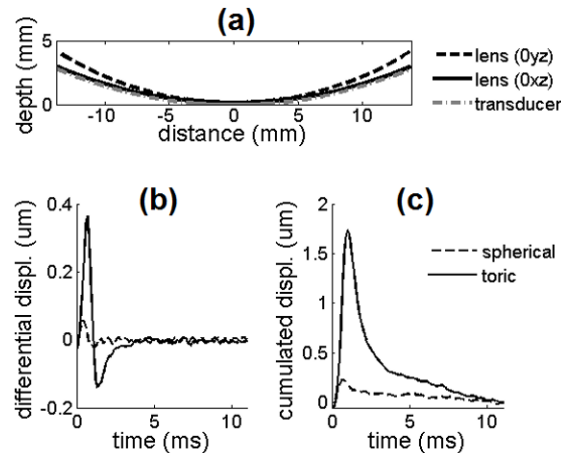
Fig. 1 – (a): Geometry of the toric lens for an aspect ratio of 5.8. The gray dash-dot curve represents the surface of the spherical transducer. The black curves represent the lens surface in the lateral (solid line) and elevational plane (dash line) respectively. (b) and (c): Axial displacement amplitude (b: frame-to-frame, c: cumulated) obtained in a 5%-gelatin phantom at ~2 mm from the source with lens (aspect ratio 5.8, solid line) and without lens (aspect ratio 1, dash line).

033   **CHARACTERIZING ABDOMINAL AORTIC ANEURYSM GROWTH IN A LONGITUDINAL STUDY USING ULTRASOUND ELASTOGRAPHY.**

Tim M. Vonk[1], V. Lai Nguyen[2], Geert-Willem H. Schurink[2], Frans N. v.d. Vosse[1], Richard G.P. Lopata[1]*
[1]Eindhoven University of Technology, Department of Biomedical Engineering, Eindhoven, THE NETHERLANDS; [2]Maastricht University Medical Center, Department of Vascular Surgery, Maastricht, THE NETHERLANDS.

Background: Abdominal Aortic Aneurysm (AAA) is a mostly asymptomatic disease and a major cause of death in the Western world. A ruptured AAA results in a fatal haemorrhage in 80-90% of all cases. The current criterion for intervention, the maximum diameter or large growth, do not account for premature rupture. Image-based mechanical characterization of AAAs has been investigated by means of computed tomography or magnetic resonance (MR) imaging based wall stress analysis, and MR or ultrasound (US) elastography.

Aims: In this study, 2D Ultrasound RF-data were obtained from a patient group suffering from AAAs with varying growth rates. The patients were followed over time to obtain several US measurements per patient. The arterial stiffness was estimated using 2D US elastography for every measurement. In this pilot, it was investigated whether this technique has the potential to detect changes in AAA elasticity.

Methods: Data were selected of three patients with no growth (< 2 mm), two patients with 5 to 6 mm growth, and two patients with significant growth of 5-10 mm during the four year study. 2D RF-data were obtained at 3 to 5 instances for each patient, over a period of four years using a Mylab70 with RF interface (Esaote, NL). The age and maximum diameter of this group was 59 - 81 years and 31 - 58 mmrespectively. The brachial pressure was measured using an arm cuff during the US examination.

An RF-based 2D displacement estimation and tracking algorithm was employed to estimate the wall motion after manually segmenting the aneursymal wall in the reconstructed B-mode images. Three consecutive cardiac cycles were selected. The diameters as a function of time were obtained and converted into distensibility (D) and incremental Young's modulus (E_{inc}), using the brachial pulse pressure. The AAAs were assumed to be axi-symmetric in the transverse direction. The results from three different cardiac cycles were averaged

Results: Distensibility ranged from 2 to 10 kPa-1 with incremental Young's moduli ranging from 1-8 MPa. The relative change in E_{inc} was -10% to 100% for the patients with no growth, 25% - 125% for the medium growth group and 75% to 700% for the patients with fast growth. Distensibility also decreased by a factor 5 for the patients with fast growth. The largest increase in stiffness corresponded to the largest increase in diameter.
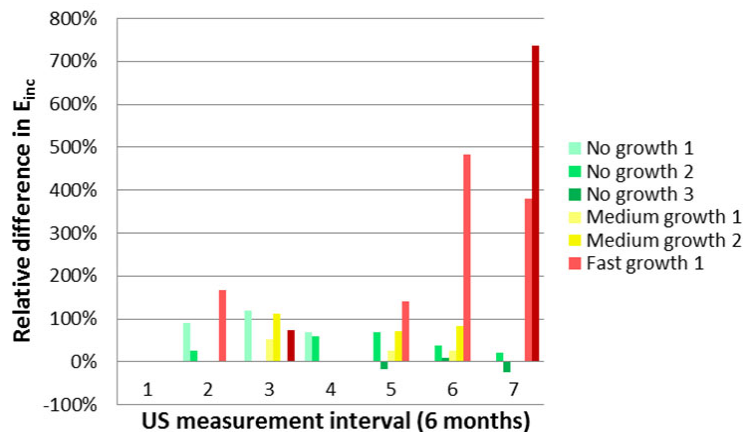
Figure 1: Relative difference in E_{inc} between consecutive US measurements. The different groups are color coded with green for no growth, yellow for medium growth, and red for fast growth.

Conclusions: The preliminary findings from this study imply that large changes in mechanical properties of the AAA wall may occur in periods of growth. If the aortic pressure curve was available, more complex material models could be used. In future work, different mechanical parameters need to be investigated, including strain. Automated segmentation and higher frame rates might decrease the intra-subject variability. Finally, the inclusion of more patients is required to strengthen the evidence found.

026 **HIFU LESION DETECTION USING PASSIVE ELASTOGRAPHY : A PRELIMINARY STUDY ON PORCINE PANCREAS.**
A Zorgani[1], J Vincenot[1], A Kocot[1], P Leduc[2] , Y Chen[2], R Souchon[1]*, D Melodelima[1], S Catheline[1.]
[1]INSERM, LabTAU 1032, Lyon, France; [2]ICE, Lyon, FRANCE.

Background: The detection of HIFU lesions in porcine pancreas with ultrasound B-Mode imaging is not satisfactory. In other applications, shear wave elasticity imaging techniques have proven their ability to retrieve the tissue elasticity locally by tracking the shear wave generated by an external source. In recent works, physiological shear waves naturally produced by the activity of the muscles, heart beating and blood network pulsatility have been shown to be efficient for elasticity tomography [1]. Furthermore, these physiological shear wave elastography techniques are fully compatible with standard ultrasound scanners working at a typical imaging frame rate of 25Hz.

Aims: The aim of this study was to demonstrate the feasibility of passive elastography in vivo in pigs to detect HIFU lesions created in the pancreas.

Methods: Passive elastography uses a diffuse shear wave field and cross-correlation interpreted in the frame of time reversal [1]. The animal experiments were carried out on six healthy pigs. HIFU ablations were created in 160 seconds using a toroidal transducer developed for intra-operative treatments. The heart beating and mesenteric vessels pulsatility creates a diffuse shear wave field measured inside the sample at a 25Hz frame rate using a 192 channel, 12 MHz ultrasonic array and a standard ultrasound scanner (Hawk system, Brujel and Kjaer Medical). In a second step, one displacement line at (x_o,z_o) is selected and correlated to the others. This can be interpreted as a virtual time reversal experiment. Thus, shear waves will virtually focalize at (x_o,z_o). By measuring the vibration amplitude, which is directly linked to the tissue elasticity and is unaffected by the temporal under sampling of the displacement field, a relative elasticity image is constructed before and after HIFU treatment.

Results: For experimental reasons that will be explained in the presentation, passive elastography experiments were successfully carried on only two pigs. The elasticity images of the pancreas are represented before HIFU in Fig. 1(b), and after HIFU Fig. 1(d). The elasticity contrast allows us to clearly observe the effect of the HIFU treatment and evaluate the lesion size compared with the B-mode image (Fig 1.a and 1.b)
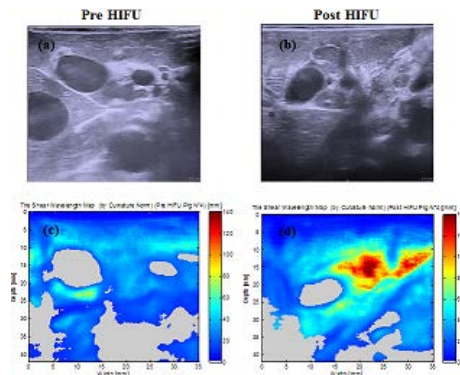
Fig 1. (a) Pre HIFU and (b) Post HIFU sonograms. (c) Pre HIFU and (b) Post HIFU shear wavelength maps. The gray regions in the wavelength maps are the zones with a low signal to noise ratio.

Conclusions: These two pre-clinical tests do not present statistically significant results. They are however very encouraging as far as the use of passive elastography for the following up of HIFU lesions is concerned.

References:
[1] S.Catheline, R. Souchon, M. Ruppin, J.Brum, A. H. Dinh, J-Y Chapelon. Tomographyfrom Diffuse Waves: Passive Shear Wave Imaging using Low Frame Rate Scanners, Appl. Phys. Lett. 103, 014101, 2013.

COMB-PUSH ULTRASOUND SHEAR ELASTOGRAPHY ASSESSMENT OF SUSPICIOUS BREAST LESIONS: UPDATES ON PRELIMINARY *IN VIVO* STUDY.

M. Denis[1]*, M. Mehrmohammadi[1], P. Song[1], D.D. Meixner[1], R.T. Fazzio[1], S. Chen[1], M. Fatemi[1], A. Alizad[1].
[1]Mayo Clinic, Rochester, MN, USA.

Background: Shear wave elastography provides a noninvasive evaluation of the stiffness of a breast lesion [1]. Since malignant breast masses are usually stiffer than benign lesions or normal soft tissue, shear wave elastography can noninvasively assess a tissue's pathology based on its mechanical properties. Differentiating benign and malignant breast lesions can limit the number of biopsies, thus reducing the number of benign breast biopsies diagnose.

Aims: Our goal is to evaluate the performance of the comb–push ultrasound shear elastography (CUSE) on pre-biopsy breast patients. CUSE is a new shear wave elastography technique for fast and robust 2D elasticity imaging [2]. In the CUSE technique a sequence of laterally spaced acoustic radiation force beams are emitted within the lesion field of view, ensuing multiple shear wave generation. Utilizing direction filtering for the left and right propagating waves a shear wave velocity map is reconstructed. Quantitative assessments of the breast lesion stiffness are obtained from the shear wave speed map. The aim for this study is to determine the diagnostic accuracy of CUSE in breast lesion detection and differentiation.

Methods: The CUSE was examined on pre-biopsy breast patients with suspicious lesions. Each patient underwent a conventional ultrasound and CUSE, using a fully programmable ultrasound platform (Verasonics V-1, Verasonics Inc., Redmond, WA) equipped with a linear array probe. A graphical user interface was developed to process the acquired CUSE data and to reconstruct the shear wave speed map. Assuming a linear, isotropic, incompressible and elastic soft-tissue the Young's modulus was obtained from the breast lesion's mean shear wave velocity. CUSE results were compared with pathology diagnosis. All patient study procedures were approved by Mayo Clinic Institutional Review Board (IRB).

Results: In total 44 pre-biopsy breast patients were examined with CUSE. Our cohort consisted of 27 malignant and 17 benign breast lesions. Our results indicate an increase in shear wave velocity in both benign and malignant lesions compared to normal breast tissue. Furthermore, the Young's modulus is significantly higher in malignant lesions (Figure 1). According to the receiver operating characteristic curve, the optimal cut-off value of 86.8 kPa yields 84% sensitivity, 89.6% specificity, 77.8% positive predictive value (PPV) and 92.9% negative predictive value (NPV). This is concordant with cut-off values ≥ 80kPa for suspicious breast lesions [1].

Conclusions: In conclusion, the CUSE imaging technique showed a significant difference with respect to the mean shear wave velocity between benign and malignant lesions.

References:
[1] Berg WA, Cosgrove DO, Doré CJ, Schäfer FK, Svensson WE, et al.: Shear-Wave Elastography Improves the Specificity of Breast US: The BE1 Multinational Study of 939 Masses. Radiology-Radiological Society of North America 262, pp. 435, 2012.
[2] Song P, Urban MW, Manduca A, Zhao H, Greenleaf JF, et al.: Comb-push Ultrasound Shear Elastography (CUSE) with Various Ultrasound Push Beams. Medical Imaging, IEEE Transactions on 32, pp. 1435-1447, 2013.

Figure 1. (a) B-mode ultrasound image of a malignant lesion ROI encircled. (b) CUSE shear wave velocity map. This figure displays a high shear wave velocity with a mean and standard deviation of 7.07 ± 1.18 m/s in the ROI. The resultant Young's modulus of 149.95 kPa is indicative of malignancy.
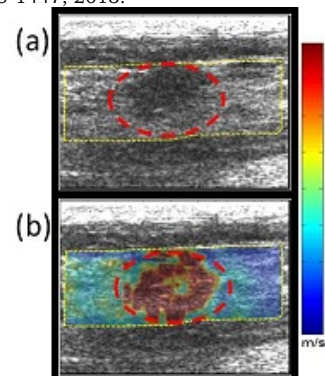
039   **DETECTION AND TREATMENT MONITORING OF EX VIVO HUMAN BREAST TUMORS USING HARMONIC MOTION IMAGING.**

Yang Han[1]*, Shutao Wang[1], Elisa Konofagou[1,2].
[1]Department of Biomedical Engineering, Columbia University, New York, NY, USA; [2]Department of Radiology, Columbia University, New York, NY, USA.

Background: Breast cancer is the most common cancer and the second leading cause of cancer death among women. High-Intensity Focused Ultrasound (HIFU) techniques are slowly emerging as less invasive, but equally effective, in the treatment of early-stage breast cancer and benign tumor. To facilitate its translation to the clinic, there is a need for a simple, cost-efficient device that can reliably monitor HIFU treatment.

Aims: We have developed the radiation-force technique of Harmonic Motion Imaging (HMI) that can be used seamlessly in conjunction with HIFU for tumor ablation monitoring, namely HMI for Focused Ultrasound (HMIFU).

Methods: Specimen collection and handling of post-surgical breast tissues were approved by the Institutional Review Board (IRB) board of Columbia University and informed consent was obtained from all enrolled patients. HMIFU was performed in 6 normal, 1 fibroadenoma specimen and 4 malignant tumors. The specimens were securely embedded in a tissue-mimicking agar phantom and merged in degassed PBS to mimic *in vivo* environment. The HMIFU setup consists of a 93-element, PZT-4 ceramic HIFU transducer confocally aligned with a 64-element phased array transducer to transmit and receive through a 4-board VDAS system. All HIFU channels were synchronously excited by a 25 Hz amplitude-modulated 4.5 MHz wave. A 2D raster scan with HMI was performed before and after thermal ablation using 1 s duration and 2800 W/cm^2 *in situ* acoustic intensity at each point. For ablation, same intensity was applied but and the duration was prolonged to 120 s to cause the lesion.

Results: After 2D raster scan, the 3D HMI displacement maps could be reconstructed representing the relative stiffness of the tissue. The average peak-to-peak displacement in the ROI of normal breast tissue, fibroadenoma and IDC were found to be 22.61±8.28 μm, 8.81±2.01 μm and 2.42 ±0.92 μm respectively. There are also significant differences between before and after HMIFU ablation in both normal and tumor specimens.

Conclusions: HMI for focused ultrasound (HMIFU) has been experimentally shown to be capable of mapping and differentiating stiffness in normal and abnormal breast tissues. HMIFU can also successfully generate and monitor the formation of thermal lesions on normal and abnormal breast tissues. The clinical objective of this technique is to develop an all ultrasound-based system for real-time thermal ablation generation and monitoring and testing in phantom and post-surgical breast specimens.

035 PROSTATE CANCER ELASTOGRAPHY WITH A SUPERSONIC IMAGINE AIXPLORER SCANNER.

Remi Souchon[1]*, Au Hoang-Dinh[1], Florence Mege-Lechevallier[2], Heldmuth Latorre-Ossa[1], Ali Zorgani[1], Stefan Catheline[1], Marc Colombel[2], Sebastien Crouzet[2], Olivier Rouviere[2].
[1]INSERM, Lyon, FRANCE; [2]Hospices Civils de Lyon, FRANCE.

Background: Prostate cancer is the most prevalent cancer in men in Western countries, and the 3rd cause of cancer-related death. Conventional imaging modalities are unsatisfactory for both detection and follow-up of the cancerous foci, which are usually detected by multiple random biopsies. Elastography gives new hopes because many cancerous prostate tumors are known to be stiffer than normal tissues. However, in the literature, the elasticity of prostatic tissues in vivo is still poorly documented.

Aims: To investigate shear wave elastography [1] feasibility in 30 patients with known prostate cancers and scheduled for prostatectomy, and to provide initial estimates of Young's modulus in *in vivo* normal and cancerous prostatic tissues.

Methods: The study was approved by the National Agency for Drug Safety (ANSM) and by the local ethical committee. 30 patients were enrolled after signing an informed consent. An experienced radiologist performed the ultrasound examinations using a commercial diagnostic ultrasound imaging scanner (Aixplorer®, SuperSonic Imagine, France [2]) and an endorectal transducer (SE12-3). Both B-mode and shear wave elastography of the whole prostate were acquired the day prior to surgery. After surgery, prostate specimens underwent conventional histological processing, and cancerous tumors were identified by a pathologist. Tumors with volume<8 mm^3 and Gleason<5 were considered clinically negligible by the pathologist and were excluded. B-mode images, elasticity images and histology slices were registered visually by the radiologist and displayed side-by-side. Regions of interest (ROI) corresponding to cancerous tissue and to normal tissues were selected by the same radiologist.

Results: Typical images are presented in figs 1 & 2. Measurements are summarized in Table 1. There is a significant difference between cancerous and normal tissues. In some patients, the anterior edge of the prostate was void of elastographic measurement (as illustrated in fig. 1) due to penetration issues.
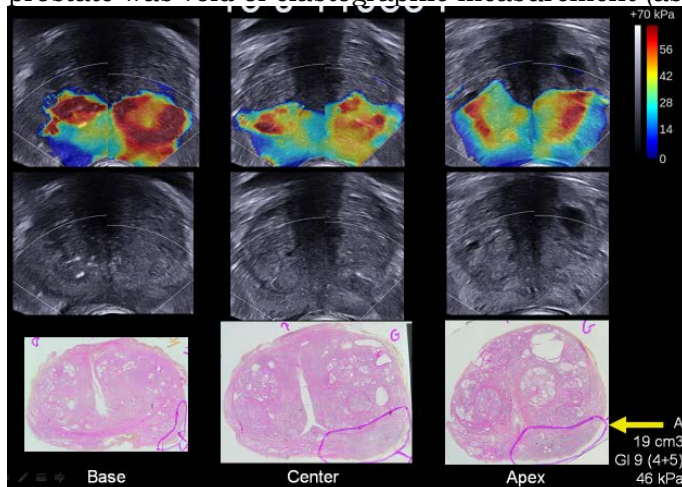
Figure 1. Case #15 - Histology slices (bottom row), B-mode (center) and elastogram (top row). Tumor A is a 19 cm^3 cancer in PZ with Gleason score 9 (4+5) and Young's modulus 46 kPa
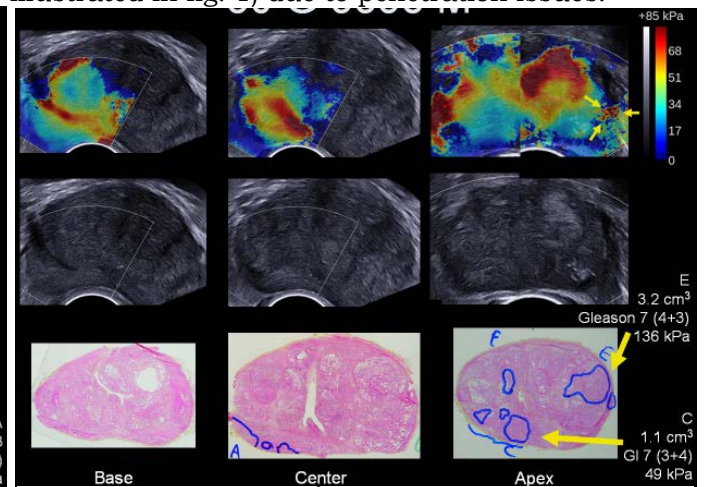
Figure 2. Case #30 - Tumor E is a 3.2 cm^3 cancer in TZ with Gleason score 7 (4+3) and Young's modulus 136 kPa. Tumor C is a 1.1 cm^3 cancer in PZ with Gleason score 7 (3+4) and Young's modulus 49 kPa

	Normal	Cancer
Peripheral zone	**26** (22-33)	**41** (21-59) (N=35)
Transition zone	**46** (36-56)	**67** (50-94) (N=6)

Table 1. Young's modulus (kPa) in prostatic tissues, with notation **median** *(25th centile – 75th centile) (N=number of cases)*

Conclusions: This study confirms the potential of shear wave elastography for imaging prostate cancer foci, and provides estimates of Young's modulus in prostatic tissues in vivo.

References: [1] Bercoff J et al.: Supersonic Shear Imaging: A New Technique for Soft Tissue Elasticity Mapping. IEEE Trans Ultrason Ferroelectr Freq Control, 51(4) pp. 396-409, 2004. [2] www.supersonicimagine.fr

046   **HIGH FRAME RATE CARDIAC DEFORMATION ESTIMATION USING COHERENT COMPOUNDING OF MULTIPLE SPHERICAL WAVES.**

MM Nillesen[1], AECM Saris*[1], HHG Hansen[1], PHM Bovendeerd[2], CL de Korte[1].
[1]Radboud University Medical Center, Nijmegen, THE NETHERLANDS; [2]Eindhoven University of Technology, Eindhoven, THE NETHERLANDS.

Background: RF-based strain imaging techniques have been developed for functional imaging of the heart. For accurate assessment of 3D deformation of the heart over the entire cardiac cycle, high frame rate 3D ultrasound imaging is compulsory. In particular, in cardiac phases with high deformation rates ultrafast transmission schemes will be of great advantage. Because of the large field of view and large imaging depth, spherical waves are preferred over plane waves for ultrafast transthoracic imaging.

Aims: To assess the performance of displacement estimation using coherent compounding of spherical waves as a preliminary step for high frame rate 3D cardiac deformation imaging.

Methods: A 3D finite element model describing the mechanics of a healthy left ventricle [1] was used to generate realistic 3D deformation fields of the cardiac muscle. Scatterers were moved according to these displacement fields and served as an input for Field II. Ultrasound element data for a 2D apical view were simulated using a phased array transducer (fc = 2.5 MHz, 64 elements, pitch = 320μm). Five spherical waves (SW) were emitted from virtual source positions behind the transducer, equally spaced across the transducer footprint, at a pulse repetition frequency of 1000 Hz (11 cm imaging depth). A subaperture of 21 elements was used for each transmit to achieve a good trade-off between lateral resolution and emitted pressure. After delay-and-sum beamforming, coherent compounding was performed to combine the 5 SW transmissions into a single RF dataset (frame rate 200 Hz). A cross-correlation based displacement estimation algorithm [2] was used to obtain axial displacements. A comparison was made between these axial displacement estimates and displacements directly derived from scatterer positions in the myocardial tissue for six characteristic phases of the cardiac cycle (begin-systole (BS): rapid ejection phase, mid-systole (MS): reduced ejection phase, end-systole (ES), begin-diastole (BD): rapid filling phase, mid-diastole (MD): slow filling phase, end-diastole (ED)).

Results: Figure 1 illustrates the good agreement between the axial displacement estimates [in mm] *(upper panel)* and ground truth displacements *(lower panel)* in all 6 cardiac phases. Root-mean-squared errors between model-based and estimated axial displacements varied from 0.2 mm in rapidly deforming phases (BS and BD) to 0.001 mm in slowly deforming phases.
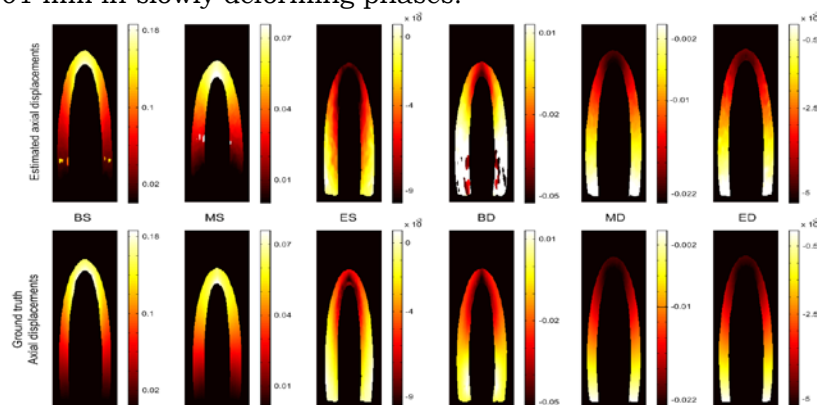
Conclusions: Cardiac displacement estimation using multiple spherical waves is feasible. Optimization of the number of spherical waves might improve image quality at large imaging depths, thereby also improving displacement estimation.

References:
[1] Bovendeerd et al.: Determinants of Left Ventricular Strain, Am J Physiol Heart Circ Physiol: 297, pp. 1058-1068, 2009.
[2] Lopata et al.: Performance of Two Dimensional Displacement and Strain Estimation Techniques using A Phased Array transducer, Ultrasound Med Biol: 35,(12),pp. 031-2041, 2009.

041 **COMPARISON OF DIVERGING WAVE AND PLANE WAVE FOR HARMONIC MOTION IMAGING (HMI) AND MONITORING OF HIFU TREATMENT IN REAL-TIME.**

Julien Grondin[1]*, Shutao Wang[1], Elisa E. Konofagou[1,2].
[1]Department of Biomedical Engineering, [2]Radiology, Columbia University, New York, NY, USA

Background: Harmonic Motion Imaging for Focused Ultrasound (HMIFU) has recently been developed to perform and monitor ablation. An Amplitude-Modulated (f_{AM} = 25 Hz) high-intensity focused ultrasound (HIFU) beam is used to induce a localized oscillatory motion at the focus which is simultaneously imaged by HMI. The feasibility of HMIFU in real-time, using a 2-D system, has recently been shown using a diverging wave to image the oscillatory motion.

Aims: The objective of this study is to compare the performance of HMI displacement estimation, using a diverging wave to that using plane wave imaging in order to achieve real-time capability with a 2D system when ablating canine livers *in vitro*.

Methods: A 93-element HIFU transducer (f_{center} = 4.5MHz) was used to induce a focal displacement while a coaxially-aligned 64-element phased array (f_{center} = 2.5MHz) was operated using a Verasonics ultrasound system for radio-frequency (RF) channel data acquisition. A continuous 120-s HIFU excitation was performed on two canine liver specimens *in vitro* at 11 different locations total. An unfocused transmit sequence using a diverging wave (5 locations) or a plane wave (6 locations) was used to image the liver at 1000 frames/second. The beamforming was performed using a delay-and-sum algorithm by multiplying a reconstruction sparse matrix by the RF channel data matrix. The data were reconstructed at 80 MHz sampling frequency axially over a 90° angle field of view for the diverging wave and 20 mm width for the plane wave. In order to achieve real-time frame rates, the data reconstruction was performed on a Graphical Processing Unit (GPU). Axial HMI displacements were estimated from the reconstructed RF signals, using 1-D normalized cross-correlation and streamed to a graphic user interface at a 1Hz display frame rate.

Results: A localized oscillatory motion was observed at the focusing depth of 70 mm. For all ablation locations in the canine liver *in vitro*, an HMI peak-to-peak displacement decrease was observed between the beginning and the end of the ablation. The average peak-to-peak displacement decrease was (64.9±8.8%). The signal-to-noise ratio in the displacement map (SNR_d) in the region of the focus at approximately 120 s was 22.3±13.3 for the diverging wave and 31.7±12.8 for the plane wave. These results show that HMIFU can provide real-time (1Hz) streaming of displacements simultaneously with HIFU treatment, using a diverging wave or a plane wave.

Conclusions: The SNR_d was found to be 1.4 times higher using a plane wave than a diverging wave suggesting that plane wave is more applicable for HMIFU. Current ongoing studies include the translation of HMIFU in a clinical setting.

008 ACCURATE MEASUREMENTS OF TISSUE DISPLACEMENT IN TWO DIMENSIONS USING HIGH FRAME RATE ULTRASOUND IMAGING.

Pieter Kruizinga[1]*, Frits Mastik[1], Nico de Jong[1,2,3,], Johannes G. Bosch[1], Gijs van Soest[1] and Antonius FW van der Steen[1,2,3,4].
[1]Thorax Center, Erasmus Medical Center, 3000CA Rotterdam; THE NETHERLANDS.
[2]Delft University of Technology, Delft; THE NETHERLANDS. [3]Interuniversity Cardiology Institute of The Netherlands, Utrecht; THE NETHERLANDS. [4]Shenzhen Institutes of Advanced Technology, Chinese Academy of Sciences, Shenzhen, CHINA.

Background: Viscoelastic properties of tissue can be assessed with ultrasound Doppler techniques [1]. Conventional Doppler techniques measure only axial (parallel to the transmit beam) displacements and not lateral (perpendicular to the transmit beam) displacements. Information on both (axial and lateral) components will improve the quality of Doppler based viscoelastic assessment of tissue. In this paper we propose a new method for measuring both axial and lateral components of tissue displacement using high frame rate ultrasound imaging.

Aims: To present a new algorithm for measuring ultra-small (< 1μm) 2D displacement vectors using non-beamformed and non-steered high frame rate ultrasound data.

Methods: Our method provides an accurate solution for a moving scatterer using non-beamformed array data. Echoes reflected from a moving scatterer will cause unique delays along the elements of an array. For each pair of elements the solution for the new scatterer position is unique. By averaging many pair-wise estimates we find a robust estimation of the new scatterer location and thereby the displacement vector. The required element specific delays between subsequent high frame rate frames were computed using an advanced instantaneous phase derivative technique. We validated our method experimentally with rotating isolated scatterers, moving diffuse scatterers and a pulsating carotid artery in-vivo. We applied HFR plane wave imaging with frame rates > 3 kHz. The plane waves (2 cycles, 8 MHz) were transmitted using a 128 element (4-9 MHz, -6dB bandwidth) linear array (Vermon, Tours, France). The array was interfaced with a 128 channel ultrasound research system using 12 bits, 80 MHz sampling (Lecoeur Electronique, Chuelles, France).

Results: In fig.1 we show three individual vector displacement frames obtained with the proposed method using data from three different experiments. The displacement estimation for isolated scatterers was found to be very precise (+/- 50 nm standard deviation). For diffuse scatterers we measured a reproducible underestimation of +/- 25% for the lateral displacement component. For the pulsating artery we found excellent agreement between the axial and lateral distension time profiles. These distension profiles contained physiological meaningful and reproducible displacements far below 1μm.

Conclusions: Here we present a new method for displacement estimation in two dimensions using high frame rate ultrasound. We provide experimental proof that with this method we can accurately measure the displacement vector in-vivo without the need for beam steering.
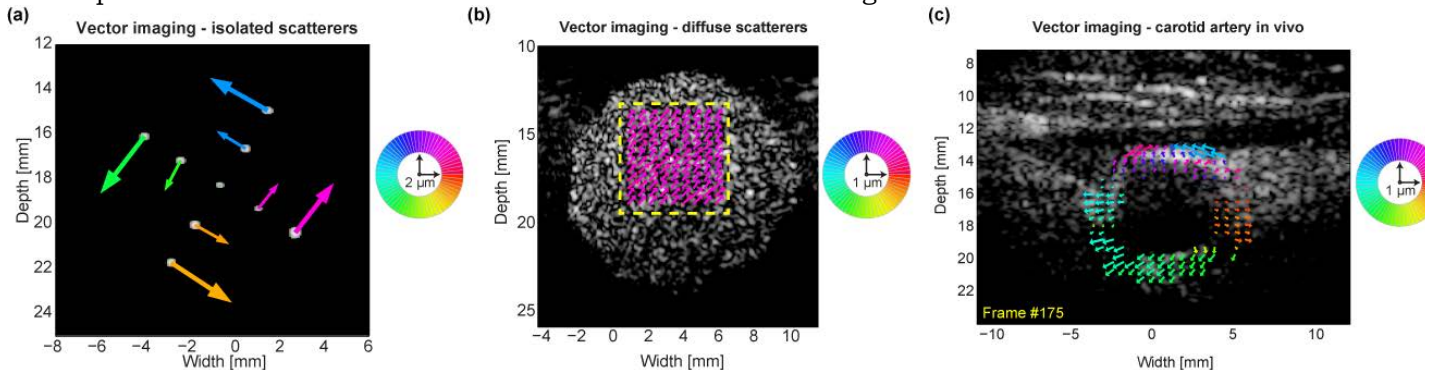
Figure 1: (a) B-mode frame with colored displacement vectors of nine rotating metallic rods (0.5 mm diameter) imaged with 3 kHz plane wave ultrasound imaging. (b) B-mode frame of moving tissue mimicking material. The uniform displacement vectors were computed for the region of interest (dashed yellow lines) and shown in color overlay. (c) B-mode frame with vectors in color overlay of a carotid artery in transverse view at maximum positive distension velocity.

References: [1] J. D'Hooge, A. Heimdal, F. Jamal, T. Kukulski, B. Bijnens, F. Rademakers, L. Hatle, P. Suetens, and G. Sutherland, Regional Strain and Strain Rate Measurements by Cardiac Ultrasound: Principles, Implementation and Limitations, Eur J Echocardiog,1,(3), pp. 154–170, 2000.

051 **THE APPLICABILITY OF PLANE WAVE IMAGING TO POROELASTOGRAPHY.**

Maria Theodorou[1]*, Jérémie Fromageau[1], Nandita de Souza[1], Jeffrey C. Bamber[1].
[1]The Institute of Cancer Research and Royal Marsden Hospital, 15 Cotswold Road, Sutton, Surrey, SM2 5NG, England, UK.

Background: Poroelastic materials contain mobile fluid that creates a time-dependent and spatially-varying strain field inside the sample under sustained compression [1]. Typically, the internal time-dependent strain is imaged dynamically with elastography by repeated scanning with ultrasound (US) under sustained global strain of the sample, the resulting technique being known as poroelastography [2]. In this paper, US poroelastography was employed to characterize the strain field behavior within poroelastic samples over a shorter timescale than employed in previous work [1], one that mimics the timescale expected for *in vivo* strain relaxation due to vascular drainage [3]. A high frame rate US system was evaluated for improving signal to noise ratio (SNR) in poroelastography over timescales on the order of seconds, introducing the opportunity to more fully characterize the fluid-related relaxations of soft tissue.

Aims: To compare plane wave to conventional transmit-focused US for poroelastography and consider its applicability in characterizing (a) the early part of slow relaxations, and (b) fast relaxations.

Methods: Poroelastic phantom experiments were performed using an Aixplorer® US scanner (SuperSonic Imagine), a linear array US transducer (SL15-4) with central frequency 7.5 MHz, and a plane-wave frame rate ranging from 100 to 500 frames per second (limited by memory buffer size). Cylindrical samples of soya-bean gel and reticulated foam were subjected to sustained axial compression (Instron 3342®) under computer control. The phantoms were scanned through an acoustic window on the side of the tank, with the US beam aligned along their radial direction. Data were acquired before and periodically after the application of the compression. The initial compression was applied over an interval of 0.1 s (top-surface displacement of 11 mm per second), inducing a global axial strain in the samples of approximately 3.5 %. This applied strain was sustained thereafter, producing stress relaxation loading conditions. The high frame rate of the single plane-wave imaging mode was used only during the first 10 s of the compression, to capture the early and rapidly changing part of the relaxation. The frame rate was then decreased to one transmit-focused image every 30 s, permitting efficient use of available buffer memory for a total data acquisition time of 15 min. Two-dimensional cross-correlation RF echo-tracking was performed between consecutive frames, followed by linear least-squares strain estimation, providing strain relative to the instant at which the compressor touched the surface of the sample. Plane wave elastography was also compared to transmit-focused elastography for a non-porous medium (gelatin). For this purpose the strain filter, which characterizes the strain SNR as a function of the applied strain [4], was used.

Results: Transmit-focused RF echo data from the Aixplorer® when imaging poroelastic media demonstrated poroelastic behavior consistent with published results [1]. However, the plane wave data obtained during the first 10 seconds produced noisy time-dependent strain images which were consistent with a degraded peak SNR observed for the plane wave strain filter compared to the transmit-focused strain filter measured using gelatin as an elastic (non-porous) medium. Nevertheless, for the small (<1%) incremental (single step) strains that are relevant to poroelastography, the plane wave imaging mode permits imaging of the fast relaxations that could not be observed using the slow frame rate of conventional line by line transmit-focused imaging.

Conclusions: A faster ultrasound poroelastography system, able to measure relaxation times on the order of seconds is necessary in order to fully characterize the poroelastic behavior of soft tissue. Although the lack of transmit focusing degrades the quality of the plane wave echo images, the high frame rate provides the ability to follow the time evolution of strain in poroelastic experiments.

References:
[1] GP. Berry, JC. Bamber, NR. Miller, PE. Barbone, NL. Bush, CG. Armstrong: Towards an acoustic model-based poroelastic imaging method: II. Experimental investigation. Ultrasound Med Biol, 32, pp 1869-1885, 2006b.
[2] E. Konofagou, TP. Harrigan, J. Ophir, and TA. Krouskop: Poroelastography: Imaging the Poroelastic Properties of Tissues. Ultrasound Med Biol, 27 (10), pp 1387–1397, 2001.
[3] R. Leiderman, PE. Barbone, AA. Oberai, JC. Bamber: Coupling between elastic strain and interstitial fluid flow: ramifications for poroelastic imaging. Phys Med Biol 51, pp 6291-6313, 2006.
[4] T. Varghese, J. Ophir: A theoretical framework for performance characterization of elastography: The strain filter. IEEE Trans Ultrason Ferroelectr Freq Contr, 44, pp 164–172, 1997b.

038 **ESTIMATION OF TISSUE VISCOELASTICITY USING INVERSE FILTER AND MULTIPLE-POINT SHEAR WAVE GENERATION.**

Tomoaki Kitazaki[1]*, Kengo Kondo[1], Makoto Yamakawa[1], Tsuyoshi Shiina[1].
[1]Kyoto University, Kyoto, Kyoto, JAPAN.

Background: Tissue viscoelasticity is measured in the diagnosis of tissue diseases such as cancer and liver fibrosis since it is related to the pathological condition. Radiation from a focused ultrasound beam has been used to produce shear waves, and the time-of-flight is measured to determine the shear wave speed. However, the method is based on an assumed propagating direction of a shear wave that is highly affected by reflection and refraction and thus might cause an error.

Aims: In this study we propose a new method for estimating tissue viscoelasticity, using shear wavelength. This method is not based on an assumed propagating direction and so is expected to improve the estimation accuracy. This study demonstrates the feasibility of the proposed method with phantom experiments.

Methods: An alternative shear elasticity estimation approach based on shear wavelength [1] was proposed and applied to passive configurations. To acquire viscoelasticity of tissue faster and more accurately, we propose a new method for estimating tissue viscoelasticity. This technique combines the shear wavelength approach and an "active" acoustic pushing configuration, i.e., multiple shear wave sources induced by acoustic radiation force (ARF). Shear waves generated at each widely separated pushing point are recorded by an ultrafast imaging method. Assuming that shear waves are impulses at each push point, shear waves measured on an arbitrary point are approximated as impulse responses. Consequently, an inverse filter can be applied to virtually focus a shear wave onto an arbitrary point. The inverse filter is implemented by singular value decomposition. The half-wavelength of the shear wave is estimated by measuring the full width at half maximum of the amplitude of the filtered signal at the focal point. Finally, wavelength is converted to shear wave speed. Viscoelasticity can be evaluated by measuring shear wave speed for each frequency. The proposed method has the potential to be robust against reflection and refraction because it does not assume the propagation direction but premises a reverberant field.

Results: The proposed method was validated by experiment using a phantom with an inclusion having a different viscoelasticity. A Verasonics ultrasound system with a 128-channel linear-array transducer (center frequency 5 MHz) was used to implement our proposed method. Tens of pushing points for shear wave generation were sparsely located. The response at each measurement point was recorded as an impulse response. The constructed image of shear wave speed clearly revealed the inclusion. The result indicated the feasibility of wavelength estimation by an inverse filter and multiple-point shear wave generation. Next, shear wave speed dispersions of surrounding medium and the inclusion were obtained to evaluate the viscoelasticity of the phantom. The region of interest (ROI) was about 10 mm^2. The obtained dispersion curves indicated the difference of material viscoelasticities. The inverse filter can be achieved more efficiently than passive configurations because it can control the shear wave generation, and the shear waves induced by the ARF impulses are good approximations of the impulse responses of shear-wave excitation.

Conclusions: We proposed a new method for estimating tissue viscoelasticity that combines the shear wavelength approach and multiple shear wave sources induced by ARF. The feasibility of the proposed method was verified using a phantom with an inclusion having different viscoelasticity. Further studies are needed to evaluate features of the proposed method by comparison with a time-of-flight-based method.

References:

[1] T. Gallot, S. Catheline, P. Roux, and M. Campillo: A Passive Inverse Filter for Green's Function Retrieval. J. Acoust. Soc. Am. Vol. 131, pp. EL21-27, 2012.

047   ***IN VIVO* 3D SKELETAL MUSCLE DEFORMATION: METHODS AND INITIAL RESULTS.**

K Gijsbertse[1]*, AMJ Sprengers[1], NJJ Verdonschot[1,2], CL de Korte[1].
[1]Radboud University Medical Center, Nijmegen, THE NETHERLANDS; [2] University of Twente, Enschede, THE NETHERLANDS.

Background: The aetiology of many musculoskeletal diseases is related to the biomechanical status of the affected muscle. Muscle contraction is characterized by large deformation and translation, requiring a multi-dimensional imaging modality to reveal the deformation of the muscle. RF-based strain imaging has been successfully used to estimate the deformation and strain of tissue during dynamic loading, and was also applied in actively deforming tissue using 2D and bi-plane techniques [1]. However, to account for out-of-plane motion and for a comprehensive mapping of the 3D muscle contraction, a full 3D technique is needed.

Aims: To assess the improvement of 3D displacement estimation using 3D phantom data, and to apply the technique to quantify the deformation of the m. gastrocnemius *in vivo.*

Methods: A phantom block (10x10x10cm) was constructed from a homogeneous 10% (wt.) gelatin (Dr. Oetker, Ede – The Netherlands) solution. 1% SiC scattering particles (15 μm SiC, E. Merck, Darmstadt – Germany) was added to mimic the scattering properties of soft tissue. The block was assumed to be linearly elastic and nearly incompressible (Poisson ratio 0.495). Using an automated plate compressor, the phantom was compressed 3 mm axially. Pre- and post-compression full volume raw ultrasound data were acquired using a Philips iE33 system, equipped with a X7-2 3D matrix array transducer (Philips, Andover, MA, USA) and an RF-interface. A cross-correlation based displacement estimation algorithm [2] was used to obtain the axial displacements. The performance of the technique was compared when using either 3D cross-correlation of 3D segments or 2D cross-correlation of 2D segments. As a measure of performance the Root-Mean-Squared errors (RMSe) was used between the expected displacement values from the controlled compression (ground truth) and the estimated displacements. To demonstrate the feasibility of 3D displacement estimation *in vivo,* data were acquired during a voluntary contraction of the gastrocnemius muscle.

Results: Figure 1 depicts the calculated axial displacements (in sample points) for a plane without (upper panel) and with (lower panel) out-of-plane motion. The results illustrate a better agreement between the estimated axial displacement and the ground truth, using 3D segments compared to 2D segments. RMSe for a plane with out-of-plane motion, were 0.62mm and 0.13mm for the 2D and 3D techniques respectively. For a plane without out-of-plane motion, the RMSe values were 0.17mm and 0.07mm respectively. Using the 3D technique, the *in vivo* data resulted in high quality axial-displacement images (Figure 2).

Figure 1

Figure 2
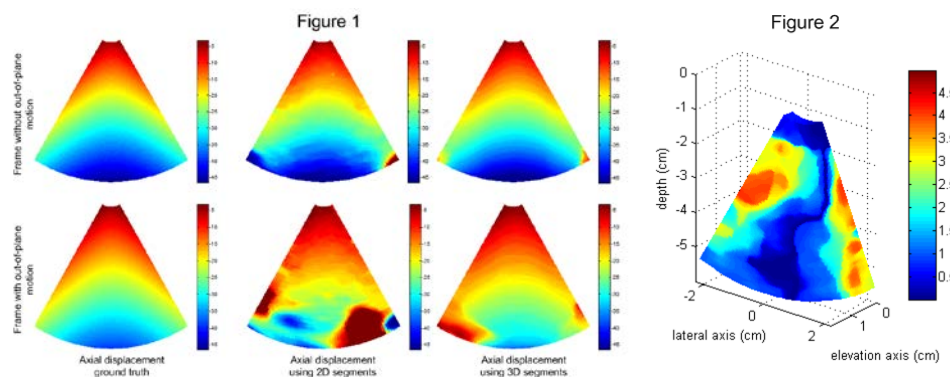
Conclusions: The usage of 3D data segments improves the axial displacement estimation. Muscle deformation estimation using full volume ultrasound RF-data is feasible. Optimization of the window settings might improve the displacement estimation even further.

References: [1] Lopata, R. G., J. P. van Dijk, et al.: Dynamic Imaging of Skeletal Muscle Contraction in Three Orthogonal Directions. J Appl Physiol, 109,(3), pp. 906-915, 1985.   [2] Lopata, R. G., M. M. Nillesen, et al.: Three-Dimensional Cardiac Strain Imaging in Healthy Children Using RF-Data. Ultrasound in Medicine and Biology, 37,(9), pp. 1399-1408, 2011.

028 **IN VIVO SHEAR WAVE DISPERSION MEASUREMENT USING MULTIFREQUENCY VIBRATION-CONTROLLED TRANSIENT ELASTOGRAPHY: FIRST RESULTS FOR LIVER STEATOSIS QUANTIFICATION.**

Jean-Pierre Remenieras[1]*, Maëlle Dejobert[2], Cécile Bastard[3], Véronique Miette[3], Jean-Marc Perarnau[2], Frédéric Patat[1,2].

[1]Université François-Rabelais de Tours, Inserm, Tours, FRANCE; [2]Inserm 1415, Tours, FRANCE; [3]Echosens, Paris, FRANCE.

Background: Nonalcoholic fatty liver disease (NAFLD) is characterized by accumulation of fat within the liver. In the most severe cases, NAFLD can progress to nonalcoholic steatohepatitis (NASH) and subsequently to liver cirrhosis. Since in many cases NAFLD can be asymptomatic, a non-invasive method for the measurement of fat concentration within the liver would be very beneficial.

Aims: The main objective of this study is to evaluate the feasibility of measuring in vivo the shear wave phase velocity dispersion $c_s(\omega)$ in the 30Hz-140Hz bandwidth, using multifrequency vibration-controlled transient elastography. This study includes some optimizations (number and different central frequency of the transient vibrations, inverse problem algorithms) dedicated to the characterization of the human liver viscoelasticity.

Methods: We use a research Fibroscan® (FS) platform with three consecutive transient vibrations (50Hz, 75Hz, 100Hz) at the same measurement point. Particle velocity $V_z(z,t)$ along the z axis under the vibrator is obtained by tissue Doppler algorithm [1] with 0.2mm spatial and 0.4 ms temporal resolution. After temporal segmentation and Fourier transform to obtain $V_z(z,\omega)$, the shear wavelength λ_s is estimated for each frequency of the transient vibration bandwidth, using a new algorithm based on a shear wave propagation model in the near field. Finally, experimental shear wave dispersion curves (Figure 1.b) are fitted using a fractional rheological model [2].

Results: Intermediate results are based on 23 healthy volunteers and 3 patients with detected steatosis. Figure 1.a shows the experimental real and imaginary part of $V_z(z,\nu=86.8Hz)$ superimposed with the theoretical propagation model. Inverse problem resolution for this frequency gives a wavelength $\lambda s=1.6cm$ i.e a phase velocity $c_s(86.8Hz)=1.1m/s$. Figure 1.b shows dispersion curve between 30Hz and 140Hz for the patient n°2. The fit by the Voigt (black line) model and the fractional rheological model [2] (red line) is shown in figure 1.b. We obtain in vivo for three different measurements on this patient $\mu=1.56\pm0.08KPa$, $\eta=2.9\pm0.89Pa.s$ for the Voigt model and $Ge=625\pm550Pa$, $\kappa=233\pm83Pa.s^n/rad^n$, $n=0.21\pm0.2$ and $\eta_\infty=2\pm1.9$ Pa.s for the Nicolle's model. Figure 1.c shows the viscosity η as a function of elasticity parameter μ for the 23 volunteers and the 3 patients with steatosis. The first preliminary results show that the three steatosis patients have the same elasticity range as the volunteers: 0.7 to 2.1kPa. The shear viscosity η for the patients (in red) is slightly higher and range between 2.9 to 4.6Pa.s. Patient 1 has 22% of fat load measured with MRI and we measure $\eta=4.6Pa.s$. Patient 3 has 13.6 % of fat and $\eta=3.9Pa.s$.**Conclusions:** Optimization of the measurement method for liver viscoelasticity measurements in the bandwith 30Hz-140Hz is encouraging and may increase the diagnostic performance of the Fibroscan® examination. Steatosis patients seem to exhibit a higher shear viscosity η than healthy volunteers. A more complete analysis on 20 steatosis patients with liver biopsy is currently in progress at Tours Hospital.
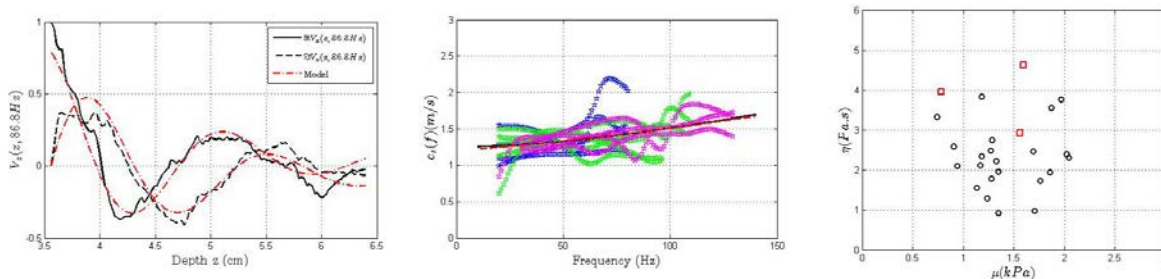
Figure 1:(a) Inverse problem for the estimation of the shear wavelength. (b) Dispersion curve of the shear phase velocity obtained for steatosis patient 2. (c) Experimental results in the parameter's space.

References: [1] R.Ternifi et al,: Measurement of Brain Tissue Motion using Extended Autocorrelation Strain Eestimator", J. Acoust. Soc. Am. 131(4), pp.3363, 2012. [2] S. Nicolle et al,; A Strain-Hardening Bi-Power Law for the Nonlinear Behavior of Biological Soft Tissues", Journal of biomechanics, 43 (201) pp. 927-932.

027 **MEASUREMENT OF SHEAR WAVE SPEED DISPERSION IN PLACENTA USING TRANSIENT ELASTOGRAPHY: A PRELIMINARY EX VIVO STUDY.**

Samuel Calle[1]*, Emmanuel Simon[1,2], Emmanuel Nicolas[1], Redouane Ternifi[1], Franck Perrotin[1,2], Jean-Pierre Remenieras[1].

[1]François Rabelais University, Inserm, Imaging and brain UMR U930, Tours Cedex 1, FRANCE;
[2]University Hospital Center of Tours, Tours Cedex 9, FRANCE.

Background: Obstetric pathologies associated with placental dysfunction are an important public health issue. Indeed, this pathology is responsible for pre-eclampsia and intrauterine growth retardation (IUGR). For clinicians, the ultrasound (US) assessment of placental function is limited to the observation of indirect parameters such as the amount of amniotic fluid, fetal growth or fetal-placental Doppler. In the case of IUGR, significant changes in the villous architecture are observed [1], which probably change the elasticity of IUGR placentas compared to normal placentas.

Aims: To this day, there have been few studies of the placenta's biomechanical properties, and no clinical device measures the elasticity of the placenta, and provides information about its architecture. Theoretical and physical considerations indicate that the presence of microscopic obstacles may influence not only the absolute value of viscoelastic tissue parameters, but also their relationship with frequency [2]. The frequency behaviour of tissue mechanical parameters may be modelled as a power law, in which case the exponent parameter represents a mechanical property inherent to a given material. In this context, the feasibility of measuring shear wave dispersion in placentas is tested *ex vivo*.

Methods: A Transient Elastography (TE) method, based on the works of Catheline *et al.* [3], is proposed. The propagation of a plane shear wave excited by a plate fixed to a low-frequency (LF) electromechanical actuator (type 4826, Brüel & Kjaer, Denmark) is measured using an ultrafast US scanner (Aixplorer, Supersonic Imagine, France). In-phase and Quadrature (IQ) demodulated complex data are acquired at 2. 8MHz (probe central frequency) and stored in 2D in the SSI system with a pulse repetition frequency of 5KHz. The tissue velocity is computed using subsample mean frequency estimation. Calculating the spatial FFTs of $Vz(x,\omega)$, *i.e.* $Vz(kx,\omega)$, the shear wave speed dispersion curve is obtained between 20Hz and 60Hz by finding for each frequency the phase velocity at which the Fourier transform amplitude is maximal. Previously validated on calibrated elasticity phantoms, the method has been applied on 8 healthy delivered placentas (<12h after delivery). Measurements (3 times with repositioning) have been performed on 2 regions: a central region (behind the umbilical cord) and a peripheral region (edge of the placenta). At the same time, measurements of the Young's modulus (3 times with repositioning) have been performed using Supersonic Shear Imaging (SSI).

Results: In agreement with literature, elasticities measured at a fixed frequency by SSI and TE methods are in the same order of magnitude for the two regions. Moreover, a low inter-individual variation has been found in the 8 healthy placentas: in the peripheral region, the elastic modulus measured with SSI is 9.9±1.15 kPa and the shear wave speed Cs measured at 50Hz using TE is 1.80±0.24 m/s. TE measurements showed high reproducibility: for example, from the 6 measurements performed in both regions of placenta 3, the shear wave speed Cs measured at 50Hz is 2.05±0.10 m/s. As presented on figure 1, two different models have been used to fit the experimental data obtained with the TE method: a classical Voigt model and a fractional rheological model [4] $(G^{*}(i\omega)=G_e+K.[i\omega]^n)$. One result is that 2 placentas which have similar elastic modulus values can present different linear constitutive parameter *n.* For example, the values of placentas 1 and 8 are, respectively: elastic modulus from SSI 9.6±0.96kPa and 9.0±1.63kPa, Cs at 50Hz from TE 1.87±0.19m/s and 1.86±0.23m/s, n=1.10±0.05 and n=1.35±0.07.

Conclusions: E*x vivo* placenta exploration using TE is feasible and reproducible. These results suggest the added-value of the elasticity frequency analysis for placental exploration. Future work will involve *ex vivo* and *in vivo* measurements comparing healthy and IUGR placentas.

References: [1] Macara L., Kingdom J.C., Kaufmann P., et al.: Placenta 17, pp. 37-48, 1996. [2] Holm S., J. Acoust. Soc. Am. 127, pp. 542-548, 2010. [3] Catheline S., Gennisson J.L., Tanter M., Fink M., PRL 91, pp. 1643011-1643014, 2003. [4] Nicolle S., Vezin P., Pallierne J.F., J. Biomechanics 43, pp. 927-932, 2010.
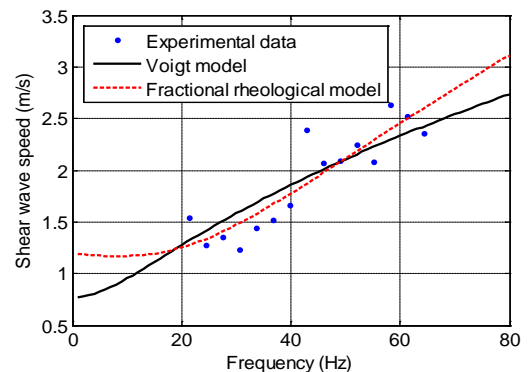
Fig.1: TE measurement in placenta 3.

013   **COMPARISON OF PLANE WAVE COMPOUNDING TECHNIQUES FOR DISPLACEMENT ESTIMATION.**

Hendrik H.G. Hansen, *Anne E.C.M. Saris, Chris L. de Korte.*
Radboud University Medical Center, Nijmegen, Geert Grooteplein 10, Nijmegen, THE NETHERLANDS.

Background: Plane wave ultrasound transmission and storage of radiofrequency (RF) element data has enabled imaging at kHz frame rates with the flexibility to beamform in any direction in receive, albeit at the cost of off-axis resolution. Multiple techniques have been developed to cope with the low off-axis resolution when performing 2D displacement estimation. Coherent compounding averages radiofrequency (RF) ultrasound data acquired sequentially at various transmit angles to suppress sidelobe levels and enhance 2D displacement estimation [1]. Displacement compounding combines axial displacements estimated at multiple plane wave transmissions angles to derive the 2D displacement vector [2].

Aims: This study compares the performance of coherent compounding and displacement compounding using simulations of a homogenously translating cube.

Methods: Ultrasound RF data for a homogeneous cube (1 x 1 x 1 cm^3) were simulated for a linear array transducer (f_c = 9 MHz, pitch = 198 µm, 192 elements) transmitting plane waves at 3 sequentially alternating angles (0°, +α, -α) at a PRF of 2 kHz using Field II [3]. Simulations were repeated for α ranging from 5° to 20° with increments of 5°. The cube moved at a constant speed of 450 µm/s at motion angles (θ) ranging from -180° to +180° in steps of 15°. Band-limited noise was added to all RF data to obtain a signal-to-noise ratio of 13 dB. Displacements were estimated at an effective frame rate of 15 Hz (30 µm inter-frame displacement) using either RF compounding or displacement compounding. For both techniques, delay-and-sum beamforming (axial spacing: 13 µm, lateral spacing: 90 µm) followed by 2D normalized cross-correlation and 2D parabolic peak interpolation was performed to estimate the displacements. To compare the performance of the techniques as a function of the maximum plane wave angle and as a function of the direction of motion, the root-mean-squared-error (RMSE) of the estimated displacements was determined with respect to the ground truth. The results for a straight-forward 0° 2D cross-correlation method without compounding were also calculated for comparison.

Results: The figure summarizes the results. Both compounding techniques outperform the 0° 2D cross-correlation technique. Displacement compounding for plane wave angles of 20° provides the most precise displacement estimates for every direction of motion. As can be expected, the best performance is obtained when the motion is in the axial direction (RMSE = 0.8 µm). The worst performance is obtained when the motion is directed laterally (RMSE = 5.3 µm).
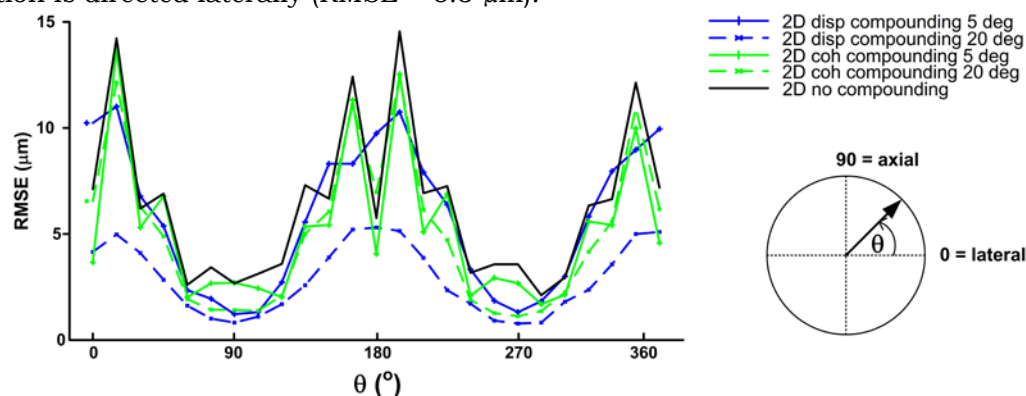
Conclusions: In a uniform motion field displacement compounding, using plane waves transmitted at large beam steering angles, outperforms coherent compounding regardless of the direction of motion.

References: [1] Montaldo et al.: IEEE Trans Ultrason Ferroelectr Freq Control, 56(3), pp. 489-506, 2009.   [2] Hansen et al.: Journal of Biomechanics, 47(4), pp. 815-23, 2014.   [3] Jensen et al.: Medical & Biological Engineering & Computing, 34(Suppl. 1, Pt 1), pp. 351–53, 1996.

044   STUDY OF ULTRASOUND STIFFNESS IMAGING TECHNIQUES USING REAL TIME BREAST IMAGING.

Kavitha Manickam[1], Ramasubba Reddy Machireddy[1]*, Bagyam Raghavan[2].
[1]Indian Institute of Technology Madras, Chennai 600036, INDIA; [2]Apollo Specialty Hospital, Chennai 600035, INDIA.

Background: The potential usefulness of stiffness imaging methods such as strain elastography imaging [1] and Acoustic Radiation Force Impulse imaging (ARFI) [2] was investigated for visualization of varying stiffness tissue mimicking phantoms [3]. From the finite element simulations and phantom experiments, it is shown that strain elastography presents a significantly improved image contrast relative to ARFI for malignant lesions [3].

Aims: In order to corroborate the above result, a pilot real time breast imaging study was conducted. The objectives of this study are twofold. 1. To analyze the performance of strain elastography and ARFI in depicting benign and malignant lesions, using observed image contrast. 2. To develop quantitative elastographic features for elastography and ARFI images and evaluate their diagnostic performance in classification of benign and malignant lesions, using observer performance.

Methods: A pilot study was conducted on 20 subjects (includes 13 malignant and 10 benign lesions). All patients underwent ultrasound B mode, real time elastography, ARFI displacement and shear wave elasticity imaging from September 2013 to November 2013, using a Siemens Acuson S2000 (Siemens, Erlangen, Germany) with a linear 9L4 transducer with a frequency of 5-8 MHz (23 X4 set of images). The true modulus contrast (C_t = Young's modulus of lesion/Young's modulus of normal tissue) is calculated from shear wave elasticity imaging ($E=3C_s^2\rho$) for benign and normal tissue, where C_s is the shear wave velocity and ρ is the density. For malignant tissue, C_t is calculated from elastogram-observed image contrast (C_o= Strain of normal tissue / Strain of lesion) [3]. The correlation between C_t from strain elastography with C_t from ARFI is analyzed and they are compared with C_o for both malignant and benign lesions. In addition to contrast analysis, we propose analyizng distinct elasticity features based on the image intensity for both ARFI and elastograms. Having manually segmented out the lesion portion, first and second order strain and displacement features were extracted to capture the heterogeneity of the lesion and background tissue.

Results: From shear wave velocity imaging, the average shear wave velocity is measured as 2.5 ±0.7 m/s and 1.8 ±0.5 m/s for benign and normal tissues respectively. From the values, C_t was calculated and they are correlated with C_t from corresponding elastograms (r=0.74). Since, ARFI reported as Indeterminate for malignant tumors, C_t was calculated from the elastogram alone and presented in Fig. 1. From the extracted feature set of ARFI, elasticity mean, variance, CNR, second order correlation and contrast were considered as significant ($\rho<0.1$), using student t test. For elastography, mean, variance, GLCM mean, GLCM variance and contrast were significant. The diagnostic significance of the extracted features was verified, using receiver operating characteristics which shows A_{roc} is above 0.5 (Fig. 2).
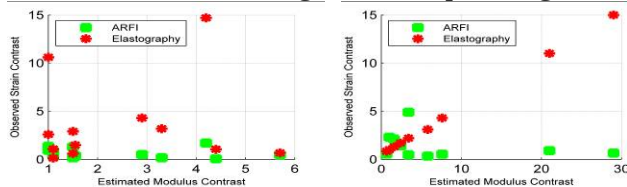
Figure 1 (a) Benign lesion (b) Malignant tumor   Figure 2 ROC (a) Elastogram (b) ARFI
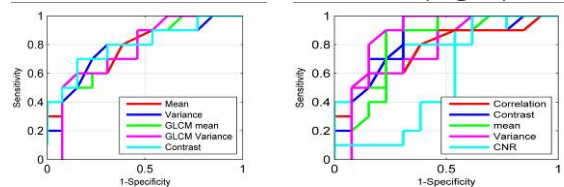
Conclusions: In this preliminary study, C_t was estimated analytically by combining ARFI shear wave velocity imaging and strain elastography which are then compared with observed image contrast. Results show that malignant lesions are easily identified with strain elastography due to their enhanced strain contrast, whereas ARFI presents a reasonable strain contrast which is close to the true modulus contrast. For quantification of the elasticity, in addition to first order statistics, second order statistics such as contrast and correlation were suggested (maximum A_{roc}) to be used as significant inputs in designing a classifier for computer aided diagnostic system.

References: [1] J. Ophir, Elastography: a Quantitative Method for Imaging the Elasticity of Biological Tissues, Ultrasound Imaging, vol. 13, pp. 111–134, 1991. [2] K. Nightingale, M. Palmeri, R. Nightingale, G. Trahey: On the Feasibility of Remote Palpation using Acoustic Radiation Force, J. Acoust. Soc. Am., vol. 110 pp. 625–634, 2001. [3] F. Kallel, M. Bertrand, and J. Ophir: Fundamental Limitations on the Contrast Transfer Efficiency in Elastography: An Analytic Study. Ultrasound in Medicine and Biology, vol. 22, pp. 463, 1996.

025 **ECHO IMAGING, DISPLACEMENT MEASUREMENT AND HIFU TREATMENT WITH NONLINEAR SIGNAL PROCESSING.**

Chikayoshi Sumi.*
[1]Sophia University, 7-1, Kioicho, Chiyodaku, Tokyo 102-8551 JAPAN.

Background: High resolution ultrasound (US) echo imaging, high accuracy tissue displacement measurement/imaging and high spatial resolution HIFU treatment are clinically important. Thus far, for instance, we have performed such processing using multiple beams in a linear sense, i.e., lateral modulation (LM) with superposition of crossed beams [1]. For HIFU treatment, the application of a high frequency US is effective, and then intense harmonic waves are often generated using micro bubbles.

Aims: In this report, with respect to variously received echo signals, increases in the carrier frequency, bandwidth and contrast are achieved via nonlinear calculations such as exponentiation or multiplications. The processing yields new high resolution echo imaging and displacement measurement.

Methods: Via nonlinear calculations, harmonic signals with wide bandwidths can be enhanced or generated newly or virtually together with a wide-band base-band signal; and with respect to the harmonic signals, detection can also be achieved in an arbitrary direction (e.g., axial, lateral directions) with fewer calculations than conventional detections. Thus, measurement of a displacement vector as well as a displacement component can be performed using a 1D measurement method such as the 1D autocorrelation method with 2D moving-average. Calculations of harmonic components will also be effective for grasping the process of heat generation with HIFU. The effectiveness of the method is confirmed using the same experimental echo data as those in [1], i.e., synthetic aperture (SA) data (US freq., 7.5 MHz) obtained on an agar phantom having a cylindrical inclusion (10mm dia.) with a higher agar concentration than the surrounding or simulations (Field II).

Results: Figure 1 shows spectra, lateral point spread functions and B-mode images obtained on an agar phantom via scanning with (1) a non-steered beam and (2) a LM using two steered beams. The squared echo data were generated from (1) and (2); and multiplied echo data were also generated from (2). B-mode images are shown only for harmonic LM with envelope and parabolic detections. In summary, the spatial resolutions increased; the side lobes decreased; the contrast increased. Figure 2 shows accurately measured displacements and strains, and shear modulus reconstruction, for instance, obtained for a lateral compression (lateral, y-axis; and axial, x-axis). Actually, spatially zoomed echo signals were used via zero-spectra padding in a frequency domain. Figure 3

Fig. 1. Phantom experiments, spectra, PSFs, B-mode images.

Fig. 2. Measurements of displacement vector;
Fig. 3. Simulations of (upper) US pressures generated using concave

shows simulated US pressures to be generated with single and duplicate concave transducers (rad. 12 mm; focus, 30mm depth). Here, only the squared pressures are shown.
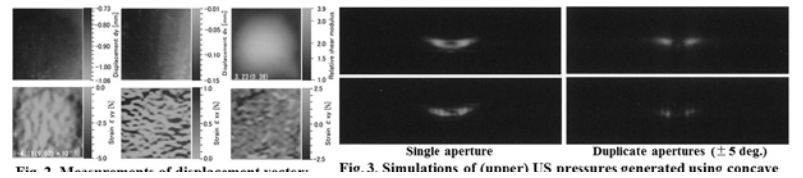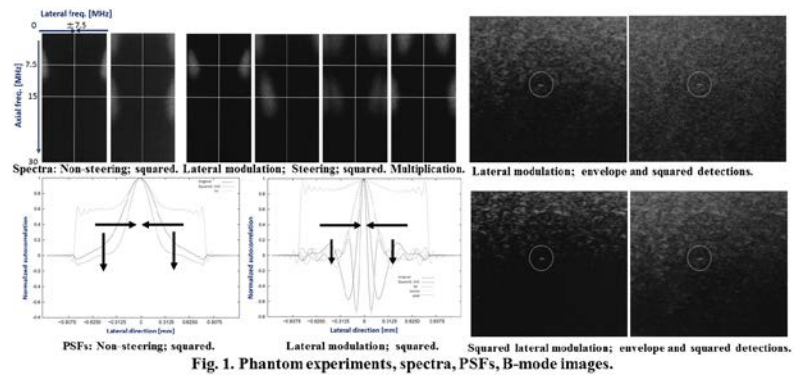
Conclusions: The nonlinear processing was effective for increasing the quality of images. Detections achieved simultaneously were also effective, i.e., for imaging and displacement measurement. Heterogeneous high and low frequency signals can also be generated via the nonlinear processing. One can anticipate that ultimately, high or low frequency signals, or mechanical sources not physically acquirable, will also be generated and used for microscopy, for deforming tissues, etc. Over-determined systems will also be generated using such quasi-waves, superposition and frequency division of spectra. These may be used for suppression of speckle as well as displacement measurement. The process of heat generation will also be experimentally investigated. Various nonlinear effects could be used, such as interference between different physical waves (electromagnetic waves, light, etc.), via transmission of harmonic waves. Nonlinear materials will also be incorporated into transducers.

References: [1] C. Sumi, IEEE Trans. UFFC, 55, pp. 2607–2625, 2008.

001   **VASCULAR ELASTOGRAPHY OF THE PORCINE CAROTID ARTERY.**

Renate W. Boekhoven*[1], Marcel C.M. Rutten[1], Frans N. van de Vosse[1], Richard G.P. Lopata[1].
[1]Eindhoven University of Technology, Den Dolech 2, Eindhoven, THE NETHERLANDS.

Background: Reliable non-invasive assessment of mechanical properties of the arterial wall, either healthy or diseased, is of great importance for patient specific diagnosis in the field of vascular disease. Vascular elastography is a promising tool to assess these mechanical properties. Validation of these techniques should be performed, preferably under matching, physiological conditions.

Aims: To compare a realistic approach for mechanical testing of arteries *in vitro*, inflation testing combined with vascular elastography, to the gold standard bi-axial testing.

Methods: Vascular elastography is applied to porcine carotid arteries (n=13). The arteries were stretched to their *in vivo* length (λ_z=1.6), submerged in and perfused with PBS, and dynamically pressurized (0 - 120 mmHg), in a circulation mock loop [1] at 38.5°C. Longitudinal RF-data were acquired with a MyLab70 scanner (Esaote, NL). Local deformations were estimated using a 2D coarse-to-fine strain algorithm [2]. For comparison, bi-axial tensile testing (CellScale, CA) was performed on two samples from each artery (9 mm by 9 mm, n=26). Samples were again stretched to a fixed length (λ_z = 1.6), and stretched in steps of 5% in the circumferential direction up to 40%. Displacements were assessed with image registration (Labjoy©). Finally, a Neo-Hookean model was used to estimate the shear modulus (G) of the carotid arteries for experiments, assuming linear elasticity, isotropy, and incompressibility. Pressure, diameter and wall thickness change were used to estimate G_{US}, while for G_{TT} estimation, force and displacements were used with the initial wall thickness at λ_z = 1.6 (from inflation).

Results: In Figure 1, the estimated shear moduli of both experiments were compared. The results show a good correspondence between the two techniques (Fig. 1a), with a shear modulus of G_{US} = 37 ± 8.5 kPa and G_{TT} = 41 ± 11 kPa, for ultrasound and tensile testing, respectively. Bland-Altman analysis revealed little bias ($G_{US} - G_{TT}$ = -3.7 ± 5.2 kPa, Fig. 1b).

Conclusions: In conclusion, vascular elastography was validated in healthy porcine carotid arteries by comparing controlled, inflation experiments with bi-axial tensile testing. In future work, these data can be used as input to compare several other hyperelastic models, which are able to describe the mechanical behaviour of arteries more realistically.
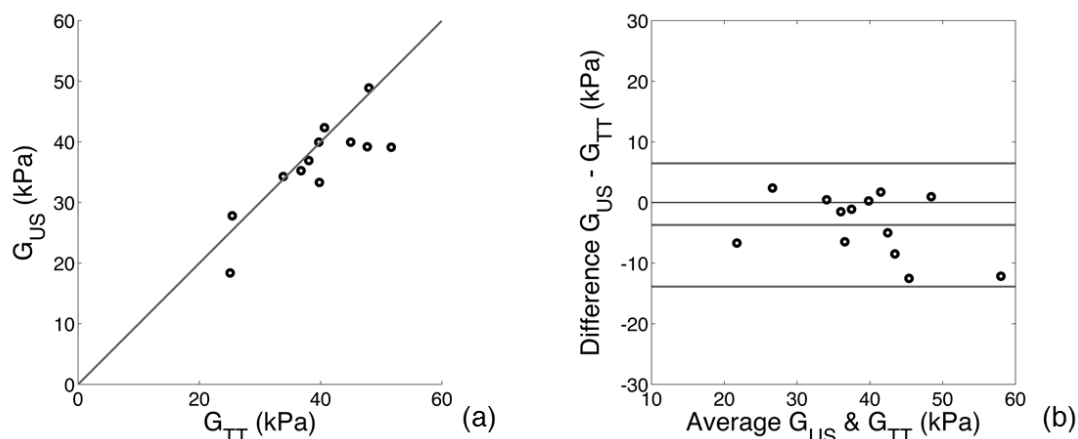
Figure 1 (a) shear moduli extracted from the tensile testing (G_{TT}) and shear moduli obtained from the inflation experiments (G_{US}). (b) shear moduli are compared by means of a Bland Altman plot.

References:
[1] van den Broek et al.: Biomech Model Mechanobiol, 2011. [2] Lopata et al.: Ultrasound Medical Biology, 2009.

040 MODULUS MAPPING OF NORMAL AND STENOTIC CAROTID ARTERIES USING PULSE WAVE IMAGING.

RX Li[1]*, IZ Apostolakis[1], EE Konofagou[1]
[1]Columbia University, New York, NY, USA.

Background: Noninvasive quantification of arterial stiffness has been shown to be of high clinical importance. The capability of Pulse Wave Imaging (PWI)[1,2] to spatio-temporally map the regional arterial wall motion and provide image-guided measurements of the local pulse wave velocity (PWV) has been demonstrated in carotid arteries *in vivo*[2]. The PWV and arterial radius measurements obtained using piece-wise linear regression can be used to generate modulus maps quantifying the stiffness along the vessel, potentially serving as a valuable tool for detecting and characterizing carotid plaques[3].

Aims: The objective of this study was to assess the feasibility of using PWI to generate modulus maps in normal carotid arteries and those with stenosis due to atherosclerotic plaques. Compared to normal carotid arteries, we hypothesize that the modulus magnitudes in the stenosis cases will be more variable, particular within and around the plaque regions.

Methods: RF signals were acquired from the common carotid arteries of five (N = 5) normal subjects and two (N = 2) patients with atherosclerotic plaque using a SonixTouch system (Ultrasonix Medical Corp., Burnaby, Canada) with a 10 MHz linear array transducer in a fixed 38mm width x 30mm depth imaging plane. A fast, normalized 1D cross-correlation-based motion estimation method[4] was used on the RF signals to compute the inter-frame pulse wave-induced wall velocities in the axial direction. The anterior wall velocities were used to generate a spatio-temporal map consisting of the wall velocity waveform at each beam location. The imaged segment was divided into five overlapping sub-segments, and piece-wise linear regression was used to estimate the PWV in each sub-segment. The modified Moens-Korteweg equation was used to compute the Young's modulus E of each sub-segment given the measured PWV value and radius.

Results: The moduli averaged across all sub-segments in the five normal subjects (in kPa) were 117.23 ± 33.05, 139.98 ± 72.49, 80.26 ± 33.42, 83.25 ± 51.80, and 56.54 ± 35.68. Compared to the normal cases, the stenosis cases exhibited higher and more variable moduli across its sub-segments (182.18 ± 182.07 and 114.63 ± 76.19). Also, both plaque cases exhibited increased PWV and E immediately preceding the plaque, as indicated by the yellow arrow in Figure 1.
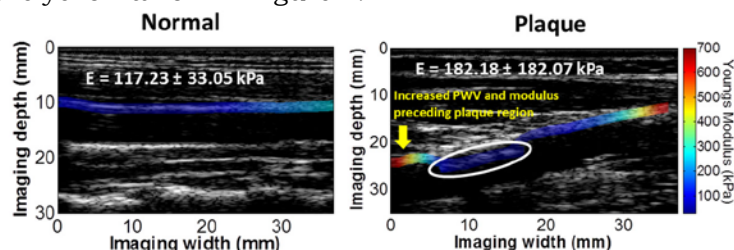
Figure 1: Modulus maps from a normal carotid artery (L) and a stenotic carotid artery (R) exhibiting atherosclerotic plaque (outlined by the white oval)

Conclusions: The potential of PWI to generate modulus maps and differentiate between normal and stenotic carotid arteries based on the modulus magnitudes and distribution was hereby shown. Future studies will be aimed at increasing the sample size to categorize individual cases based on plaque size and percentage of stenosis.

References:
[1] Li RX, Luo J, Balaram SK, Chaudhry FA, Shahmirzadi D, Konofagou EEE, Pulse Wave Imaging in Normal, Hypertensive, and Aneurysmal Human Aortas *In Vivo*: A Feasibility Study: Phys Med Biol, 58(13): pp. 4569-62, 2013.
[2] Luo J, Li RX, Konofagou EE, Pulse Wave Imaging of the Human Carotid Artery: An *In Vivo* Feasibility Study. IEEE TUFFC. 59(1), pp. 174-81, 2012
[3] Ino-Oka E et al,: Evaluation of Carotid Atherosclerosis from the Perspective of Blood Flow Reflection. Clin Exp Hypertens, 31(3), pp. 188-200, 2009
[4] Luo J and Konofagou EE, A Fast Normalized Cross-Correlation Calculation Method for Motion Estimation. IEEE Trans Ultrason Ferroelectr Freq Control; 57(6), pp. 1347-57, 2010.

INTRACARDIAC MYOCARDIAL ELASTOGRAPHY IN HUMANS IN VIVO DURING RADIO-FREQUENCY ABLATION.

Julien Grondin[1]*, Elaine Wan[2], Alok Gambhir[2], Hasan Garan[2], Elisa E Konofagou[1,3].
[1]Department of Biomedical Engineering, [2]Medicine, [3]Radiology, Columbia University, New York, NY, USA.

Background: Intracardiac echocardiography (ICE) is commonly used during radio-frequency (RF) ablation procedures for procedural guidance. Besides its imaging function, ICE could be used to assess mechanical properties of the myocardium to improve the ablation outcome.

Aims: The objective of this study was to demonstrate that ICE can be used at high frame rate using a diverging beam transmit to image myocardial strain and differentiate myocardial tissue properties before, during and after ablation for a clinical ablation procedure.

Methods: A 5.8-MHz center frequency ICE probe was used to image the heart of three normal canines and six humans with atrial fibrillation (AF) *in vivo* before, during and after RF ablation at high frame rates (1200 Hz) and the channel data were acquired on a clinical ultrasound system. The RF signals were reconstructed on a 9cm depth and 90° field of view region with a delay-and-sum algorithm and axial cumulative displacement estimation was performed using 1-D cross-correlation using a window size of 2.6mm and 95% overlap. Axial cumulative strains were obtained from the axial displacements using a least-squares estimator with a kernel of 5.1 mm.

Results: In the canine case, radial thickening was detected in the lateral wall and in the interatrial septum during left atrial (LA) systole. For AF patients, mean absolute strain in the ablated region was lower (8.3±6.3%) than before the ablation (17.1±9.7%) in LA at end LA systole.

Conclusions: Myocardial strains in the LA of an AF patient were approximately 2.1 times lower in the ablated region than before ablation. This initial feasibility may suggest Myocardial Elastography as a new imaging modality to be used in adjunct with ICE in RF ablation guidance and lesion monitoring.

010 **MYOCARDIAL PASSIVE SHEAR WAVE DETECTION.**

HJ Vos1*, BM van Dalen2, AFW van der Steen1, JG Bosch1, N de Jong1.
1 Biomedical Engineering (room Ee2302), Erasmus MC, NL-3000 CA, Rotterdam, THE NETHERLANDS;
2 Cardiology (room BA328), Erasmus MC, NL-3000 CA, Rotterdam, THE NETHERLANDS.

Background: Accurate echocardiographic diagnosis of diastolic heart failure is needed to face the epidemic proportions of this syndrome. Since diastolic dysfunction and myocardial stiffness are correlated, various studies have addressed shear wave elastography to measure the myocardial stiffness non-invasively. We revisit the passive method by Kanai [1] and Brekke et al. [2] that exploits naturally-occurring Lamb waves in the septal wall caused by aortic valve closure, and apply this method to diseased pigs. We also address the mechanical waves after mitral valve closure, to provide potentially more functional information about the myocardium.

Aims: To investigate myocardial elastography by imaging and interpretation of the mechanical wave phenomena, caused by mitral and aortic valve closures.

Methods: We examined Göttingen minipigs (N=14, weight: 37±7 kg) that are a model for the development of diastolic heart failure. Most pigs were measured both at baseline, and when diseased. To date, the results are still blinded. Each measurement contained 1 to 3 heart beats, recorded in a parasternal long-axis view. We used a custom-programmed research scanner (SonixTOUCH, Ultrasonix/Analogic Ultrasound, Richmond, BC, Canada) with DAQ raw data acquisition module for offline data processing. The transmission consisted of a 1.5 cycle pulse at 2.5 MHz, radiating in a diverging beam from the probe (75° effective opening angle). A full frame was produced from each single transmit, yielding a frame rate of approximately 4,000 frames / second. The frames were processed with an IQ-based correlation technique and smoothed to obtain the local tissue displacement [2]. Wave phenomena in the intraventricular septum are displayed in a 2D map of tissue displacement as function of time and position [2]. Various techniques were tested to extract the wave propagation velocity (via manual tracking, cross-correlation, and Hough transform) and wave dispersion (via 2D Fourier transform) from this map.

Results: Out of 27 recordings, 22 recordings resulted in estimates of wave velocities. After aortic valve closure, mechanical waves were readily visible in the processed data, and could be extracted by all techniques listed above, yielding median velocities of 3.6 m/s (50% interval: 3.2 m/s – 4.4 m/s). This is close to values found earlier with active shear wave detection in healthy pigs (4.1 m/s, [3]). In 4 out of 22 recordings the wave dispersion closely followed an analytical prediction of Lamb waves in the septum [1, 4], while the remaining recordings showed large discrepancy. The discrepancy was generally caused by various co-existing waves. After mitral valve closure, wave phenomena were more difficult to assess automatically, and up to now only manual tracking resulted in stable velocity estimation. The median propagation velocity of these waves was 2.1 m/s (50% interval: 1.7 m/s – 2.8 m/s), larger than values reported earlier for healthy pigs (1.4 m/s, [3]). In general, the propagation velocities were found to be larger than expected from the Lamb wave model.

Conclusions: Mechanical waves in the septum after aortic valve closure were easily visible and their velocity could be detected automatically, while spurious signals during mitral valve closure inhibited automated detection and classification of these waves. The origin and nature of the mechanical waves in the septum still need to be elucidated.

References:
[1]   Kanai: IEEE T Ultrason Ferr; 52, pp. 1931-1942, 2005.
[2]   Brekke et al.: Ultrasound Med Biol; 40, pp. 222-231, 2014.
[3]   Hollender et al.: Ultrasound Med Biol; 38, pp. 1271-1283, 2012.
[4]   Nenadic et al.: Phys Med Biol; 56, pp. 6723-6738, 2011.

005 **3-D SPECKLE TRACKING WITH TWO-PASS PROCESSING AND PHASE-ROTATED CORRELATION COEFFICIENT FILTERING FOR 4-D ECHOCARDIOGRAPHIC STRAIN ESTIMATION.**

Emily Y. Wong[1]*, Colin B. Compas[2], Ben A. Lin[2], Albert J. Sinusas[2], James S. Duncan[2], Matthew O'Donnell[1].
[1]University of Washington, Seattle, Washington, USA; [2]Yale University, New Haven, Connecticut, USA.

Background: In 4-D echocardiography (4DE) strain estimation using speckle tracking, large interframe strains resulting from moderate volumetric frame rates can cause significant peak hopping artifacts. Conventional correlation filters applied spatially at constant lags are effective for reducing peak hopping in low strain cases, but can exacerbate false peak artifacts when large strains are present. Alternatively, a tilted method of filtering correlation coefficients can correct for strain-induced incoherence across the correlation function by applying phase rotations in accordance with the local strain distribution prior to filtering [1]. As well, an iterative or multi-pass process for speckle tracking, using displacement estimates from the previous pass as the initial guess for a subsequent pass, can improve displacement accuracy.

Aims: The goal is to reduce peak hopping artifacts in 3-D speckle tracking using a two-pass approach combined with 3-D tilt filtering.

Methods: 4DE data were acquired in an open chest canine at six weeks following surgical coronary occlusion using a commercial 2-D phased array. Initial estimates were obtained using a combined 3-D tracking method, which integrated displacements from 3-D phase-sensitive correlation-based speckle tracking and 3-D shape tracking in an adaptive manner based on local confidence values. Tilt filtering was applied in first- and second-pass speckle tracking, where the coefficients of the 3-D normalized cross-correlation function were filtered in 3-D space at constant lags following phase rotation according to the local strain estimate from the combined method [1]. Second-pass tracking was performed with a small search region around the initial estimate (1 x 2 x 1 pixels (lateral x axial x elevational)).

Results: Tilt filtering reduced peak hopping compared to filtering without phase rotation. The most notable improvements were seen in the transitions zones where axial displacements had a high degree of variation along the orthogonal directions. In the transition zones, larger correlation filters without tilting exacerbated peak hopping, whereas larger tilt filters were able to overcome peak hopping artifacts (Figure 1). The lowest peak hopping was seen when both tilt filtering and multi-pass methods were applied.

Conclusions: Tilt filtering and two-pass processing can improve the quantification of myocardial deformation using 3-D speckle tracking and may be valuable in the assessment of cardiac function using echocardiography. The 3-D speckle tracking algorithms will be iteratively integrated into an adaptive 3-D motion tracking method to achieve robust, high-resolution strain quantification from 4DE data.

References: [1] Huang L, et al., "Phase rotation methods in filtering correlation coefficients for ultrasound speckle tracking," IEEE Trans Ultrason Ferroelectr Freq Control. 2009;56(7):1368-82.
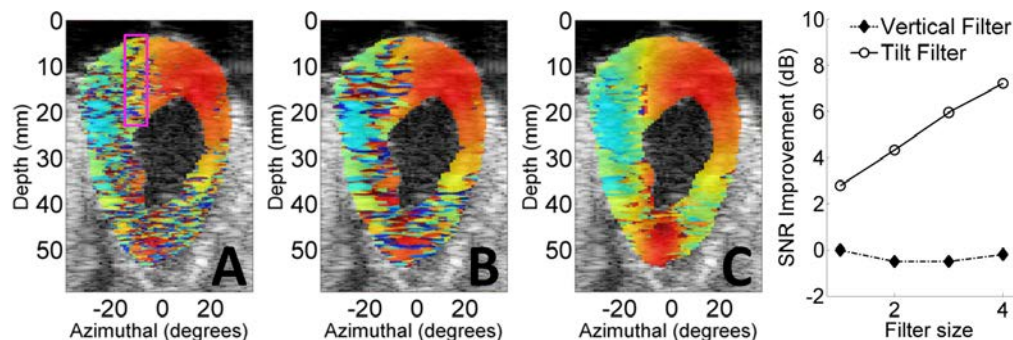
Figure 1. Myocardial axial displacement estimates from 3-D speckle tracking for the first-pass using (a) small and (b) large filters without phase rotation, and (c) second-pass using a large tilt filter. Graph shows SNR improvement with increasing filter size in the transition zone (magenta box), where SNR is defined as $10\log_{10}($[variance using small filter without phase rotation]/[variance using filter]).

056   IN VITRO VALIDATION OF VASCULAR ELASTOGRAPHY: FROM INFLATION TEST TOWARDS *IN VIVO* MEASUREMENTS

EJS Mascarenhas[1], MFJ Peters[1], MCM. Rutten[1], FN van de Vosse[1], RGP Lopata*[1.]
[1]Eindhoven University of Technology, Eindhoven, THE NETHERLANDS.

Background: Rupture of aortic aneurysms (AA) is a major cause of death in western countries. Currently, clinical decision upon surgical intervention is based on maximum diameter measurement, which is proven to be an unreliable criterion [1]. From a biomechanical perspective, rupture of AA occurs when wall stress locally surpasses the strength of the wall. Thus, noninvasive assessment of the elastic properties of the vessel wall by means of vascular ultrasound (US) elastography might be a better indicator for AA growth and rupture risk. US elastography has been introduced to estimate material properties in coronaries, carotids and aortas [2-4]. To validate these *in vivo* elastography measurements, *ex vivo* inflation testing of aortas was performed and validated using bi-axial tensile testing [5].

Aims: To estimate the mechanical properties of the aortic wall, using inflation testing and 2D US elastography, and investigate the performance of the method for physiological conditions.

Methods: Twelve porcine aortas were mounted in an experimental setup filled with physiological saline solution at a set temperature of 37°C. A physiological longitudinal pre-stretch of 1.22 was applied to all aortas. Two different types of *in vitro* inflation US-experiments were performed: 1) a static US-experiment, wherein the elasticity of the aortic wall was tested for a complete pressure range (0 – 140 mmHg) for uniform steps in strain (1.2 %); 2) a dynamic experiment in a sophisticated mock circulation setup in which the aorta was subjected to physiological pressures closely mimicking the *in vivo* hemodynamics (70 – 130 mmHg). One longitudinal and two cross-sectional 2D US datasets were acquired for both experiments using a Mylab70 US scanner equipped with a 7MHz linear array probe and RF interface (Esaote, NL). The RF-data were manually segmented, yielding the initial wall thickness and diameter. RF-based 2D displacement tracking [5] was applied to all datasets to obtain the diameter as a function of time. A linear elastic, isotropic material model (Neo-Hookean) was chosen to describe the mechanical behavior. The shear modulus G was estimated. In addition, an incremental study based on the static data was performed to: 1) investigate the changes in G for increasing mean arterial pressure (MAP) for a certain pressure difference (30, 40 and 50 mmHg), and, 2) compare the results with those obtained from the analysis of the dynamic US data sets, taking into account the same physiological pressure range.

Results: The resulting shear moduli G were 100 ± 18 kPa for the static experiment, which is in agreement with a previous study [5]. The dynamic data revealed a G of 263 ± 20 kPa. In general, a linear dependency on MAP was found for G in the incremental analysis, however, the effect of the pressure difference was negligible. For the same pressure range, the incremental shear modulus (G_{inc}) was 252 ± 41 kPa and good agreement was found with the dynamic US-experiment, using Bland-Altman analysis. However, the dynamic US-experiment revealed a higher precision reproducibility. In all experiments, no significant differences were found in G between the different image planes, with the exception of the two cross-sections during dynamic testing (paired sample Student's t-test, p-value=0.01<0.05).

Conclusions: In this study, 2D US elastography of aortas during inflation testing is feasible under controlled and physiological circumstances. Dynamic moduli were estimated with low variability (< 10%) and were in good agreement with standard inflation tests (bias < 11 kPa). In future studies, the *in vivo*, dynamic experiment should be conducted for a range of MAPs and pathological vessels should be examined. Furthermore, the use of more complex material models needs to be considered to describe the non-linear behavior of the vascular tissue.

References:
[1] Choksy et al.: Ruptured abdominal aortic aneurysm in the Huntingdon district: A 10-year experience. Annals of The Royal College of Surgeon of England. 81(1), pp. 27-31, 1999.
[2] de Korte et al.: Morphological and Mechanical Information of Coronary Arteries obtained with Intravascular Elastography; Feasibility Study *in vivo*. European Heart Journal, 23(5), pp. 405-413, 2003.
[3] Ribbers et al.: Noninvasive Two Dimensional Strain Imaging of Arteries: Validation in Phantoms and Preliminary Experience in Carotid Arteries *in vivo*. Ultrasound in Medicine and Biology, 33(4), pp. 530-540, 2007.
[4] Fromageau: Noninvasive Vascular Ultrasound Elastography applied to the Characterization of Experimental Aneurysms and follow-up after Endovascular Repair, Physics Med Biol., 30(9), pp. 1173-83, 2008.
[5] Lopata et al.: Vascular Elastography: A Validation Study, Ultrasound Med Biol., 40(8), pp. 1882-95, 2014.

002 FATTY PLAQUE PHANTOM FOR ULTRASOUND IMAGING

Renate W. Boekhoven[*][1], *Marcel C.M. Rutten*[1], *Frans N. van de Vosse*[1], *Richard G.P. Lopata*[1].
[1]Eindhoven University of Technology, Den Dolech 2, Eindhoven, THE NETHERLANDS.

Background: Prior to the clinical application of novel techniques, such as vascular elastography and photo acoustic imaging, validation studies are of great importance. Gelatin, agar and polyvinyl-alcohol (PVA) phantoms are commonly used. However, more realistic phantoms are needed with complex geometry and different constituents, such as lipids, all with known properties.

Aims: To design and construct a fatty plaque phantom (fPP) which is ultrasound compatible.

Methods: A 15 weight percent (wt%) PVA solution was made, and 1 wt% of silica scatters was added (3 –8 nm). The solution was poured into a custom-designed fPP mold. The outer wall (2.5 mm) was freeze thawed in two cycles of 16/8 hrs at -4°C / 24°C, respectively. After 2 freeze / thaw cycles, porcine lard was injected. The structure was kept in the fridge for 30 minutes for the lard to set. Next, PVA was added and the luminal mold was inserted, to create a second layer of 0.5 mm, resulting in a total wall thickness of 3 mm, and luminal diameter of 5 mm, including a cap covering the lipid pool. The maximum wall thickness of the fatty plaque was 3.5 mm. RF-data were acquired using a MyLab70 (Esaote, NL) during dynamic pressurization (0-80 mmHg). Next, a 3D echo-CT strain imaging method (Boekhoven et al. 2013a-c) was used to determine 3D geometry, distension and radial strains.

Results: B-mode data revealed the different layers and fat inclusion in the phantom (Fig. 1a) and good natural echogenicity of the lard. Distension of the different regions, as revealed in Figure 1a and b, indicates that the distension of the healthy part, region i and iii, are similar. Distension of the fatty region is significantly larger, due to the soft lipid inclusion. Radial strains are shown (at end-systole) in both longitudinal and transverse (reconstructed) cross-sections, and in 3D (Fig. 1c). Radial strains revealed the typical $1/r^2$ relation. In accordance with the distension data, higher radial strains were found at the lipid inclusion location. The relatively low strain at the tip of the lipid inclusion is due to the high speckle density, causing strain underestimation.

Conclusions: In future work, strain data will be compared to numerical models that match the phantoms and experimental conditions to validate the strains measured. Additional stiffening of the PVA using a coagulation bath will be explored to increase the systolic pressure. Furthermore, fiber-enforced materials are currently investigated.
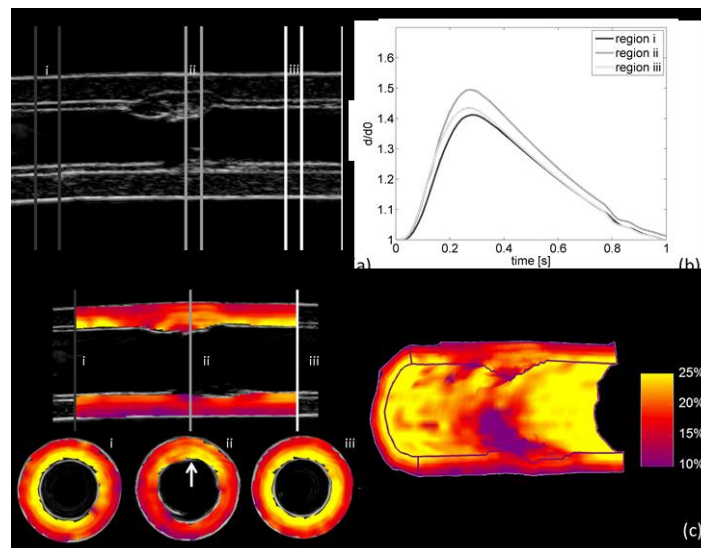
Figure 1, (a) longitudinal B-mode cross-section of the fatty plaque phantom, regions i-iii indicate the diameter stretch in (b);
(c) strain renderings of the transverse cross-sections in full 3D, both at maximum pressure. The arrow indicates a lipid inclusion.

References: [1] van den Broek et al.: Biomech Model Mechanobiolog, 2011. [2] Lopata et al.: UMB, 2009.

007 **INTRAVASCULAR ARFI TRANSDUCER FOR ELASTICITY IMAGING OF CORONARY ARTERIES.**

Carl D. Herickhoff[1]*, Jeremy J. Dahl[1].
[1]Duke University, Durham, NC, USA.

Background: Coronary heart disease (CHD) affects 15.4 million people [1] and is the leading cause of death in the U.S. [2]. CHD involves a buildup of plaque along the vessel wall, which results in a narrowing and hardening of the arteries (atherosclerosis), restricting the supply of blood and oxygen to the heart muscle. Vulnerable plaques, characterized by a thin fibrous cap and a soft, lipid-rich necrotic core, are prone to rupture and can eventuate in a heart attack or stroke [3]. Our long-term goal is the development of an IVUS probe capable of high-resolution acoustic radiation force imaging in the coronary arteries to identify and characterize vulnerable plaque [4].

Aims: The aim of this work is to simulate and demonstrate a prototype transducer capable of generating sufficient acoustic radiation force (ARF) and displacement for elasticity imaging in coronary vessels.

Methods: Our design concept augments a 3.5-Fr, 0.75-mm long cylindrical phased array of a Volcano Eagle Eye IVUS catheter with a 2.2-mm long cylindrical transducer to generate ARF pushes. Field II was used to simulate a 10-µm maximum ARF displacement at a range of 1 mm from the 2.2-mm long transducer operating at 6 MHz; the original Volcano IVUS phased array was then used at 20 MHz to track and create an image of the resulting scatterer displacement using correlation-based methods.
A prototype transducer was fabricated from a 4.6-Fr tube of radially-poled PZT-4 (Morgan Advanced Materials, Windsor, Berkshire, UK), which was the smallest piezoceramic cylinder commercially available nearest to 3.5 Fr. The tube was cut to a length of 2.2 mm with a dicing saw (DAD 3220, Disco USA, Santa Clara, CA), bonded to a length of stainless steel needle tubing, and electrically connected to a micro-coaxial cable (TE Medical, Wilsonville, OR). Measurements of the acoustic field were taken at a range of 6mm using a membrane hydrophone in a water tank to determine optimal drive frequency. The transducer was then placed in contact with a gel phantom (2.9 kPa Young's modulus, 1.0 m/s shear wave speed) and driven by a Verasonics system at 7.5 MHz, with a peak-to-peak drive amplitude of 96V.

Results: Our simulation's tracking pulses measured a 5.6-µm peak displacement from the actual 10-µm displacement (Figure 1). The prototype transducer tracked an average maximum displacement of 19.6 µm (σ = 6.0 µm) at a range of 5.1 mm when using a 111-µs long, 7.5-MHz pushing pulse (Figure 2).

Conclusions: Our simulation demonstrated that a Volcano IVUS array could achieve acceptable spatial resolution and measurement of displacement generated by a cylindrical transducer element. The correlation-based tracking measured a 5.6-µm peak displacement—an underestimation of 44% (consistent with underestimation by current radiation force methods—approx. 45-50%). The 4.6-Fr cylindrical prototype transducer was able to generate and track an average displacement of 19.6 µm at a range of 5.1 mm in an elasticity phantom, indicating a sufficiently-high level of radiation force. These results demonstrate that intravascular radiation force imaging is feasible on IVUS-sized devices.

References: [1] AS Go, D Mozaffarian, et al.: Heart Disease and Stroke Statistics, 2014 Update. American Heart Association – Circulation. Published online Dec 18, 2013. [2] KD Kochanek, JQ Xu, et al.: Deaths: Final Data for 2009. National Vital Statistics Reports. 60(3), 2011. [3] AV Kinn, M Nakano, et al.: Concept of Vulnerable/Unstable Plaque. Arterioscl Throm Vas. 30 pp. 1282-92, 2010. [4] V Patel, JJ Dahl, et al.: ARFI Imaging on an IVUS Circular Array. Ultrason Imaging 36(2) pp. 98-111, 2014.
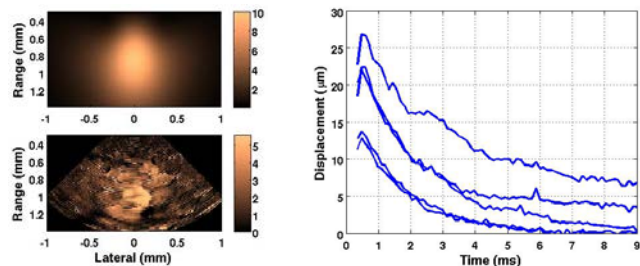
Figure 1: [top] Input displacement profile, brightness scale in µm. [bottom] Field II simulated ARFI displacement image using 20-MHz Volcano IVUS array.

Figure 2: Displacement vs. time data at 5.1 mm depth (5 acquisitions) for 2.2-mm, 4.6-Fr cylindrical prototype.

032 **MECHANICAL CHARACTERIZATION OF ASCENDING THORACIC AORTIC ANEURYSMS USING 4-D ULTRASOUND.**

Emiel M. J. van Disseldorp[1]*, Jan Nijs[2], M. Erwin S.H. Tan[3], Marc R. van Sambeek[4], Frans N. van de Vosse[1], Richard G.P. Lopata[1].
[1]Eindhoven University of Technology, Department of Biomedical Engineering, Eindhoven, THE NETHERLANDS; [2]University Hospital Brussels, Center for Aortic and Cardiovascular Connective Tissue Disease, Brussels, BELGIUM; [3]Catharina Hospital Eindhoven, Department of Cardiothoracic Surgery, Eindhoven, THE NETHERLANDS; [4]Catharina Hospital Eindhoven, Department of Vascular Surgery, Eindhoven, THE NETHERLANDS.

Background: Aortic aneurysms are a hazardous, asymptomatic condition and the 13th cause of death in Western society. The major complication of aneurysms is rupture, which leads to death in 75 to 90% of all cases[1]. Surgery is recommended for aneurysms with a diameter exceeding 5.5 cm and for small aneurysms if the aneurysm has grown over 1 cm in the last year[2]. However, this method has proven to be inadequate as a criterion for intervention planning. Hence, a new approach for rupture risk assessment is needed. The aneurysm will rupture if the mechanical stress exceeds the local strength of the vessel wall. Therefore, the state of the aortic wall (i.e. the mechanical properties) will be a better predictor for rupture risk.

Aims: To characterize the mechanical properties of the aortic wall, using 4D ultrasound (US) *in vivo*. This characterizationis based on a patient specific finite element model (FEM) that is fit to the US-based motion data. This study is focused on aneurysms in the ascending thoracic aorta (ATAAs).

Methods: 4D US data were collected for five patients who underwent graft replacement surgery. The US data were acquired using a 3D phased array probe for transesophageal echocardiography and captured by 4 beats ECG triggered full volumes with a frame rate of 30-36 Hz.
The 4D US data were segmented manually at diastolic pressure in order to determine the geometry of the ATAA. To avoid sharp edges in the geometry, an in-house developed smoothing algorithm was applied. This smoothed geometry was subsequently used as input for the US tracking algorithm.
For the FEM, the same geometry was converted into a quadratic tetrahedral element mesh. A Neo-Hookean model was calculated explicitly using a hybrid element formulation accounting for incompressibility. A backward incremental method was used to determine the initial wall stress at diastolic pressure. Finally, the *in vivo* shear modulus was found by optimizing the model using a Gauss-Newton optimization method for different shear moduli until the difference between simulated and measured displacements was < 5%. Finally, the shear modulus estimated using the FEM/US method was verified by a direct estimation of the shear modulus, using a Laplace approximation of the stresses, based on the diastolic and systolic geometry and pressures in the ATAA.

Results: The resulting shear moduli from the FEM/US tracking method were 272 ± 104 kPa. The moduli estimated directly from the US – pressure data were 294 ± 64 kPa. In one case, the two methods showed poor agreement, 150 vs. 332 kPa, however, in the other four cases a good correspondence was found.

Conclusions: In this study, a combined FEM/US-approach was introduced that showed the feasibility of *in vivo* characterization of ATAAs. A good agreement was found for the incremental shear modulus between the two methods, although the standard deviation between samples is relatively high. This is presumably caused by the patient specific pathogenic state of the aortic wall.
In future work, the complexity of the material model will be increased, as well as the number of patients included. Finally, verification of the *in vivo* results needs to be performed, using mechanical testing

References:
[1] T.Gasser, A. Nchimi, J. Swedenborg, J. Roy, N. Sakalihasan, D. Böckler, A. Hyhlik-Dürr: A Novel Strategy to Translate the Biomechanical Rupture Risk of Abdominal Aortic Aneurysms to their Equivalent Diameter Risk: Method and Retrospective Validation; European Journal of Vascular and Endovascular Surgery., 47,(3), pp. 288-295, 2014.
[2] K.Khanafer, A. Duprey, M. Zainal, M. Schlicht, D. Williams and R. Berguer: Determination of the Elastic Modulus of Ascending Thoracic Aortic Aneurysm at Different Ranges of Pressure using Uniaxial Tensile Testing; The Journal of Thoracic and Cardiovascular Surgery., 142,(3), pp. 682-686, 2011.

057   **BEAM-FORMING CHOICES: WHAT ARE THEY, HOW DO THEY WORK, AND WHAT IS THEIR IMPACT FOR ELASTOGRAPHY**

Marvin M. Doyley[1].*
[1]University of Rochester, Rochester, NY, USA.

Background and overview of presentation: Elastography is traditionally performed using only the axial component of displacements because ultrasound cannot measure the lateral component precisely without substantially sacrificing temporal and/or spatial resolution. However using faster ultrasound scanning techniques and advanced beam-forming methods, we can now measure the lateral component of displacements with high precision while maintain temporal and spatial resolution. In this tutorial, we review the general principles of ultrasound beam-forming. More specifically, we discuss

(a) the delay-and-sum and minimum variance beam-forming methods,

(b) ultrafast imaging techniques such as plane-wave,

(c) beam-forming methods which can work with plane-wave echo data, such as synthetic aperture imaging, and

(d) choices for the apodization function.

We also provide clinical and phantom examples to illustrate how different beam-forming strategies influence elastographic imaging.

Conclusion: Improvements in ultrasound imaging systems and beam-forming methods is revolutionizing elastography. Future elastographic systems need not be limited to using only the axial component of displacement, and yet may retain high frame rate and good spatial resolution.

036   ***IN VIVO* ARFI SURVEILLANCE OF SUBCUTANEOUS HEMORRHAGE (ASSH) FOR MONITORING RCFVIII DOSE RESPONSE IN HEMOPHILIA A DOGS.**

Rebecca E. Geist[1]*, Timothy C. Nichols[2,3], Elizabeth P. Merricks[3], Melissa C. Caughey[2], and Caterina M. Gallippi[1,4,5].

[1]UNC-NCSU Joint Department of Biomedical Engineering, [2]UNC Department of Medicine, [3]UNC Department of Pathology and Laboratory Medicine, [4]UNC Department of Radiology, [5]NCSU Department of Electrical and Computer Engineering, University of North Carolina at Chapel Hill, Chapel Hill, North Carolina, USA

Background: Bleeding is a frequent and deadly complication of hematologic and cardiovascular disorders. To control bleeding in inherited bleeding disorders, innovative therapeutic proteins, e.g., recombinant factor VIII (rFVIII), are available for replacement therapy for hemophilia A. However, translating such treatments from clinical trials to optimal dosing regimens for clinical use is challenged by insufficient assays for *in vivo* dose response.

Aims: A new *in vivo* hemostasis assay, ARFI Surveillance of Subcutaneous Hemorrhage (ASSH), has previously been demonstrated to distinguish bleeding phenotype between normal and naïve hemophilia A dogs. The purpose of this investigation is to evaluate ASSH for monitoring dose response. *We hypothesize that ASSH will differentiate bleeding phenotype in hemophilia A dogs treated with different levels of rFVIII.*

Methods: The UNC-CH IACUC approved all procedures. ASSH was performed using a Siemens SONOLINE Antares imaging system in association with a standardized, B-Mode-guided puncture of a ~2 mm diameter hind leg vein in 13 dogs (N=6 hemostatically normal, 7 hemophilia A). Hemophilia A dogs were examined in the naïve state and with three prophylactic treatment doses: infusion of rFVIII to approximately 3%, 10% and 100% of normal FVIII level. The ASSH observation period was 60 min following puncture, with serial ARFI data acquisitions every 1 to 5 min. Acquired raw RF data were processed with one-dimensional cross-correlation to measure axial displacement, and displacement variance in response to ARFI excitation discriminated hemorrhagic pixels. Then, from the hemorrhagic area temporal dynamics, ASSH bleeding rate (BR) and time to hemostasis (TTH) were estimated. ASSH was performed in each dog at each dose level with 2 repeated measures at least 2 weeks apart.

Results: Fig. 1A shows ASSH TTH dichotomized to normal (10-30 min) and abnormal (>30 min) outcomes in all dog cohorts. The percent within each cohort with abnormal TTH (red) progressively decreased with increasing rFVIII dose. Fig. 1B depicts box plots describing ASSH BR per cohort. The median BR decreased with increasing dose, although only the naïve hemophilia A and 100% rFVIII treatment levels exhibited statistically different BRs ($p < 0.05$).
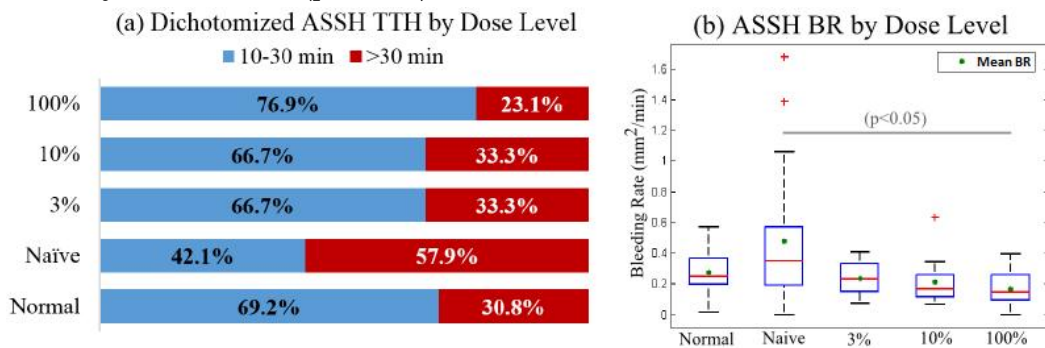
Figure 2: ASSH TTH and BR by Dose Level: (a) percent of abnormal (>30 min) TTH decreased with increasing rFVIII dose. (b) Median BR decreased with increasing rFVIII dose, with statistically different (p<0.05) BR between naive and 100% treatment levels.

Conclusions: There was an observable difference between the naïve and 100% treatment level in BR, but not the 3% or 10% treatment levels. This suggests that ASSH may be relevant for differentiating responses to different treatment levels.

021 **AGE-DEPENDENT EVOLUTION OF NATURAL BRAIN TISSUE PULSATILITY: A CLINICAL ULTRASOUND STUDY.**

R. Ternifi [1], G. Chassagnon [2,3], C. Destrieux [1,4], F. Patat [1,2,3], J.P Remenieras* [1].

[1]Université François-Rabelais de Tours, Inserm, Imagerie et Cerveau UMR U930, Tours, FRANCE; [2]CHRU de Tours, pôle imagerie, Tours, FRANCE; [3]Inserm CIC 1415, Tours, FRANCE; [4]CHRU de Tours, service de neurochirurgie, Tours, FRANCE.

Background: Cerebral pulsatility is mainly related to arterial beat during the cardiac cycle, intracranial pressure and tissue elasticity. However, the relationships between the mechanical cerebral tissue properties and natural aging have been barely studied.

Aims: The purpose of this study was to assess the relation between cerebral pulsatility and aging, using estimation of cerebral tissue movements by ultrasound (US).

Methods: Forty healthy volunteers aged from 20 to 80 years old were included. Every volunteer had 4 US tissue Doppler acquisitions centered on the Basilar artery in a transverse plane via the right temporal acoustic window. We used a homemade transcranial linear probe comprising 128 elements with a center frequency of 2.8 MHz. A brain imaging platform was developed by connecting a neuronavigation system (BrainLab®) with an US system (Aixplorer®) to spatially locate the regions of measured pulsatility. The Aixplorer allowed us to make fast ultrasonic acquisitions varying from 100 Hz to 1 kHz. Besides, the superposition of MRI and US images in real time allowed us to precisely identify the regions of interest. The determination of tissue displacement u, and strain ε along the ultrasonic axis was calculated by extended autocorrelation algorithm from ultrafast complex signal IQ data. We implemented two criteria to differentiate between artifacts and tissue pulsatility. We estimated the maximum value of u_{max} and ε_{max} peak to peak time-averaged after segmentation of 10s cycles, which corresponds to a 1s elementary cardiac cycle.

Results: Our results show a significant correlation of estimated u_{max} and ε_{max} with age (Figure 1). These two parameters decreased significantly with age, from u_{max} and ε_{max} of 71.21μm and 2.70% for 20 year old, down to 22.80μm and 0.93% for 78 year old, respectively.

Conclusions: Together, these results suggest that brain tissue pulsatility ranges widely with a stiffening of cerebral arteries and are significantly age-dependent. Biomechanical analysis tools for brain study seem to be a prerequisite for clinically valuable conclusions.

Keys word: Tissue pulsatility imaging, Strain imaging, Neuronavigation, Brain aging.
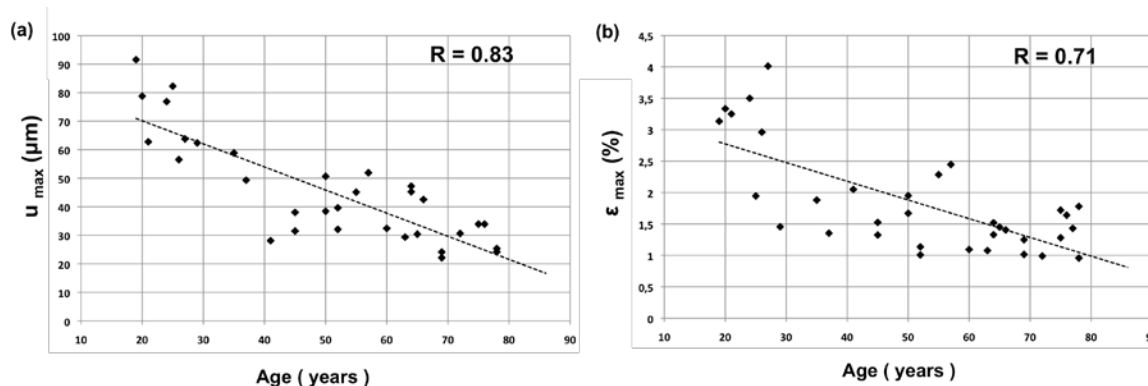
Figure 1: Brain tissue pulsatility as a function of age. (a) The maximum tissue displacement u_{max} decreases significantly with age. (b) The maximum strain tissue ε_{max} decreases significantly with age.

References:
[1] Krejza et al.: Transcranial Color Doppler Sonography of Basal Cerebral Arteries in I 82 Healthy Subjects: Age and Sex Variability and Normal Reference Values for Blood Flow Parameters. American Journal of Roentgenology. pp. 213-218, 1999. [2] Kiening et al.: Assessment of the Relationship between Age and Continuous Intracranial Compliance. Acta Neurochir. 95, pp. 293–297,2005. [3] Atsumi et al.: Measurements of Intracranial Pressure and Compliance Index using 1.5-T clinical MRI Machine. Tokai J Exp Clin Med., 1, pp. 34-43, 2014.

053 **VISCOELASTICITY AS A BIOMARKER OF CELL DEATH: A COMPARISON WITH ADC IN AN ORTHOTOPIC BREAST CANCER XENOGRAFT MODEL.**

Jin Li[1], Yann Jamin[1], Jessica KR Boult[1], John C Waterton[2], Ralph Sinkus[3], Michelle D Garrett[1], Jeffrey C Bamber[1]*, Simon P Robinson[1]
[1]Institute of Cancer Research and Royal Marsden NHS Foundation Trust, London, England, UK; [2]AstraZeneca, Macclesfield, England, UK; [3]King's College London, King's Health Partners, St Thomas' Hospital, London, England, UK.

Background: Recent pre-clinical investigations with magnetic resonance elastography (MRE) show reductions in tumour elasticity and viscosity following treatment with conventional chemotherapy or vascular disrupting agents, associated with a pathologically-confirmed reduction in cell proliferation and increased necrosis [1-3]. Quantitation of the tumour apparent diffusion coefficient (ADC), measured by diffusion-weighted imaging (DWI), is also being evaluated as an oncology imaging biomarker [4,5], where treatment-induced tumour necrosis typically causes ADC to increase. In evaluating novel MRE biomarkers, pathological validation and correlation with established biomarkers is needed [6].

Aims: To compared the relationship between change of (a) MRE, (b) DWI and (c) pathology, of orthotopically propagated BT474 breast cancer xenografts during tumour progression and/or treatment with the novel multi-kinase inhibitor AT13148, previously shown to induce apoptosis in this model [7].

Methods: All experiments were performed in accordance with the UK Animals (Scientific Procedures) Act 1986. BT474 breast carcinoma cells were injected subcutaneously in the mammary fat pad of female NCr nude mice. A 7T MicroImaging horizontal MRI system (Bruker Instruments) was used to acquire 3D MRE data from anaesthetised mice bearing size-matched tumours prior to, and 24h after, treatment with either 40mg/kg AT13148 p.o. (n=6) or vehicle alone (n=6). A spin-echo sequence modified with sinusoidal motion-sensitizing gradients was used, synchronized to a continuous 1kHz wave applied via a square piston to the tumour. Maps of the magnitude of complex shear modulus $|G^*|$, elasticity G_d, viscosity G_l, shear wave attenuation α, and shear wave speed c_s were reconstructed with an isotropic pixel size of 300µm, and mean values were determined from the whole tumour from two central slices. Diffusion-weighted images (TE/TR=32/1500ms, b values=200, 300, 500, 750, 1000 s/mm-2, three 1mm thick slices) were also acquired for determination of tumour ADC. Following the post-treatment scan, tumours were excised, formalin fixed, and paraffin-embedded sections cut and stained with haematoxylin and eosin (H&E) and picrosirius red for the histological assessment of necrosis and collagen respectively.

Results: The hyperintense T2-weighted signal was associated with a region of dying cells, with the pattern of cell shrinkage, cell-cell membrane detachment and maintenance of collagen revealed by histology (Fig. 1). The spatial distribution of $|G^*|$ and ADC were closely associated with the T2-weighted image contrast, with reduced $|G^*|$ and elevated ADC within the T2-weighted hyper-signal area. Changes in $|G^*|$, G_d, G_l, c_s and ADC for each tumour over 24 hours were significantly correlated with the change of the % hyper-signal area, with the MRE biomarkers showing a higher significance, although correlation with change in tumour ADC was not significant (Fig. 2).
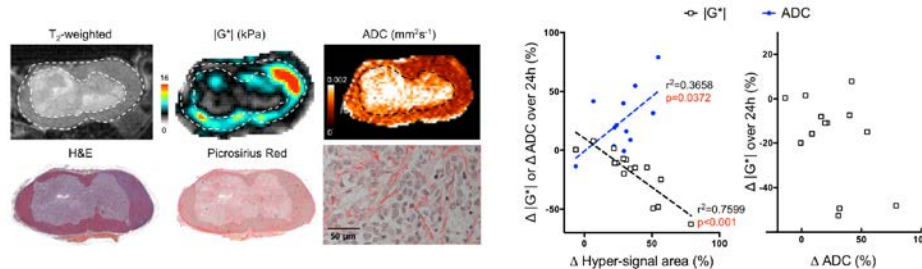
Figure 1   Figure 2

Conclusions: Both the MRE measured tissue viscoelastic properties and ADC are robust imaging biomarkers of cell death, and may interrogate different biophysical characteristics. $|G^*|$ is a potentially earlier biomarker of cell death than ADC.

References: [1] Juge et al., Radiology;264(2):436-44, 2012. [2] Pepin et al., Mag Res Med; in press. [3] Li et al, Proc ISMRM; 1049, 2013. [4] Padhani et al., Neoplasia;11:102-25, 2009. [5] Sinkus et al, Eur J Cancer; 48:425-31, 2012. [6] Waterton and Pylkkanen, Eur J Cancer; 48:409-15, 2012. [7] Yap et al., Clin Cancer Res;18:3912-23, 2012.

* indicates Presenter

049 **INVESTIGATING THE EFFECT OF PIA ON THE YOUNG'S MODULUS MEASUREMENTS OF GREY AND WHITE MATTER IN *EX VIVO* PORCINE BRAINS USING SHEAR WAVE ELASTOGRAPHY.**

Huan Wee Chan[1,2]*, Chris Uff[2], Aabir Chakraborty[3], Neil Dorward[2], Jeffrey C Bamber[1]
[1]Institute of Cancer Research and the Royal Marsden NHS Foundation Trust, London, England, UK; [2]The National Hospital for Neurology and Neurosurgery, London, England, UK; [3]Southampton General Hospital, Southampton, England, UK.

Background: Brain is composed of grey and white matter. White matter is thought to be stiffer than grey matter because it contains axons, which are myelinated nerve fibres aligned in a compact fashion. In contrast, grey matter contains neurons, which are nerve cell bodies arranged sparsely. Young's modulus (YM) measurements of grey and white matter have been controversial, with some studies showing lower grey matter YM [1,2] whilst some showing higher grey matter YM [3,4]. It is hypothesised that pia mater contributes to higher YM measurements in grey matter.

Aims: To investigate the effect of pia mater on the grey and white matter YM measurements.

Methods: Three post-mortem porcine brains were scanned using the SuperSonic Aixplorer® (Aix-en-Provence, France) with a 4-15 MHz linear array probe (SL15-4). In all 3 brains, the pia matter on one hemisphere was removed carefully (Figure 1). After that, the scans were acquired in the coronal plane with the brains immersed in warm saline solution of $37 \pm 1°C$. An example of the shear wave elastography (SWE) display is shown in Figure 2.

Results: Figure 3 showed that grey matter with pia mater had a significantly higher YM than that without (p = 0.011). There was no significant difference between the grey matter and white matter with or without pia mater, and between the white matter with and without pia mater.

Figure 1: The pia mater has been removed from the left hemisphere.
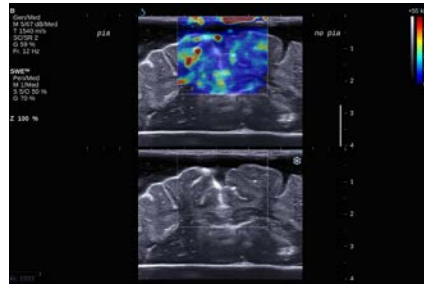
Figure 2: SWE display on the scanner with the pia absent on the right side of the scan.
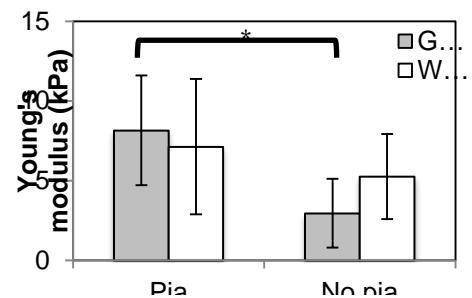
Figure 3: The YM measurements of grey and white matter with and without pia. *p = 0.011.

Conclusions: This study showed that pia mater resulted in significantly higher grey matter YM measurements. It also showed that the white matter had higher YM than grey matter without pia mater, which agreed with majority of the studies on ex-vivo samples when the pia mater was absent. Further validation with a mechanical rheometer is needed for confirmation of this finding.

References:
[1] Kruse et al.: Neuroimage 39, p. 231-7, 2008.
[2] Uffmann et al.: Proceedings of ISMRM, p. 1768, 2004.
[3] Green et al.: NMR in Biomedicine 21, p. 755-764, 2008.
[4] Uff et al.: Proc. ITEC, p. 116, 2010.

050 **DETECTING MRI-NEGATIVE EPILEPTOGENIC LESIONS WITH INTRAOPERATIVE SHEAR WAVE ELASTOGRAPHY.**

Huan Wee Chan[1,2]*, Chris Uff[2], Aabir Chakraborty[3], Neil Dorward[2], Jeffrey C Bamber[1]
[1]Joint Department of Physics, Institute of Cancer Research and the Royal Marsden NHS Foundation Trust, London, England, UK; [2]The National Hospital for Neurology and Neurosurgery, London, England, UK; [3]Southampton General Hospital, Southampton, England, UK.

Background: Focal symptomatic epilepsy is epilepsy with onset in a cerebral hemisphere, caused by an abnormality in the brain, known as an epileptogenic lesion, and is usually resistant to medical therapy. Up to 43% of these patients do not have identifiable lesions on magnetic resonance imaging (MRI) [1]. As the success rate of resective surgery in these patients depends on the extent of resection [2], it is important to detect these lesions on images that guide resection and electrode implantation for seizure monitoring. Intraoperative shear wave elastography (SWE) has been shown to successfully detect an MRI-negative lesion in a patient [3].

Aims: To determine the ability of intraoperative SWE in detecting MRI-negative epileptogenic lesions in further patients.

Methods: Four patients were included in the study (aged 7-49 years, M:F = 3:1). In addition to the standard epilepsy workup, including PET, SPECT and invasive EEG, intraoperative SWE was performed using SuperSonic Aixplorer® (SuperSonic Imagine, France) prior to placement of invasive electrodes. Linear (SL15-4; 4-15 MHz bandwidth) and sector transducers (SE12-3; 3-12 MHz bandwidth) were used for scan acquisitions in 2 patients each. Young's modulus (YM) measurements were performed using the in-built Q-box™ function. Surgical opinion of lesion stiffness relative to brain was obtained blind to the SWE measurements of YM.

Results: Epileptogenic lesions were visible in all 4 patients. The SWE appearances for all 4 patients are shown in Figures 1-4. All the lesions were graded surgically as stiffer than brain. The lesions were 3 focal cortical dysplasia (FCD) and 1 dysembryoplastic neuroepithelial tumour (DNT). Three of the lesions had YM of 74.7 kPa (FCD), 96.9 kPa (FCD), and 43.4 kPa (DNT), respectively, which agreed with stiffness grading. In contrast, 1 patient (FCD) had YM of only 22.5 kPa, which was less than brain although for this case there was particularly low confidence in the YM measurement in brain with high SWE measurement noise (seen when the SWE gain was put to 100%). Nevertheless, the lesion was clearly visible as a noise-free region.
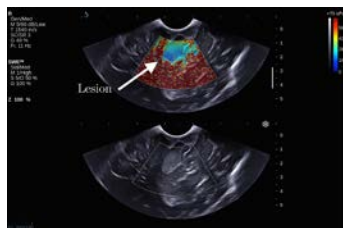
Figure 1: SWE for FCD case where YM of the lesion is less than brain.

Figure 2: SWE for FCD case delineating the lesion clearly.
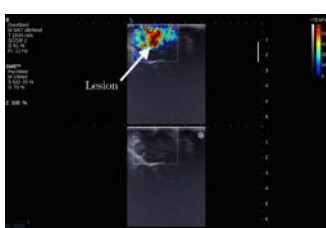
Figure 3: SWE for FCD case demonstrating the lesion clearly.
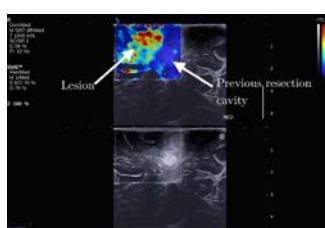
Figure 4: SWE for DNT case, where the lesion adjacent to previous resection cavity was clearly demonstrated.

Conclusions: This study showed that intraoperative SWE successfully detected MRI-negative epileptogenic lesions in 4 of 4 patients. When the SWE measurement quality was adequate, the YM contrast agreed with surgical finding. Unexplained low quality SWE measurements were sometimes obtained in brain, in which case the brain appeared artefactually stiff on the elastogram when the SWE gain was set too high. The results show the feasibility of SWE being used as an intraoperative adjunct for MRI-negative cases for guiding electrode placements and resection in the future.

References: [1] McGonigal et al.: Brain 130, p. 3169-3183, 2007. [2] Cohen-Gadol et al.: J Neurosurgery 101, p. 55-65, 2009. [3] Chan et al.: Epilepsia 55, p. e30-33, 2014.

003   **PHASE-SENSITIVE OPTICAL COHERENCE TOMOGRAPHY AND CODED ACOUSTIC RADIATION FORCE FOR SHEAR WAVE ELASTOGRAPHY.**

Thu-Mai Nguyen[1]*, Shaozhen Song[1,2], Bastien Arnal[1], Emily Y Wong[1], Ruikang K. Wang[1,3], Matthew O'Donnell[1].
[1]University of Washington, Department of Bioengineering, Seattle, WA 98105, USA;
[2]University of Dundee, School of Engineering, Physics and Mathematics, Dundee, Scotland, UK;
[3]University of Washington, Department of Ophthalmology, Seattle, WA 98104, USA.

Background: Optical coherence tomography (OCT) provides micron scale resolution and nanometer scale sensitivity. Thus, it has great potential for elastography, especially for ophthalmic applications (cornea and intraocular lens characterization).

Aims: We implemented a shear wave elastography method using ultrasound radiation force as a remote shear source and phase-sensitive OCT (PhS-OCT) for detection. We propose a pulse compression approach to increase the signal-to-noise ratio (SNR) of the detected shear wave. It spreads the instantaneous peak energy over a long coded emission, and then digitally compresses the recorded signal into a short, high-energy pulse.

Methods: A single-element transducer (frequency 7.5 MHz, Sonic Concept, Bothell, WA, USA) was driven with 3-ms long emission (peak pressure <3 MPa). The amplitude was modulated by a linear-swept frequency square wave (1 to 7 kHz, 50% duty cycle). The resulting shear wave was tracked using PhS-OCT at an equivalent frame rate of 44.8 kHz, with a pixel size of 4.15 μm x 23.4 μm (axial x lateral). An inverse filter was designed to digitally compress the shear wave, as described in [1]. Then, elastic maps were reconstructed using a time-of-flight algorithm. Results of the compressed coded excitation were compared to those of a standard excitation (200-μs burst).

Results: At a pressure of 3 MPa in a 0.5%-agarose phantom, a standard excitation gives a 16.8 dB SNR while the pulse compression (see Fig. 1) has a 46.5 dB SNR. In both cases, the shear wave speed was estimated to be 2.6 ± 0.4 m/s. At a pressure of 2 MPa, the standard excitation does not provide any significant signal (SNR = 1.1 dB) whereas pulse compression produces a 37.2 dB SNR.

Conclusions: We demonstrated that PhS-OCT and ultrasound radiation force can map the elasticity of tissue-mimicking phantoms. We implemented a pulse compression method that paves the way for shear wave generation at low ultrasound pressure. This is essential for ocular tissues where there are very restrictive limitations on ultrasound exposure according to FDA regulations. Further studies will aim at optimizing the transducer and the coded excitation for *in vivo* implementation.
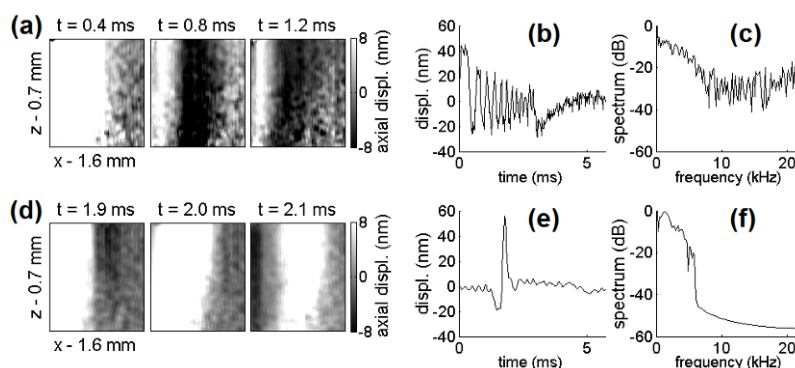
Fig. 1 – Frame-to-frame axial displacements in a 0.5%-agarose phantom obtained at a pressure of 3 MPa with coded excitation before *(a-c)* and after *(d-f)* compression. *(a,d)*: Snapshots of the shear wave propagation at different time steps. *(b,e)*: Temporal profile at one location. *(c,f)*: Normalized spectrum at one location. SNRs are respectively 14.3 and 46.5 dB before and after compression.

References:
[1] Nguyen et al.: "Shear Wave Pulse Compression for Dynamic Elastography using Phase-Sensitive Optical Coherence Tomography" J. of Biomed. Opt., 19, 016013, 2014.

055 **SHEAR-WAVE ELASTOGRAPHY USING MULTI-CHANNEL OPTICAL COHERENCE TOMOGRAPHY: A COMPARISON OF RELATIVE AND ABSOLUTE SHEAR-WAVE TIME OF FLIGHT METHODS.**

Eli Elyas[1], Alexander Grimwood[2], Janine Erler[3], Simon P Robinson[1], Thomas Cox[3], Daniel Woods[4], Peter Clowes[1], Jeffrey C Bamber[1]*

[1]Institute of Cancer Research and Royal Marsden NHS Foundation Trust, London, England, UK; [2]Royal Surrey County Hospital, Guildford, Surrey, UK; [3]University of Copenhagen, Copenhagen, Denmark; [4]Michelson Diagnostics, Orpington, Kent, UK.

Background: The cellular microenvironment plays a critical role in cancer initiation, progression, and the ability to invade and metastasise [1], with the stiffness of the extracellular matrix (ECM) regulating many cellular processes. Elastographic methods are well developed for macroscopic clinical imaging and provide useful information about pathological processes, which is complementary to that provided by conventional ultrasound, magnetic resonance imaging, etc. The extension of elastography to the microscopic level should ply the field of cellular biology with valuable information, and optical coherence tomography (OCT) offers a way to do this noninvasively with resolutions of the order of tens of μm and penetration depths of 1-2 mm [2]. We are evaluating the potential to develop microelastography using a commercial OCT scanner (Michelson Diagnostics VivoSight™) to measure the speed of shear waves propagating in a three-dimensional (3-D) medium, which would in eventual applications contain cells in culture. This paper extends previous work [3] by automating the shear wave speed measurement using a regularised method to track OCT speckle and by comparing two alternative approaches to speed measurement, one that uses absolute time of arrival (TOA) and another that uses a novel relative TOA measurement which takes advantage of parallel data acquisition and mimics important features of the method of supersonic shear wave elastography in medical ultrasound. In this study, both methods employed only the envelope-demodulated OCT signal, and simple synchronization signals, which were readily available without modifying the commercial OCT system.

Aims: To test an automated version of a novel parallel 4-channel OCT approach to shear-wave speed measurement using relative TOA and compare it with a single channel method based on absolute TOA.

Methods: A needle, embedded in a 5 mm thick gelatin layer containing optical scatterers, was excited to vibrate along its long axis with five-cycle bursts of a 500 Hz sinusoid. The displacement as a function of time and distance from the needle associated with the resulting shear waves was detected using four M-mode images acquired simultaneously using a commercial four-channel swept-source OCT system. Shear-wave TOA was detected for each channel and at each distance from the needle by tracking the axial OCT-speckle motion using cross-correlation methods. Shear-wave speed was calculated from inter-channel differences of TOA for a single burst (the relative TOA method) and compared with the shear-wave speed determined from positional differences of TOA for a single channel over multiple bursts (the absolute TOA method). Both methods were further evaluated by studying the increase in the measurement precision that may be gained at the expense of lateral resolution.

Results: Only the relative TOA method provided shear-wave speed with acceptable lateral resolution, precision and accuracy when judged against the expected linear dependence of shear modulus on gelatine concentration ($R^2 = 0.95$). Its performance was also independent of the quality of synchronization between shear excitation and OCT data acquisition; to be useful, the absolute method would require hardware and software modification of the commercial OCT system.

Conclusions: The relative multichannel TOA approach shows promise for the eventual provision of microelastography using a current commercial OCT system as a research tool in cancer cell biology. Further work is required to optimize parameters such as vibration frequency, burst length and amplitude, and to fully assess the lateral and axial resolutions as well as to create 3D elastograms.

References:
[1] Paszek MJ, et al., Tensional homeostasis and the malignant phenotype. Cancer Cell; 8:241–254, 2005.
[2] Kennedy BF, Kennedy KM, Sampson DD, A review of optical coherence elastography: fundamentals, techniques and prospects. IEEE J Selected Topics in Quantum Electronics; 99, 2013. [3] Elyas E, Erler J, et al., Potential for quantitative microelastography using a multi-channel optical coherence method, IEEE Ultrasonics Symposium (IUS), 2567-2570, 2012. [4] Bercoff GJ, Tanter M, Fink M, Supersonic shear imaging: a new technique for soft tissue elasticity mapping, IEEE Tans. UFFC; 51:396-409, 2004.

052   **UNWRAPPING PHASE IN SWEPT-SOURCE OPTICAL COHERENCE ELASTOGRAPHY USING A COMBINED CORRELATION METHOD.**

Alexander Grimwood[1], Jeffrey C Bamber[2]*.
[1]Royal Surrey County Hospital, Guildford, Surrey, UK; [2]Institute of Cancer Research and Royal Marsden NHS Foundation Trust, London, England, UK.

Background: Detecting phase shifts in the image signal from optical coherence tomography (OCT) systems has been demonstrated as a viable displacement estimation method [1]. However, unless phase unwrapping is employed, this confines displacement estimation to a magnitude of no more than half the image signal's carrier wavelength (typically 0.5 – 1.5 μm). Correlation based tracking of the amplitude demodulated OCT signal, on the other hand, is sensitive to large (greater than the coherence length) displacements but not very sensitive to sub-wavelength displacements [2]. We demonstrate a displacement estimation method incorporating the sensitivity of phase detection without having to explicitly unwrap the phase shift. This is achieved through a combined correlation tracking method analogous to one previously developed for ultrasound elastography [3].

Aims: The application of a combined correlation tracking method in OCT is demonstrated and its effectiveness is highlighted by comparison with a standard phase shift estimator.

Methods: M-mode images were acquired of a transverse wave passing through an agar phantom. The OCT system, actuation method and phantom have been previously described [4]. They comprise a commercially available OCT device, modified to enable M-mode acquisition synchronized to the generation of the transverse wave within the phantom via a shaker attached to a needle. For the time-dependent combined correlation displacement estimation, the amplitude and phase associated with sequential pairs of adjacent A-lines from the M-mode image are compared, where both signals are assumed equivalent except for a shift along the optical axis caused by an associated displacement induced by the arrival of the transverse wave. A rough estimate of displacement, ΔU, rounded to the nearest carrier half-wavelength, is made by identifying the absolute peak in the normalized cross correlation function between the two amplitude A-lines in any pair. Next, the phase shift, $\Delta \phi$, at this location is calculated and the two values are combined to produce a final displacement estimate, u:

$$u = \Delta U + \frac{\Delta \phi \; \lambda_c}{2\pi}$$

where $\Delta \phi$ is calculated in radians, and λ_c is the centre wavelength of the OCT source laser.

Results: For the phase detection technique, wrapping is observed in the image regions where axial displacement between A-scans is greater than the OCT's carrier wavelength. Combined correlation displacement maps demonstrate the technique's ability to track larger displacements, whilst remaining sensitive to those shifts smaller than the coherence length.

Conclusions: Combined correlation tracking is robust to inter A-line displacements larger than the wavelength. Potential limitations requiring further investigation arise from comparatively high noise in the envelope estimation, which reduces the sensitivity advantage of phase estimations. However, the method can still be used to combine the sensitivity of phase shift estimation with the displacement range of cross correlation.

References:
[1] Razani M, Mariampillai A, et al., Feasibility of optical coherence elastography measurements of shear wave propagation in homogenous tissue equivalent phantoms, Biomedical Optics Express; 3(5):972, 2012.
[2] Schmitt J, OCT elastography: imaging microscopic deformation & strain of tissue, Opt. Express; 3:199-211, 1998.
[3] Shiina T., Nitta N., Ueno E., Sum S. J., and Bamber J C., Real time tissue elasticity imaging using the combined autocorrelation method, J. Med. Ultrasonics; 29:119-128, 2002.
[4] Elyas E., Erler J., et al., Potential for quantitative microelastography using a multi-channel optical coherence method, IEEE Ultrasonics Symposium (IUS), 2567-2570, 2012.

012 **ANALYTICAL PHASE TRACKING BASED STRAIN ESTIMATOR FOR QUASI-STATIC ELASTOGRAPHY.**

Lili Yuan[1]*, Peder C. Pedersen[1].
[1]Worcester Polytechnic Institute, 100 Institute Road, Worcester, MA, USA.

Background: Most current strain methods are correlation based and as such are usually less efficient, may suffer from limited resolution and are error prone for large displacements.

Aims: To develop fast and robust method for extracting axial displacement and strain with improved resolution, referred to as analytical phase tracking strain estimation (APTE).

Methods: The APTE method is implemented in two ways - zero phase search with moving window (I) and zero phase band tracking using connected component labeling (II). Based on acquired RF signals, the analytical amplitude and wrapped phase matrices firstly are produced via Hilbert transform as a function of axial range (fast time) and the applied force (slow time). As illustrated in Fig. (a), APTE-I subsequently seeks zero phases in the sequence of slow time (e.g. $\varphi_0(p,0)$ as initial and $\varphi_0(q,M)$ as end points) and obtain the fast time shifts (e.g. p-q). Axial location of previous estimated zero phase is used as the center of the current 1 wavelength searching range. As for APTE-II, it creates zero phase bands across the phase matrix with only phase values in a small range retained, e.g. $+/-0.2\pi$. It then tracks zero phase bands across the phase matrix to obtain the fast time shifts of the zero phase bands between pre- and peak-compression. Finally, both strategies convert the time shifts to displacement and calculate strain.
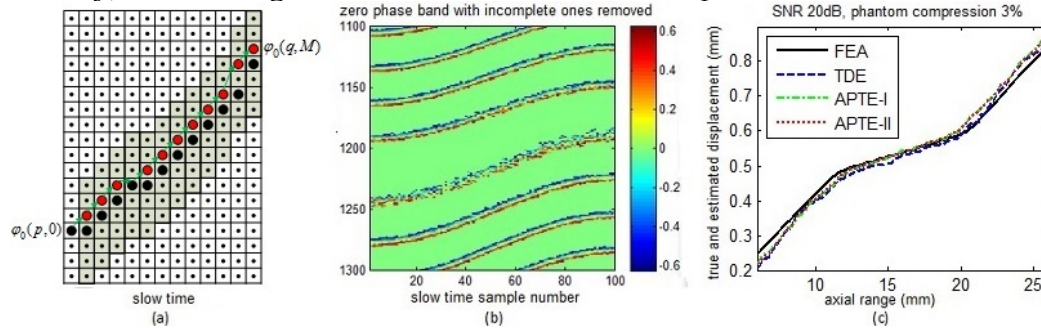
While most of the zero phase bands in APTE-II are continuous across the slow time dimension of the phase matrix, discontinuities, bifurcations or mergers occur, correlated with low analytical signal amplitudes. This is remedied as follows: 1) applying an amplitude threshold filter to the zero phase bands, eliminating bifurcating or merging phase bands; 2) removing discontinuous phase bands using connected component labeling, leaving only the complete phase bands (Fig. (b)). Figure (c) displays three displacement curves: A reference curve determined by Finite Element Analysis (FEA); estimation based on standard time domain cross correlation estimator (TDE); estimation based on APTE-I and APTE-II.

Computation complexity analysis based on the number of multiplications and summations and maximum/minimum/connected-components searching reveals that the cost of APTE is almost 1/20 of TDE, assuming window size is 3 wavelengths and search region is 1 wavelength for TDE. Its efficiency is also superior to other reported algorithms such as time-domain cross correlation with prior estimates (TDPE), phase root seeking (PRS) and combined autocorrelation method (CAM) [1].

Results: Numerical simulation and actual experiments on inhomogeneous phantoms were performed with inclusion of various stiffness contrasts and sizes. Both results indicate that APTE estimates tissue displacement roughly 20 times faster than TDE with comparable or better accuracy. Specifically, at compression level 3% and 6% with SNR 20 dB, statistical simulation assessment demonstrates average strain error of 10% for APTE versus 18% for TDE. Estimated displacement and strain curves using APTE from 5 phantom experiments also show good agreement with true value from FEA simulations.

Conclusions: The APTE method achieves its advantages of faster processing, higher axial resolution and less susceptibility to large displacement errors by zero phase tracking across all RF lines.

References: [1]. Reza Zahiri-Azar et al.: IEEE Transaction on Biomedical Engineering; 53(10), pp. 1990-2000.

011 **A FAST HYBRID MOTION TRACKING ALGORITHM FOR 3D ULTRASONIC ELASTICITY IMAGING.**

Yuqi Wang[1]*, Timothy Hall[1]
[1]University of Wisconsin, Madison, WI, USA;

Background: Displacement tracking is an important basic step for ultrasonic elasticity imaging. An efficient method for displacement tracking, named the "quality-guided" method, which can reduce the computational expense was reported by Chen [1]. This method estimates the local displacement guided by its neighboring point's 'known' displacement. "Seeds" to initiate this guidance process come from an exhaustive search with a large search region. Those seed displacement estimates are rank ordered according to their displacement estimation cost function values, and the highest ranked seed is used to guide displacement estimation in a small search region for its neighboring point. However, this method is easily affected by its initial seed selection. Peak-hopping error may occur during the exhaustive seed search with large search region. Later, Jiang reported a method to validate high quality seeds using the Viterbi algorithm considering both the continuity and the correlation [2, 3]. The Viterbi method selects seeds more strictly and hence improved the tracking performance. Both methods were validated in 2D breast strain imaging. We combined and modified these two methods to obtain a faster algorithm, and extend it to 3D motion tracking.

Aims: The purpose of our research is to develop a computationally efficient, accurate and robust motion tracking method for 3D ultrasonic elasticity imaging.

Methods: The proposed hybrid tracking method for 3D motion tracking includes two steps. The first step finds high quality seeds and the second step performs motion tracking with the quality-guided method. In the first step, high correlation and continuity are the criteria to select true seeds. The displacements of the potential seed center point and its 6 nearest-neighbor points are first estimated by maximizing the sum of their correlation coefficients. If the resulting displacement estimates all have high correlation (between pre- and post-displacement echo signals) and continuity (the displacement difference between each neighboring point and the center point is less than a threshold value), those displacement estimates will be selected as true seeds. The true seed center point will be unchangeable during later quality-guided search. In the second step, quality-guided displacement estimation (a region-growing method) will be performed to obtain displacement of all points on the region of interest (ROI) grid according to the initial inner (true seed points) and exterior (its neighbor) points. To test our method, several phantoms were compressed and scanned. RF ultrasonic echo data was acquired using a Siemens Acuson S2000 Ultrasound system and their Automated Breast Volume Scanning system. The displacement field ROI included 106 points (every 9th RF sample) in the axial direction, 57 in lateral (skipping every other A-line) and 66 in elevation (no skip in elevation). Seeds are evenly spaced in the ROI forming a grid of 6 in the axial, 4 in lateral and 5 in elevation. Therefore, there are a total of 398,772 displacement points to be tracked and a total of 120 potential seeds. Our method was evaluated using the phantom data, and compared with the Viterbi method (2) and the original quality guided method (1). The displacement images and strain images were finally obtained with each of these algorithms.

Results: The new 3D method demonstrated less peak-hopping errors on the displacement fields compared with the original quality-guided method. Both the new method and the Viterbi method had smooth displacement field but the new method was approximately 20 times faster than the Viterbi method. Tests in 3D breast elasticity imaging are ongoing.

Conclusions: This improved hybrid tracking method achieves the balance of accuracy and efficiency for 3D ultrasound motion tracking. It is potentially more accurate than the original quality-guided method by selecting seeds more carefully. It products the same good performance as the Viterbi method but can be much faster than the Viterbi method.

References: [1] Chen, L., Treece, G. M., Lindop, J. E., Gee, A. H., & Prager, R. W: A Quality-Guided Displacement Tracking Algorithm for Ultrasonic Elasticity Imaging. Medical Image Analysis, 13(2), pp. 286-296, 2009. [2] Jiang, J., & Hall, T. J: A Fast Hybrid Algorithm Combining Regularized Motion Tracking and Predictive Search for Reducing the Occurrence of Large Displacement Errors. IEEE Transactions on Ultrasonics, Ferroelectrics and Frequency Control 58(4), pp. 730-73 2011. [3]Jiang, J., & Hall, T. J: A Generalized Speckle Tracking Algorithm for Ultrasonic Strain Imaging using Dynamic Programming. Ultrasound in Medicine & Biology, 35(11), pp. 1863-1879, 2009.

006 **ASSESSMENT OF MYOCARDIAL STRAIN USING ADAPTIVE SIGNAL PROCESSING FOR THE SUPPRESSION OF HIGH-INTENSITY INTERFERENCES: A SIMULATION STUDY.**

S Okumura[1]*, A Kita[2], H Taki[1], T Sato[1].
[1]Kyoto University, Yoshida-Hommachi, Kyoto, Kyoto, Japan; [2]Sakai Rumi Clinic, Kobe, Hyogo, JAPAN.

Background: Tissue strain imaging is the technique for assessing myocardial strain by ultrasound and some tissue strain imagers employ the tissue velocity information estimated by a Doppler technique [1]. High-intensity interferences, such as echoes from bones and ribs, seriously corrupt the performance of the Doppler technique in estimating tissue velocity. To suppress the contribution of high-intensity interferences, moving target indicator (MTI) filters are widely used. However, an MTI filter only suppresses the stationary components of interferences and their time-varying components still remain.

Aims: In this study, we propose a technique to suppress high-intensity interferences using adaptive signal processing to improve the performance of the Doppler technique in estimating tissue velocity under the condition that high-intensity interferences exist.

Methods: We first employ an MTI filter which completely suppresses the stationary component of interferences. Second, to suppress time-varying components of interferences, we apply the Capon method to the signal after the MTI filtering. The Capon method is one of the adaptive signal processing techniques used for high resolution imaging. The method requires the estimation of the spatial covariance matrix which shows the cross-correlation between two signals received at two elements. Because the assessment of myocardial strain needs high-temporal resolution, we estimate the covariance matrix by averaging five received signals with the averaging process along the axial direction. In the simulation study, we suppose a liner array probe consists of 8 elements, the center frequency is 4.5 MHz and the pulse length is 0.80 mm. The arrival direction of the desired signal is the front of the probe and the tissue velocity is 0.20 m/s.

Results: Fig.1 shows the estimation error of the tissue velocity by using the proposed method and a conventional delay and sum (DAS) beamformer, where both methods employed an MTI filter. The conventional method failed to estimate the tissue velocity when the signal to interferences ratio (SIR) was less than -30dB. Conversely, the proposed method with the axial averaging length of d_a = 1.7 mm succeeded in estimating tissue velocity with an average error of less than 0.015 m/s, even when SIR is -80 dB.

Conclusions: When the axial resolution is 1.7 mm and the measurement time for a single axial line is 0.50 ms, the proposed method succeeds in estimating the tissue velocity with an average estimation error of less than 10%. This result shows the high potential of the proposed method to improve the accuracy of the Doppler technique in estimating tissue velocity, indicating the possibility of achieving a high-accuracy tissue strain imager using the Doppler technique.

References: [1] H. Skulstad, et al.: Detection of Ischemia and New Insight into Left Ventricular Physiology by strain Doppler and tissue velocity imaging. Assessment during Coronary bypass Operation of the Beating Heart. J. Am. Soc. Echocardiogr, 17, (12), pp. 1225–1233, 2004.
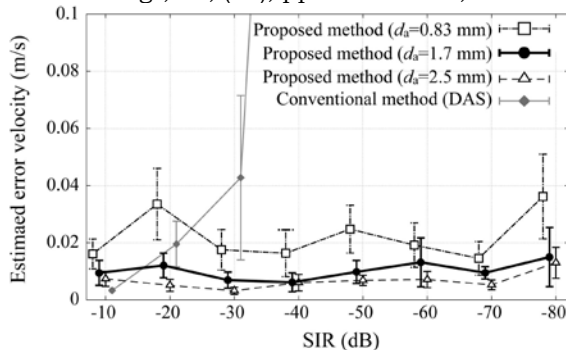
Figure 1: Tissue Doppler velocities estimated using the conventional and the proposed methods, where the ratio of the desired signal intensity to the interference intensity (SIR) ranges from −10 to −80 dB. The interference arrived at an incident angle of 5.0 degrees, and the intensity of the time-varying component of the interference was 40 dB lower than that of the whole interferences. Each error bar shows the standard deviation.

014 **TWO-DIMENSIONAL ULTRASOUND STRAIN IMAGING IN A TRANSVERSELY ISOTROPIC MEDIUM.**

He Li[1]*, Wei-Ning Lee[1]
[1]The University of Hong Kong, Hong Kong, CHINA.

Background: Lateral motion estimation has always been a major challenge in two-dimensional (2D) ultrasound speckle tracking and strain imaging, owing to the inherent poor resolution and lack of phase information in the lateral direction. The presence of axial deformation further leads to lateral decorrelation, thus reducing lateral estimation accuracy. Moreover, the strain filter [1, 2] implies that lateral and axial strain estimation may require different frame-pairing paradigms to achieve comparable strain quality. However, to our knowledge, little is known about the performance of 2D ultrasound strain imaging in orthogonal planes of an anisotropic tissue under quasi-static compression.

Aims: In our study, we aim 1) to improve the estimation accuracy of the lateral displacement based on a previously developed radio-frequency (RF)-based speckle tracking technique [3], 2) to obtain two-dimensional (2D) strain images of high quality, and (3) to investigate the performance of ultrasound strain imaging in both fiber- and cross-fiber planes in a transversely isotropic tissue model in a quasi-static compression configuration.

Methods: We proposed a series of strategies to improve the RF-based speckle tracking method [3]: a two-dimensional (2D) matching kernel, a material point-wise axial motion correction incorporating local displacement variation, an exhaustive peak search on an interpolated 2D normalized cross-correlation (NCC) map, and a multi-step framework achieving the optimal range of strain filters [1, 2]. Compression (4.5% axial strain) was realized in a $40\times40\times40$ mm^3 finite element analysis (FEA) model, and a linear convolution model [4] was utilized to generate simulated US images, with 5MHz center frequency, 60% fractional bandwidth, 1mm beam-width and 128 elements used.

Results: The findings in the 2D isotropic model show a higher accuracy of lateral displacement (mean absolute error (MAE): 0.006±0.008 mm v.s. 0.032±0.027 mm) and strain (MAE: 0.06±0.06% v.s. 0.21±0.18%) estimates yielded from the proposed methodology than the previous technique in [3]. In the 3D transversely isotropic model, displacement MAE of 0.017±0.034 mm and 0.028±0.038 mm, strain MAE of 0.16±0.13% and 0.34±0.32%, and elastographic signal-to-noise ratio (SNR$_e$) of 3.5±0.9 dB and 9.9±1.2 dB were found in the fiber plane and cross-fiber plane, respectively. Figure 1 shows the lateral displacement and strain images obtained by the proposed method.

Conclusions: The 2D window kernel, material point-wise motion correction, and exhaustive peak search on the interpolated 2D NCC map were found to collectively improve speckle tracking accuracy and strain image quality in the lateral direction. Higher strain quality in the cross-fiber plane than the fiber plane suggests that asymmetric frame-pairing be used for depicting a deforming anisotropic tissue to achieve comparable lateral strain image quality in different ultrasound imaging planes.

References: [1] T. Varghese and J. Ophir: A Theoretical Framework for Performance Characterization of Elastography: The Strain Filter. IEEE Transactions on Ultrasonics Ferroelectrics and Frequency Control, 44, pp. 164-172, 1997. [2] E. Konofagou et al.: Theoretical Bounds on the Estimation of Transverse Displacement, Transverse Strain and Poisson's Ratio in Elastography. Ultrasonic Imaging, 22, pp. 153-177, 2000. [3] W.-N. Lee et al.: Theoretical Quality Assessment of Myocardial Elastography with *In Vivo* Validation. IEEE Transactions on Ultrasonics Ferroelectrics and Frequency Control, 54, pp. 2233-2245, 2007. [4] J. Meunier and M. Bertrand: Echographic Image Mean Gray-Level Changes with Tissue Dynamics - A System-Based Model Study. IEEE Transactions on Biomedical Engineering, 42, pp. 403-410, 1995.
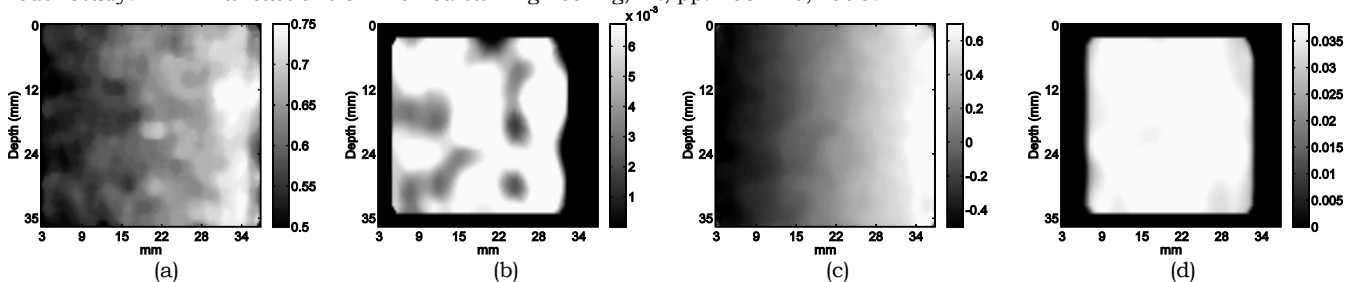
Fig. 1 Lateral displacement and lateral strain in the fiber plane ((a) and (b)) and in the cross-fiber plane ((c) and (d)) of the transversely isotropic model.

030 **OVER-DETERMINED SYSTEMS USING PLURAL STEERED BEAMS OR PLANE WAVES FOR DISPLACEMENT VECTOR MEASUREMENT AND SUPER-RESOLUTION IMAGING.**

*C Sumi. *[1]*

[1]Sophia University, 7-1, Kioicho, Tokyo 102-8554 Japan.

Background: We have been developing ultrasound (US) high spatial resolution echo imaging and high accuracy tissue displacement vector measurement methods. For instance, simultaneous use of our previously developed multidimensional autocorrelation method (MAM) and a lateral modulation (LM) using steered beams or steered plane waves permits a high accuracy measurement. We also generate over-determined sets of data from large numbers of LMs for performing the least squares solution (LST), averaging of measurements (AVE), and coherent superposition (compounding) of beams or waves (CS). Although small inclusions were visualized in [1], the synthetic aperture echo data used had low echo SNR due to the scanner employed. In [2], data with a more realistic echo SNR was used, but only a single LM was performed. Nevertheless, this generated the highest measurement accuracy with MAM to date. We should clarify accuracies achievable via LST, AVE and CS on realistic (high) SNR echo data.

Aims: To clarify the tissue displacement and strain vector measurement accuracies achievable using the above methods for realistic SNR echo data obtained from an agar phantom [2] (US freq., f = 7.5 MHz).

Methods: The agar phantom had a cylindrical inclusion (10mm dia.) with higher shear modulus than the surrounding, and was compressed in a lateral direction (about -0.2%). The MAM was used. Super-resolution imaging was also performed by CS of plane waves.

Results: Figure 1 shows, for scanning with parabolic transmission and apodized reception, and spherical transmission and dynamic reception synthetic focusing (SF), the standard deviations (SDs) of measured axial, lateral and shear strains vs LM frequency. Note that although increasing LM frequency decreases the axial frequency, increments up to 3/8f increase the measurement accuracy of axial strain together with that of lateral strain. This is achieved by the simultaneous measurements of both axial and lateral displacements. Figure 2 shows, for SF scanning, lateral strain images obtained using single or plural LMs with the indicated LM frequencies. In [2], the most accurate lateral strain measurement achieved with a single LM was with an LM of ½f and had a SD of 0.28%. Here, as shown in the figure, using a LM frequency = f, yields a more accurate measurement, with SD of 0.22%. Furthermore, by using plural high LM frequency beams, smaller SDs of 0.16%, 0.16% and 0.20% were respectively achieved for: 16 beams LST (1/8f to f with an interval of 1/8f), 10 beams AVE and 10 beams CS (1/2f to f with an interval 1/8f) (images omitted). However, using independent LM frequencies obtained using large steering angle differences (Fig. 2) achieves the same accuracies using fewer beams, i.e., 8 beams LST, and 6 beams AVE and 4 beams CS. When using plane wave (PW) transmissions with spherical dynamic reception focusing and Gaussian reception apodization, single LMs with frequencies f/2 and f yielded SDs of 0.50% [2] and 0.42% respectively (images omitted). Similar combinations for LST, AVE and CS yielded respectively: 0.27% (6 waves, 2 each with LMs of f, ¾f and f/2), 0.27% (the same 6 waves) and 0.31% (4 waves, 2 each with LMs of f and ¾f). When using more waves, however, only 14, 12 and 14 waves, for LST, AVE and CS respectively, yielded more accurate measurements than the best single LM with SF scanning (0.22 %), i.e., SDs of 0.19, 0.20 and 0.21% respectively. For super-resolution imaging using SF scanning and a single LM frequency of ½f, superposition using CS with 10 plane waves (Fig. 3) yielded a high spatial resolution, particularly demonstrating strong scattering depicted by the circle indicated.
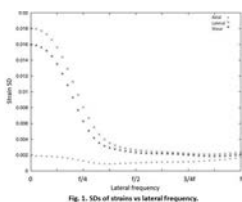
Fig. 1. SDs of strains vs lateral frequency.
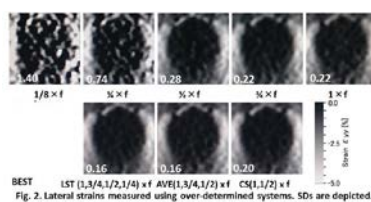
Fig. 2. Lateral strains measured using over-determined systems. SDs are depicted.

Parabolic SP (1/2)f   Gaussian PW (3/4, 5/8, 1/2, 3/8, 1/4)f   Super-resolution
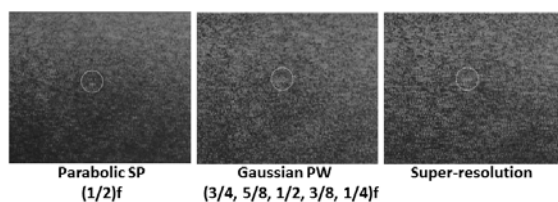
Conclusions: For SF scanning, over-determined datasets with high LM and independent frequencies yielded the highest strain measurement accuracies for LST, AVE and CS (SDs 0.16 or 0.20% for 16 or 10 steered beams), whereas for PW transmissions, accuracies of 0.19 to 0.21% were obtained using 14 or 12 steered waves respectively. The accuracy of CS was the lowest of all the methods, particularly for SF scanning. However, CS of only 10 waves achieved almost the same high strain image spatial resolution as that of a single LM with SF scanning.

References: [1] C. Sumi et al, Proc of 2013 ITEC. [2] C. Sumi, IEEE Trans. UFFC, vol. 55, pp. 2607–2625, 2008.

045   **LONGITUDINAL SHEAR WAVE AND TRANSVERSE COMPRESSIONAL WAVE IN SOLIDS.**

R.Souchon[*1], S. Catheline[1], N. Benech[2.]*
[1]LabTau, INSERM, University of Lyon, Lyon, FRANCE; [2] Laboratorio de Acústica Ultrasonora, Instituto de Física, Facultad de Ciencias, Montevideo, URUGUAY.

Aims: What general definition can one give to elastic P-waves and S-waves, especially when they are transversely and longitudinally polarized respectively? This question is the main motivation of the analysis of the Green's function in elastic solids reported in this letter.

Methods: The anomalous polarization of the S-wave was observed in seismology [1] in non-destructive testing [2] and medical imaging [3]. It is in this latter field called elastography, that this special wave has been systematically studied [4,5] and even commercialized [6] for fibrosis diagnostic. In this paper, it is shown that this latter longitudinal S-wave has a symmetrical counterpart: the transverse P-wave.

Results: These unexpected waves are shown to be special parts of the solution of the wave equation known as coupling terms. Similarly to surface water waves, they are divergence and rotational free. Their special motion is carefully described and illustrated.

Conclusions: Some practical applications of this work could consist in using a longitudinal transducer or a laser to measure both P-wave and S-wave arrivals from a point source. Equivalently a transverse transducer is able to detect both waves if placed in the correct direction. Thus only one measurement can determine the elastic properties of solids.

References:
[1] K. Aki and P. Richards, "Quantitative seismology: Theory and methods: Elastic Waves from a Point Dislocation Source; pp. 63-121, 2002.
[2] P.Gendreu, M.Fink, D.Royer: Optical Imaging of Transient Acoustic Fields Generated By Piezocomposite Transducers; IEEE Trans.Ultrason. Ferroelec.Freq.Contr., 42, pp. 135-143, 1995.
[3] Y. Yamakoshi, J. Sato, and T. Sato: 'Ultrasonic Imaging of Internal Vibration of Soft Tissue under Forced Vibration: IEEE Trans. Ultrason. Ferroelectr. Freq. Control UFFC-37, pp. 45–53, 1990.
[4] S.Catheline, F. Wu, and M. Fink; A Solution to Diffraction Biases in Sonoelasticity: The Acoustic Impulse Technique: J. Acoust. Soc. Am., vol. 105, (5), pp. 2941–2950, 1999.
[5] S. Catheline, J. L. Thomas, F.Wu, and M. Fink: Diffraction Field of a Low Frequency Vibrator in Soft Tissues using Transient Elastography: IEEE Trans. Ultrason. Ferroelectr. Freq. Control 46, pp. 1013–1019, 1999.
[6] L. Sandrin, S. Catheline, M. Tanter, X. Hennequin and M. Fink: Time-Resolved Pulsed Elastography with Ultrafast Ultrasonic Imaging: Ultrasonic Imaging 21, pp. 259-272, 1999.
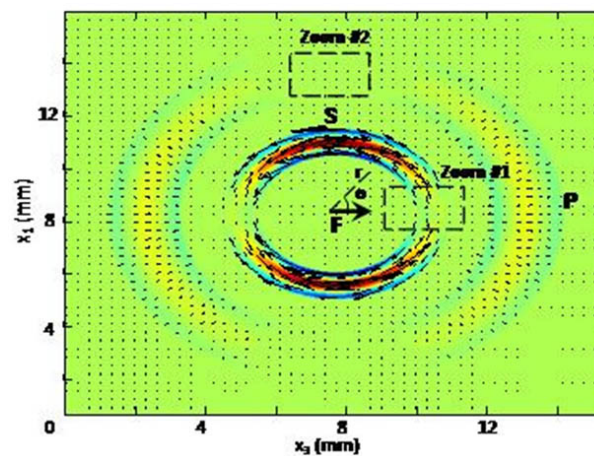
Fig.1 Elastic Green's function. The P and the S wave are clearly visible at $\theta=0$ and $\theta=\pi/2$. The longitudinal S-wave and the transverse P-wave are located inside dashed boxes called Zoom #1 and #2.

009 **DEVELOPMENT OF AN EXPERIMENTALLY VALIDATED NUMERICAL TOOL TO ASSESS THE ACCURACY OF SHEAR WAVE ELASTOGRAPHY.**

Annette Caenen[1]*, Darya Shcherbakova[1], Benedict Verhegghe[1], Clément Papadacci[2], Mathieu Pernot[2], Patrick Segers[1], Abigail Swillens[1].
[1]Ghent University, Ghent, BELGIUM; [2]Institut Langevin, Paris, FRANCE.

Background: There is increasing interest in applying shear wave elastography (SWE) in arteries for the purpose of cardiovascular risk assessment. However, the artery's thin wall (typically < shear wavelength), multi-layered configuration and anisotropic tissue properties induce complex wave phenomena, complicating the link between the measured shear wave (SW) characteristics and the true arterial tissue properties.

Aims: To assess the accuracy and robustness of SWE for assessment of arterial stiffness, a flexible testing ground for SWE in variably complex conditions is needed. For this purpose, we built a 3D finite element (FE) model with its numerical settings validated and optimized according to SWE measurements performed in a bounded, visco-elastic medium. This modelling strategy has been previously demonstrated by [1] and [2], but in bulky media.

Methods: We modelled the SWE-experiment we conducted on a thin (4.35 mm) gelatin-agar phantom (setup illustrated in fig.A) in the FE-software Abaqus (Providence, RI, USA). The FE-model required two inputs: (i) the employed acoustic radiation force (ARF), obtained by modeling the ultrasonic excitation from the Aixplorer system (SuperSonic Imagine, France)using the ultrasound simulation software Focus (Michigan state university, MI, USA), and (ii) the phantom's visco-elastic material properties, determined by using a uniaxial mechanical test bench. Furthermore, these mechanical tests served as a ground truth for the Young's modulus derived from the SWE experiments. To validate the numerical framework, we compared the experimental and numerical shear wave speed (SWS) obtained by tracking the SW front via the peak tissue velocity.

Results: Fig. B depicts the axial tissue velocity in the middle of the phantom (dashed line in fig. A) versus time, both for experiment and simulation, used to derive the SWS. AnSWS of 4.58m/s is obtained in the simulation, matching well the 4.63 m/s of the experiment. This corresponded to an E-modulus of 62.9kPa (simulation) and 64.3kPa (experiment), deviating 9% from mechanical testing (E=68.1kPa). The simulated displacement field caused by the ARF excitation is illustrated in fig. C.
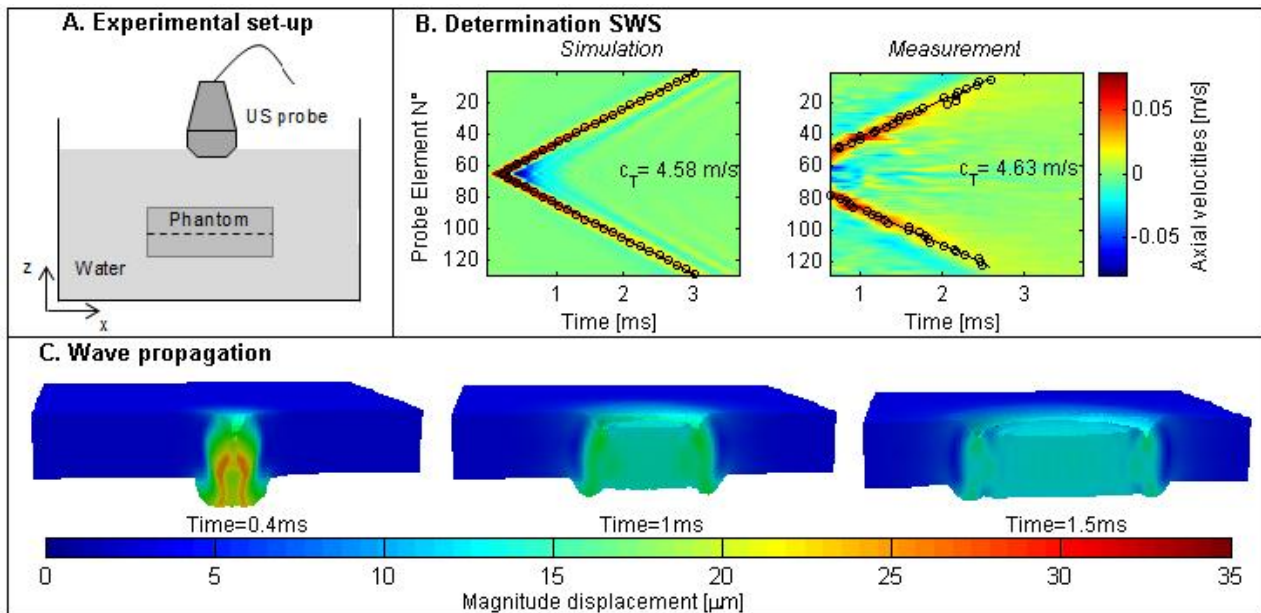
Conclusions: The developed numerical framework reproduces the experimental data obtained and provides a solid basis for further exploration of the complex link between tissue geometry/material properties and SW propagation in (diseased) arteries.

References: [1] Palmeri et al, Ultrason. Ferroelectr. Freq. Control IEEE Trans. On, 52, pp. 1699–1712, 2005. [2] Lee et al, Int. J. Numer. Methods Biomed. Eng., 28, pp. 678–696, 2012.

031 **DEVELOPMENT OF OPEN-SOURCE TOOLS TO VALIDATE SHEAR WAVE IMAGING: AN INTEGRATED QIBA EFFORT.**

Jingfeng Jiang*[1], Steve McAleavey[2] , Jonathan Langdon[2], and Mark Palmeri[3]
[1]Michigan Technological University, Michigan, USA; [2]Universtiy of Rochester, Rochester, New York, USA; [3]Duke University , Durham, North Carolina, USA.

Background: In ultrasound-based shear wave imaging (SWI) [1, 2], local shear wave speed inferred from ultrasonically-tracked tissue motion can be used as a surrogate of local tissue stiffness. The great potential for SWI to improve characterizations of liver steatosis and fibrosis has resulted in several major manufacturers (*e.g.,* FibroScan, Siemens, Philips and SuperSonic Imagine) releasing commercially-available SWI packages. Early inter-laboratory comparisons of SWI [3] demonstrate that there are still several sources of bias and variance that need to be addressed though the overall results were consistent among different systems.

Aims: The goal of this effort is to build a virtual (open source) ultrasound-based simulation platform for public use. The intended virtual simulation system will enable rigorous testing of SWI systems using known but complex media to accelerate the development of SWI, as strongly advocated by the Radiological Society of North America (RSNA).

Methods: Main thrust of this work is to streamline SWI simulations by leveraging existing open source software packages including Field II [4], VTK, and FEBio. The integration of these four open source packages is based on a simple message-passing scheme to facilitate its use among imaging scientists. Modeling of shear wave propagation in soft media has been explored using two open-source packages and one commercial tool: FEBio (http://mrl.sci.utah.edu/software/febio/), a finite difference wave simulation tool by Dr. Steve McAleavey's group at University of Rochester, and LS-DYNA3D (http://www.lstc.com/). Simulation results obtained from elastic CIRS (CIRS Inc., VA, USA) phantoms were analyzed and compared to mechanical testing results.

Results: Simulation scripts and functions that are currently publically available are on GitHub (https://github.com/RSNA-QIBA-US-SWS/fem). The initial results with the Phase I elastic CIRS phantoms have been posted online for public download (http://qibawiki.rsna.org/index.php?title=Ultrasound_SWS_tech_ctte). Comparisons between commercial FEM packages yield <1% relative solutions differences, which comparisons with open-source tools is ongoing.

Conclusions: The preliminary results demonstrated the use of open-source packages for SWI simulations is indeed feasible and commercial solutions agree well with one another. In the future, the proposed virtual software infrastructure will be further developed for hepatic applications, including the incorporation of viscoelastic materials for a second phase of viscoelastic phantom measurements.

References:
[1] K. Nightingale, S. McAleavey, and G. Trahey: Shear-Wave Generation using Acoustic Radiation Force: *In Vivo* and *Ex Vivo* Results. Ultrasound Med Biol*;* 29, pp. 1715-23., 2003.
[2] S. Chen, M. W. Urban, C. Pislaru, R. Kinnick, Y. Zheng, A. Yao, and J. F. Greenleaf, "Shear-Wave Dispersion Ultrasound Vibrometry (SDUV) for Measuring Tissue Elasticity and Viscosity," IEEE Trans Ultrason Ferroelectr Freq Control*;* 56, pp. 55-62, Jan 2009.
[3] T. J. Hall, A. Milkowski, B. Garra, et al., "RSNA/QIBA: Shear-Wave Speed as a Biomarker for Liver Fibrosis Staging, Ultrasonics Symposium (IUS), IEEE International, pp. 397-400, 2013.
[4] J.A. Jensen and N. B. Svendsen "Calculation of Pressure Fields from Arbitrarily Shaped, Apodized, and Excited Ultrasound Transducers; IEEE Trans. Ultrason, Ferroelec., Freq. Contr.*,* 39, pp. 262-267, 1992.

017   **STRAIN-BASED SPARSITY REGULARIZATION FOR DIRECT FEM INVERSION OF TISSUE ELASTOGRAPHY.**

M Honarvar[1]*, R Rohling[1], S E Salcudean[1.]
[1] The University of British Columbia, Vancouver, CANADA.

Background: Dynamic steady state elastography, also called vibro-elastography, can be performed by vibrating tissue and then solving an inverse problem to calculate the elasticity map from the measured steady state tissue motions. Direct finite element inversion is one of the methods used for this purpose [1], and sparsity regularization has been used to stabilize the inverse problem [2]. In this approach, the original variables are transformed into another set of variables using a sparsifying transformation (e.g. Discrete Cosine Transform (DCT)) which results in a sparse representation of the original variables. Therefore, in the new domain, most parameters can be removed, resulting in a system of equations with fewer unknowns and greater stability. The challenging part is to determine an appropriate sparsity pattern in the new domain. In our previous study, we used a circular pattern in the lower frequency part of the DCT domain (Fig.1c), but it is preferable to choose an optimal sparsity pattern based on prior knowledge of the unknown parameters.

Aims: To use the quasi-static strain images of the region as a prior knowledge of the elasticity distribution to choose a more efficient sparsity pattern for sparsity regularization.

Methods: The linear system of equations used in the direct FEM inversion with sparsity regularization is $[\mathbf{A}\mathbf{R}_1]\{\boldsymbol{\mu}^*\}+[\mathbf{C}\mathbf{R}_2]\{\boldsymbol{p}^*\}=\{\boldsymbol{f}\}$ in which $\mathbf{R}_i$ (i=1,2) are the sparsity filters and $\boldsymbol{\mu}^*$ and $\boldsymbol{p}^*$ are the truncated shear modulus and pressure parameters in the DCT domain. In order to derive the filter $\mathbf{R}_1$, we suggest tochoose the sparsity pattern based on the quasi-static strain image. Basically the DCT transform of the strain image is calculated and the parameters with higher magnitudes are selected to be inside the sparsity pattern. For example, Fig.1b shows the quasi-static (10Hz) strain image resulting from the region shown in Fig.1a and Fig.1d shows the sparsity pattern obtained based on the strain image. For deriving the filter $\mathbf{R}_2$, which is for the pressure, we still use the circular pattern.

Results: Validation is performed on simulated data obtained from the model shown in Fig.1a. Frequency of 100Hz is used to generate the dynamic data and down-sampled into a coarser mesh grid of size 46×46. We used both the strain-based sparsity pattern and the circular pattern for deriving the sparsity filter. We changed the number of parameters selected in the sparsity pattern for the shear modulus, solved the inverse problem, and calculated the RMS error of the reconstructed modulus for the cases with and without noise (Fig.1e). The lines with error bars in this figure show the mean and standard deviation of the RMS error. It can be seen that the strain-based pattern selection is more efficient. For example, in the case without noise, the strain-based method using only 180 parameters out of the total number of 45×45=2025 leads to the same level of error as using 800 parameters in the circular pattern. Also, from the noise analysis result, we can see the strain-based method is much more robust to noise than using the circular pattern. An example of reconstructed shear modulus using 180 parameters with the circular sparsity pattern (Fig.1f) and the strain-based pattern selection method (Fig.1g) is shown here.

Conclusions: This simulation study shows that, by using sparsity regularization with strain-based sparsity, we can efficiently find the shear modulus parameters by solving a system of equations with fewer unknowns. From the noise analysis, we can see the strain-based regularization produces lower errors in the presence of noise compared to using the circular pattern
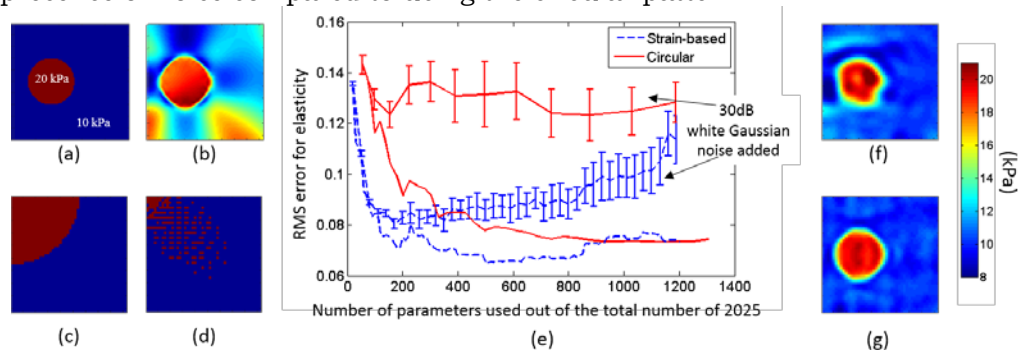
References: [1] E Park and A M Maniatty, Phys Med Biol 51:3697, 2006. [2] M Honarvar, et al. Phys Med Biol 57:5909, 2012.

048 **EFFECT OF ISOTROPIC ASSUMPTION ON MATERIAL PROPERTY MAPS OF THE HUMAN BRAIN USING NON-LINEAR INVERSION FOR MR ELASTOGRAPHY.**

A Anderson[1]*, C Johnson[1], J Holtrop[1], E Van Houten[2], M McGarry[3], K Paulsen[3], B Sutton[1], J Georgiadis[1].
[1]University of Illinois at Urbana-Champaign, Urbana, IL, USA; [2]Universite of Sherbrooke, Sherbrooke, Quebec, CANADA; [3]Dartmouth College, Hanover, NH, USA.

Background: Magnetic resonance elastography (MRE) is an MR imaging contrast used to palpate physically unreachable biological tissues. MRE is used clinically to stage liver fibrosis and as a research tool for studying millimeter-scale tissue mechanical property changes in animals and humans.

Aims: The present study looks at the effects of the common isotropic material assumption in the material property algorithm for applications of MRE on the brain.

Methods: MRE uses an external actuator to induce shear waves in the material of interest; MR imaging techniques measure the steady-state displacement field; and an offline inversion to estimate the viscoelastic material properties. For these experiments, the external shear waves are introduced into the human brain using a Resoundant® pneumatic actuator, at 50 Hz, in two consecutive directions: at the bottom of the head in the anterior-posterior (A-P) direction and on the side of the head in the left-right (L-R) direction. The excitation directions (A-P and L-R) produce shear displacement fields with different propagation directions, and should interrogate anisotropic materials differently. The whole-brain, full vector displacement fields from each excitation were measured using a 3D multislab, multishot spiral MRE sequence [1], and diffusion tensor imaging (DTI) data was collected on a co-registered imaging volume. An isotropic, viscoelastic, finite element based, non-linear inversion (NLI) is employed, using the 3D displacement field, to estimate the full-brain mechanical material property maps [2-3]. The material maps were computed for each direction and both directions were combined, within the NLI framework, using the sum of the mean square error between the measured and calculated displacement fields.

Results: The two excitation directions, A-P and L-R, produced two distinctly different shear wave maps and NLI reconstructed two distinctly different material property maps (Fig. 1). The disparities in material property maps, upwards of 2 kPa in storage modulus (G'), are likely due to shear being applied to the anisotropic axon bundles in different directions. In the brain, G' at the genu of the CC estimated from the A-P excitation is higher than from L-R excitation. This can be attributed to the fact that A-P excitation corresponds to higher displacement normal to the local fiber direction and thus higher values of stiffness. Using NLI to combine both displacement fields provides more information for a more representative reconstruction, and can provide improved property estimates of important white matter tracts.

Conclusions: This study highlights the potential limitations of the isotropic assumption used in NLI, but combining multiple excitation fields during inversion provides a potential solution for capturing the salient features of the brain microstructure, until a more representative model can be employed. Extracting the wave propagation relative to well-ordered fiber bundles will be crucial in extracting representative anisotropic properties of the underlying microstructure.

References: [1] C.L. Johnson, et al.: 3D Multislab, Multishot Acquisition for Fast, Whole-Brain MR Elastography with High Signal-to-noise Efficiency. Magnetic Resonance in Medicine, 71, (2), pp. 477-485, 2014. [2] E.E.W. Van Houten, et al.: Subzone Based Magnetic Resonance Elastography using a Rayleigh Damped Material Model. Medical Physics, 38, (4), 2011.1993-2004. [3] M.D.J. McGarry, et al., "Multiresolution MR Elastography using Nonlinear Inversion. Medical Physics 39(10)pp.6388-6396, 2012.
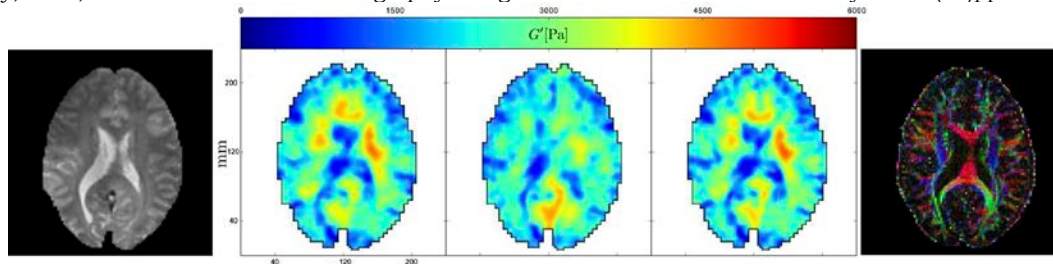
Figure 3: T2 anatomical; MRE multi-excitation stiffness (A-P, L-R, NLI-combined), and DTI fractional anisotropy.

034   **ALGORITHMS FOR QUANTITATIVE QUASI-STATIC ELASTITY IMAGING USING FORCE DATA.**

Mohit Tyagi[1]✱, Sevan Goenezen[2], Paul E. Barbone , Assad A. Oberai[1].

[1]Rensselaer Polytechnic Institute, Troy, USA ; [2]Texas A&M University, College Station, USA; [3]Boston University, Boston, MA 02215, USA.

Background: Quasi-static elasticity imaging can improve diagnosis and detection of diseases that affect the mechanical behavior of tissue[1]. In this methodology images of the shear modulus of the tissue are reconstructed from the measured displacement field. This is accomplished by seeking the spatial distribution of mechanical properties that minimizes the difference between the predicted and the measured displacement fields, where the former is required to satisfy a finite element approximation to the equations of equilibrium. However, in the absence of force data, the shear modulus is determined only up to a multiplicative constant[2]. In this study we address the problem of calibrating quantitative elastic modulus reconstructions created from measurements of quasi-static deformations.

Aims: The aim of this study is to develop algorithms for reconstructing quantitative shear modulus images using quasi-static displacement and force measurements.

Methods: We present two methods that make use of the knowledge of total applied force and/or a measured traction distribution along a portion of the boundary. The first method involves solving for the relative shear modulus field by minimizing the displacement mismatch, and then rescaling it so as to best match the measured force data. This approach is easy to implement but neglects the spatial distribution of traction measurements. The second involves adding a force-matching term to the original minimization problem followed by a simple change of variables, wherein we seek to determine the log of the shear modulus instead of the shear modulus itself.

Results: We have tested the performance of both methods on synthetic data and on experimental data obtained from tissue-mimicking phantoms. We have found that (a) The simple rescaling approach is effective (see Figure1(a) and 1(b)). (b) Without a change in variables, the approach of simultaneously minimizing the displacement and force matching term yields incorrect results because of the conflict between the force matching and regularization terms (see Figure 1(c)). (c) This problem is effectively handled by simply changing the problem from one of determining the shear modulus to that of determining the log of the shear modulus (see Figure 1(d)).

Conclusions: We have developed and tested algorithms for generating quantitative shear modulus images from quasi-static displacement and force measurements.

References:
[1]. Sevan Goenezen, J-F Dord, Zac Sink, Paul E Barbone, Jingfeng Jiang, Timothy J Hall, and Assad A Oberai. Linear and Nonlinear Elastic Modulus Imaging: An Application to Breast Cancer Diagnosis. Medical Imaging, IEEE Transactions on, 31(8) pp. 1628–1637, 2012.
[2] Paul E. Barbone and Nachiket Gokhale. Elastic Modulus Imaging: On the Uniqueness and Nonuniqueness of the Elastography Inverse Problem in 2D. Inverse Problems, 20 (1) pp. 283–296, 2004.

(a)   (b)   (c)   (d)
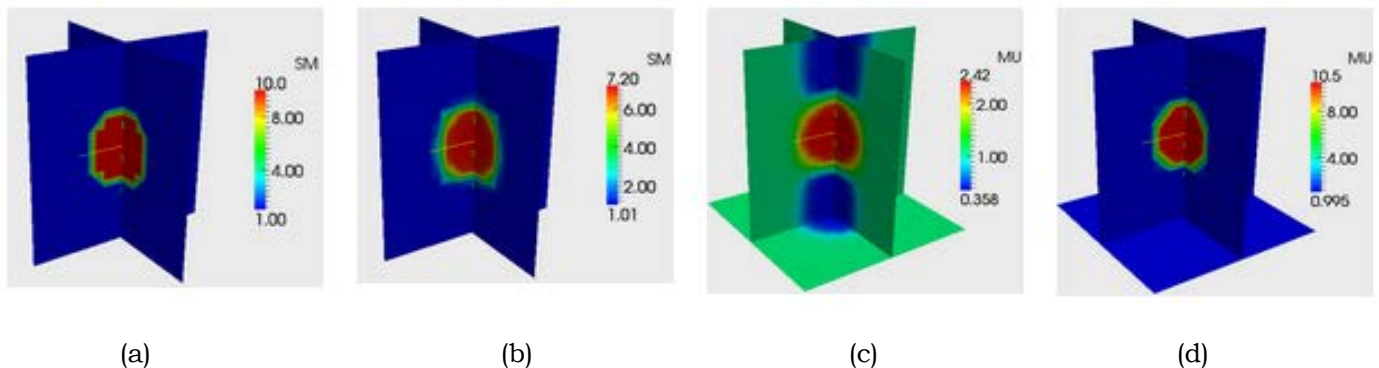
Figure 1. Shear modulus distribution for a problem with synthetic data: (a) Exact distribution. (b) Reconstructed distribution by rescaling modulus. (c) Reconstructed distribution with displacement and force matching. (d) as (c) but with change of variables.

024 **CALIBRATION-FREE BLOOD PRESSURE ESTIMATION USING A MODIFIED ELASTOGRAPHY APPROACH: SIMULATION RESULTS.**

Aaron M. Zakrzewski[1]*, Brian W. Anthony[1].
[1]Massachusetts Institute of Technology, Cambridge, MA, USA.

Background: Current blood pressure estimation techniques either require calibration by the user or are not suited for continuous measurement. Further, various blood pressure estimation techniques are hard to use and make many physical assumptions during the estimation process.

Aims: This study aims to apply elastography methods to estimate pulse pressure and mean arterial pressure within a simulated vessel in a way that does not require any calibration procedures. This method makes minimal physical assumptions, uses data from an ultrasound probe, and is suitable for continuous estimation.

Methods: The finite element program Abaqus (Dassault Systems, France) is used to compress simulated tissue using a linear elastic material model. The applied force is recorded from the finite element model and is a clinically recordable value [1]. Pre- and post-compression B-Mode images are formed with the Matlab program Field II [2, 3]. Displacements and strains are calculated from the pair of B-Mode images using a block-matching method. An inverse problem is solved, such that the objective function compares displacements calculated from the B-Mode images with those from a finite element model. This inverse problem takes the force and displacement data as an input and solves for an estimate of the pulse pressure and elastic modulus distribution around the vessel. The results are used as input into another inverse problem, whose objective function compares the radius and location of the vessel at points along the pressure pulse curve from the finite element model with the values recorded from manual B-Mode image segmentation. The solution to this inverse problem gives an estimate of the mean arterial pressure in addition to the unloaded dimensions and configuration of the vessel. By combining the estimated mean arterial pressure and the estimated pulse pressure, the total pressure is obtained.

Results: Figure 1 shows a simulated B-Mode image (a), the corresponding elastogram (b) where the ground truth is a homogeneous material with an elastic modulus of 4 kPa, and the total pressure estimation result (c). Because the artery is neglected in this simulation, pressures are chosen to be smaller than clinical values. Simulation results show that the mean arterial pressure is estimated in 8 iterations to within 5 percent of the true value and pulse pressure is estimated in 8 iterations to within 20 percent of the true value.

Conclusions: The simulation results show that the method can estimate blood pressure without the need for calibration. While the artery was neglected and quasi-static deformations were assumed, the framework of this research can be used in a final clinically relevant blood pressure estimation device.

References: [1] Gilbertson MW, and Anthony BW: An ergonomic, instrumented ultrasound probe for 6-axis force/torque measurement. IEEE Eng. Med. & Biol., 2013. [2] Jensen JA: Field: A program for simulating ultrasound systems. Presented at 10th Nordic-baltic conf. biomed. imag., 34(1), pp. 351-353, 1996. [3] Jensen JA, and Svendsen NB: Calculation of pressure fields from arbitrarily shaped, apodized, and excited ultrasound transducers. IEEE Trans. Ultras., Ferroelec., Freq. Contra., 39, pp. 262-267, 1992.
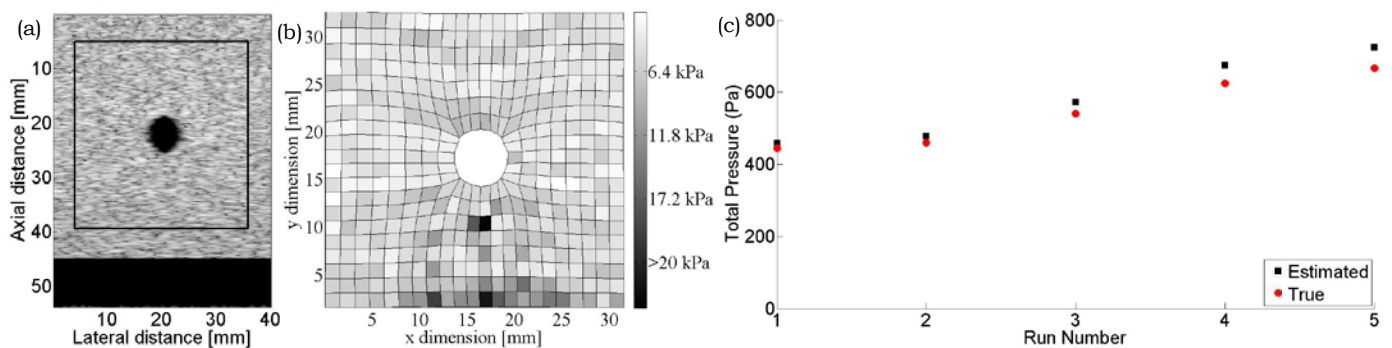
Figure 1: (a) B-Mode image simulated with Field II, (b) corresponding elastogram, (c) total pressure estimation, including mean arterial pressure and pulse pressure results.

Snowbird Village Map

CLIFF LODGE

Aerie Restaurant
Aerie Lounge & Sushi Bar
(A private club for members)
Atrium Restaurant
Boot Teck Bootfitting (winter only)
Camp Snowbird Children's Center
Cliff Spa, Salon & Spa Shop
Cliff Sundries
Cliff Sports (winter only)
Cliff Sports Gear Rental, Tuning & Repair (winter only)
Conference Center
Keyhole Junction
Keyhole Cantina
(A private club for members)
Marco Polo's Silk Road Treasures
Superior Snacks

SNOWBIRD CENTER

Activity Center
Aerial Tram
Alpine Slide (summer only)
Baked & Brewed at the Bird
Birdfeeder
Bungy Tramp (summer only)
Canyon Designs
Center Sundries & Pharmacy
Cottonwood Canyons Realty
Christy Sports & Gear Rental
Event Center (summer only)
Forklift Restaurant
General Gritt's Grocery & Deli
Meeting Rooms
Pier 49 San Francisco Sourdough Pizza
Powder Shots/Superior Photo
Rendezvous Restaurant (winter only)
O Zone–The Oakley Store
Superior Ski Tuning and Repair (winter only)
Ticket Sales
Legend Demo Center (winter only)
Steak Pit Restaurant
Tram Club
(A private club for members.)
Wasatch Powderbird Guides (winter only)
Wine & Liquor Store
Wings

LODGE AT SNOWBIRD

Aspen Room
Lodge Bistro
Lodge Bistro Lounge
(A private club for members)

THE INN

IRON BLOSAM LODGE

Wildflower Restaurant
Wildflower Lounge (winter only)
(A private club for members)

(S) Resort Shuttle stops

Resort Shuttle routes— Operates on
an as needed basis from 5 p.m. nightly.
Call Ext. 5034

(B) B.A.S.S. Shuttle stops

B.A.S.S. Shuttle routes—please check
the posted schedules for arrival and
departure times. Operates from
8 a.m. to 5 p.m. daily.

Walking path between lodges
Snowbird is a pedestrian village.
Cars are not necessary once
you arrive.

To Alta:
1.5 Miles

Wasatch Powderbird Guides

Family
Tubing Hill

Superior
Parking Lot

Covered
Parking

Ski Trail from
Whodunnit to Gad Valley

Entry Four

Zip
Rider

In winter these walking
paths are on snow across
the Chickadee Slope

Handle Tow—
Chairlift Access

Chickadee
Chairlift

Peruvian Chairlift

Snowbird Aerial Tram

Ski Trail to Gad Valley

Entry Three

Main
Parking

Entry Two

Wilbere Chairlift

Gad
Valley
Parking

Gad Valley Lift Ticket Booth

Mid-Gad Chairlift

Little Cottonwood
Canyon Road ➡

GADZOOM Detachable Quad Chairlift

Creekside Lodge

To Baby Thunder
Chairlift

Entry One

Scale: 400 feet

0   200 ft.   400 ft.

To Salt Lake City: 25 Miles

Cliff Lodge Conference Center

THE CLIFF LODGE (Level B)

Lecture Hall
Posters Exhibits
Ballroom I
Ballroom II
Ballroom III
Ballroom Lobby
Conference Registration
phones
Elevators
Valet
Bell Desk
Entry
Escalators
Elevators
Golden Cliff
Magpie B
Magpie A
Atrium Lounge
Creekside Patio
Atrium Patio

CLIFF LODGE (Level C)

Conference Center Terrace w/Tent
(June - September; not to scale)

Maybird
Service Center
Board Room
Superior B
Superior A
Superior Terrace
Conference Services
Elevators
Sundries Shop
Mezzanine Lobby
Business Center
Offices
Lobby
Front Desk
Concierge
Superior Lobby
Eagle's Nest
White Pine
Red Pine
Little Pine
Posters & Exhibits Wednesday
Amphitheatre Lobby Patio
Elevators
Atrium Overlook
Escalators
Wasatch B
Wasatch A

78

Conference Evaluation and Questionnaire

OVERALL CONFERENCE

	Poor		Mid		Excellent
Overall Conference Evaluation	1	2	3	4	5
General comments/suggestions:					

SCIENTIFIC PROGRAM

	Poor		Mid		Excellent
Quality of the Presentations	1	2	3	4	5
Relevance of Presentations to the Conference's Theme	1	2	3	4	5
Time Allotted for Presentations	1	2	3	4	5
Time Allotted for Discussion	1	2	3	4	5
~~Poster Session~~	~~1~~	~~2~~	~~3~~	~~4~~	~~5~~
Tutorials	1	2	3	4	5
Short Presentation Category	1	2	3	4	5
Student Participation	1	2	3	4	5
Equipment Exhibit	1	2	3	4	5
Additional comments/suggestions:					

CONFERENCE MATERIALS

	Poor		Mid		Excellent
Printed Proceedings Book	1	2	3	4	5
CD Proceedings	1	2	3	4	5
Other Registration Materials	1	2	3	4	5
CD only or Printed Proceedings Book and CD	CD Only		Proceedings Book and CD		
Additional comments/suggestions:					

CONFERENCE FACILITIES AND SOCIAL PROGRAMME

	Poor		Mid		Excellent
Lecture Hall	1	2	3	4	5
Registration Desk	1	2	3	4	5
Meals: Dining facilities	1	2	3	4	5
Conference Lunches	1	2	3	4	5
Conference Dinner and Entertainment	1	2	3	4	5
Coffee Breaks	1	2	3	4	5
Opening Dinner Reception	1	2	3	4	5
Closing Dinner Reception	1	2	3	4	5
Audio–Visual: Screen Visibility	1	2	3	4	5
Sound Level	1	2	3	4	5
Presentation Transition	1	2	3	4	5
Internet Connectivity:	1	2	3	4	5
Additional comments/suggestions:					

Conference Evaluation and Questionnaire

VENUE AND HOTEL

	Poor		Mid		Excellent
Venue: Snowbird, Utah, USA and Environs	1	2	3	4	5
Would you return to this city?	Yes		Perhaps		No
Area Attractions	1	2	3	4	5
Hotel: Overall	1	2	3	4	5
Reservations	1	2	3	4	5
Transportation and Accessibility	1	2	3	4	5
Reception and Check–In	1	2	3	4	5
Accommodations	1	2	3	4	5
Facilities	1	2	3	4	5
Parking	1	2	3	4	5
Would you return to this hotel?	Yes		Perhaps		No

Additional comments/suggestions:

CONFERENCE ADMINISTRATION

	Poor		Mid		Excellent
Website	1	2	3	4	5
Registration off–site	1	2	3	4	5
Registration on–site	1	2	3	4	5
Administrative staff	1	2	3	4	5
Correspondence	1	2	3	4	5

Additional comments/suggestions:

GENERAL INFORMATION

I am a Returning Delegate	Yes		No
I plan to attend the next conference in 2015	Yes	Perhaps	No
and present a paper(s) / poster(s)	Yes	Perhaps	No
Other(s) from my lab would attend the next conference	Yes	Perhaps	No
and he/she / they would present a paper(s) / poster(s)	Yes	Perhaps	No

How did you learn of this conference? (Check all that apply)
- ☐ Email Announcement
- ☐ Internet
- ☐ Website
- ☐ Other
- ☐ Colleague

Tutorial Topic Suggestions for next year:

Additional Comments/suggestions:

If you would be willing to host the Conference in your city, please give your name to the Conference Staff.
Questions or comments are welcome at any time at <secretariat@elasticityconference.org> Thank You!